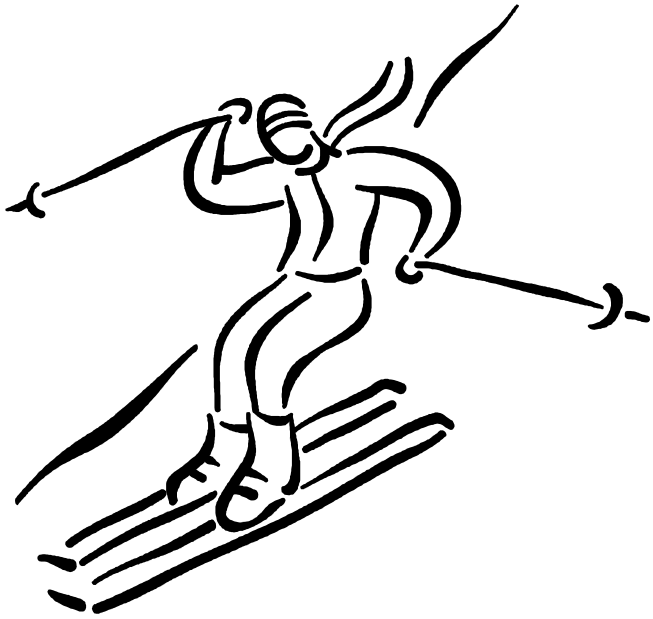

Proceedings of the 2nd Winter Education Seminar

Rokytnice nad Jizerou 2011, February 16—18

Published by the FZÚ AV ČR, v. v. i.
Cukrovarnická 10, 162 53, Praha 6, Czech Republic
Editors: Mgr. Zdeněk Remeš, PhD., Ing. Alexander Kromka, PhD., RNDr. Martin Ledinsky, PhD.
http://www.fzu.cz/~remes/Rokytnice/workshop.html

ISBN 978-80-260-0911-5

CONTENT

PREFACE

The Proceedings publish the selected English written papers presented at the 2nd Winter Educational Seminar which took place in February 16-18, 2011 in the Ski center Horni Domky, Rokytnice nad Jizerou http://www.skiareal-rokytnice.cz/cs/zima/skiareal-horni-domky/, as a joint activity of the Department of Thin Films and Nanostructures and the Department of Optical Materials of the Institute of Physics AS CR, v. v. i. (FZU) in the frame of the CABIOM-Carbon-based Biomaterials and Biointerfaces http://cabiom.fzu.cz/ (Virtual Research Center of the Institute of Physics AS CR, v. v. i.). The evening lectures and discussions took place between 16:00-22:00. The aim of the seminar was to promote the discussion about the problems the students face during their PhD. studies. The research workers referred about the scientific research at the Institute of Physics of the ASCR, v. v. i. to explain special methods used in their laboratories. The main subject of the given talks was **CVD deposition and processing** as well as **optical spectroscopy of thin films**. The discussions were focused on technology, measurement, data analysis and theoretical modeling. The seminar was enjoined by students because of the possibility to spend the free time by sport activities, especially skiing.

The number of participants at the 2nd Winter Educational Seminar was as follows: 3 research workers from the Institute of Physics of the ASCR, v. v. i. (Mgr. Zdeněk Remeš, PhD., RNDr. Martin Ledinský, PhD. and Ing. Alexander Kromka, PhD.), 3 PhD. students and 2 undergraduate students. The seminar was attended by guests from the International Laser Centre in Bratislava and from Slovak University of Technology in Bratislava with whom we closely collaborate in the frame of the agreements on international cooperation in research & development supported by the Ministry of Education, Youth and Sports (MŠMT) under the project no. MEB0810081 *Study of electrical and optical properties of nanodiamond and diamond-like thin films* and the project MEB0810082 *Directed manipulation of surfaces of diamond nanostructures and their characterization* as well as by the Slovak Research and Development Agency projects SK-CZ-0148-09 and SK-CZ-0122-09.

The 3rd Winter Educational Seminar will take place at the same place **in February 1-5, 2012**, please see http://www.fzu.cz/~remes/Rokytnice/workshop.html for more information. The seminar is open for PhD. students and the undergraduate students working in the Institute of Physics of the Academy of Sciences, v. v. i. as well as for the invited guests. The attendance to the seminar is free of charge for the participants of the seminar under the condition that they will give in English an oral talk about their work or a topic that can be interested for others.

Mgr. Zdeněk Remeš, PhD.
in Prague September 28, 2011

200–1600 NM MICRO-SPECTROMETER & LASER SCANNING OPTICAL MICROSCOPE (LSOM)

Zdeněk Remeš[1], Julien Pernot[2], T. N. Tran Thi[2]

[1]*Institute of Physics AS CR, v. v. i., Cukrovarnická 10, Praha 6, 162 53, Czech Republic*

[2]*Institut NEEL, CNRS and Université Joseph Fourier, BP166, 38042 Grenoble Cedex 9, France*

remes@fzu.cz

Abstract In this paper we describe our prototype micro-spectrometer & laser scanning optical microscope (LSOM) build in the last two years at the Department of the Optical materials at the Institute of Physics of the ASCR, v.v.i. The micro-spectrometer is capable to operate in a broad spectral range 200-1600 nm with the spatial resolution below 10 micrometers. Possible configurations include micro-transmittance and micro-reflectance spectroscopy, steady-state photoluminescence spectroscopy, electroluminescence spectroscopy, confocal microscopy with focused laser beam: laser Scanning Optical Microscope (LSOM) and micro-photoluminescence mapping, Laser scattering, dual beam photocurrent spectroscopy (DBP) and high resolution LBIC (light beam induced current) mapping with focused laser beam.

Keywords*:* spectroscopy, chemical, photoluminescence, electroluminescence, thin films

INTRODUCTION

Optical spectra have been usually measured on homogeneous samples with the spatial resolution not better then about Ø 1 mm [1,2]. However, there is a growing need to increase the lateral resolution in the optical measurements, for example:

- to measure homogeneity of the thin films
- to measure optical properties of microscopic objects such microscopic particles or planar microstructures prepared by photolithography
- to reduce the number of light emitting objects in photoluminescence to avoid broadening of the spectral features due to statistical fluctuations

It is the optical microscopy that provides the tool to measure the optical properties with a spatial resolution down to the wavelength of the light. It is therefore ideal solution for many applications to connect the optical spectrometer to an optical microscope. The modern micro-Raman spectrometer offers the Raman spectra to be collected in the visible range with the lateral resolution in micro-scale dimensions down to Ø 1 µm or less. Unlike Raman spectroscopy that uses for excitation the lasers at selected wavelengths (typically red 633, green 532 or blue 488 nm) and measures with a very high spectral resolution and high spatial resolution down to diffraction limit below 1 µm, the steady-state photoluminescence usually requires Xe lamp attached to double gratings monochromator as a source of monochromatic light at tunable wavelength in a broad spectra range (excitation is typically in near UV or visible region, emission spectra are collected in visible and near IR) that cannot be focused as simply as the laser beam. So, the confocal optical microscope is required for the photoluminescence to achieve the spatial resolution down to diffraction limit below 1 µm. Near field scanning optical microscope (NSOM, based on AFM principles) and cathodoluminescence via SEM are the most advanced tools for the optical spectroscopy on nanoscale down to about few tens of nm. However, these sophisticated systems cost typically more than 100 k€.

In our FTIR laboratory we use the commercial IR-Plan Advantage Spectra-Tech microscope connected to the Nexus Nicolet 870 FTIR spectrometer which allows the transmittance and reflectance spectra to be collected with the spatial resolution Ø 100 µm in the spectral range 10000–600 cm^{-1} (1–16 µm) using the build-in liquid nitrogen cooled MCT detector. Recently, we extended the spectral range of the microscope to 400–1000 nm using the internal halogen lamp and the external BWTEK BTC112E TE Cooled CCD array spectrometer mounted via optical fiber to the trinocular port of the microscope. This simple solution

works well and is now commonly used for fast evaluation of the homogeneity of thin film thickness from the interference fringes.

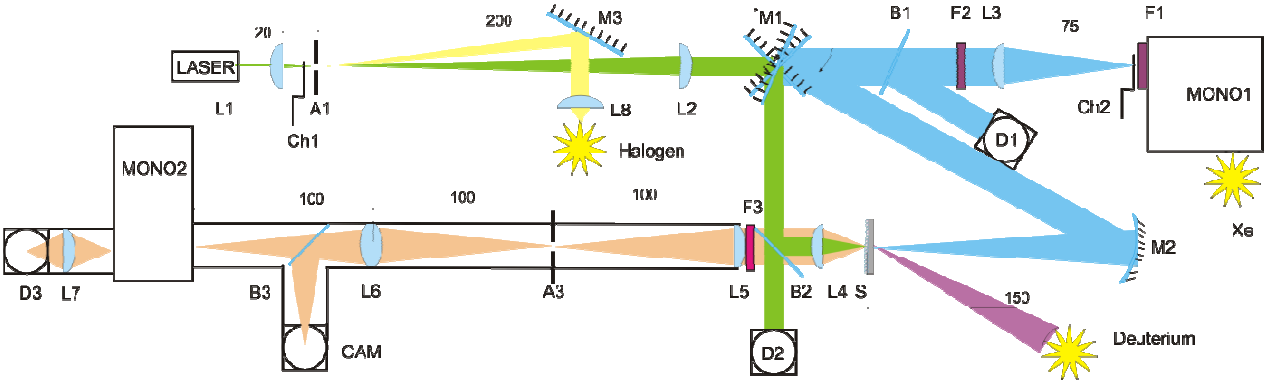

Figure 1 *The schematic view of our micro-spectroscopic setup: L1-8 lenses, M1-3 mirrors, Ch1-2 choppers, A1 aperture, D1-3 detectors,F1-3 filters, B1-3 beamsplitters, CAM videocamera, MONO1-2 monochromators, S sample*

	Spectral range (nm)	dispersion (nm/mm)	Groove density (gr/mm)	note
SP150, grating #1	200 – 500	5	1200	bl. 250 nm
SP150, grating #2	400 – 1000	10	600	bl. 500 nm
H10IR	500 – 1600	16	600	holographic
H10UV	200 – 600	8	1200	holographic
UV-Si APD	200 – 1000			bias -150V
Newport Si918-UV	200 – 1000			calibrated
InGaAs	600 – 1600			
50W QTH lamp	400 – 4000			
75W Xe lamp	200 – 2000			ozon
30W D2 lamp	180 – 350			ozon

Table 1 *The gratings, detectors and lamps used in μ-spectrometer. Available laser wavelengths 532, 635, 830 and 1064 nm.*

PRINCIPLES OF OUR μ-SPECTROMETER

I have built at the Department of Optical materials the infinity-corrected optical microscope that can be applied to different kinds of spectroscopy measurements in a broad spectra range 200–1600 nm with a spatial resolution about 10 μm, see Fig. 1. Lenses of diameter Ø25 mm are made from fused silica to minimize the autofluorescence and chromatic aberration due to the low dispersion of the index of refraction in visible and near IR regions. The system provides sufficient image quality with the optical magnification 50x[1]. The main components of the μ-spectrometer are: 75 W Xe lamp and several solid state lasers (532, 635, 830 and 1064 nm) as a light sources, monochromator SpectraPro-150 (Acton Research, focal length 150 mm, aperture ratio f/4), monochromators H10IR or H10UV, (HORIBA Scientific, focal length 100 mm, aperture ratio f/3.5), HD videocamera, UV-enhanced Si APD (avalanche photodiode) or InGaAs photodiode as light detectors and fused silica aspheric lens (objectives) *L1* with N.A 0.25 (f = 50 mm, plano-convex) N.A 0.5 (f = 25 mm, aspheric) as microscope objectives. The monochromator H10 is placed in front of the detectors to analyze the transmitted, reflected or emitted light. The key parameters are summarized in the Table 1.

[1] Objective *L1* (f = 50 mm) provide together with the lens *L2* (f = 100 mm) the optical magnification 2x. The magnification provided by the 1:1 mapping between camera and monitor pixels is about 25x depending on the ratio between diameter of the monitor (around Ø200 μm for 96 dpi) and camera pixels (Ø 8 μm).

Micro-transmittance spectroscopy at 300-1600nm	Use 75W Xe lamp and SP150 as a monochromatic light source. Use mirrors M1 and M2 to focus the light on S from right side. The μ-T is a ratio of intensities of monochromatic light passed through the aperture A1 measured with and without the sample. Below 300nm large chromatic aberration.
Micro-reflectance spectroscopy at 300-1600nm	Use 75W Xe lamp and SP150 as a monochromatic light source. The μ-R is the spectrum of light reflected by the sample and passed through the aperture A1 and the spectrum of the reference Al mirror.
Steady-state photoluminescence with Xe lamp and narrow band filters, 77-500K (using cryostat Oxford Instruments Optistat DN-V)	Use 75 W Xe lamp together with SP150 monochromator and narrow band filters F3. Use long pass filters in front of HR10.
Confocal microscopy with focused laser beam: Laser Scanning Optical Microscope (LSOM) and Micro-photoluminescence mapping	Measure 2D scan of the intensity of reflected or emitted light at selected wavelength under focused laser beam. For PL use laser together the razor edge filter F1 (absorbing 6 orders of magnitude at laser wavelength)
Laser scattering	Shift the mirror M1 to the right so the sample is illuminated from it's edge. Lens L1 (f=50mm) collects the intensity if the light scattered by 90deg.
Dual beam photocurrent spectroscopy (DBP) in 200-1000nm	Use mirrors M1 and M2 and auxiliary detector D1 to measure ac photocurrent under constant voltage bias. Use auxiliary broad band illumination provided by deuterium lamp to keep the dc photocurrent constant. Requires ohmic contacts on the sample.
High resolution LBIC (light beam induced current) mapping with focused laser beam	2D scan (matrix typically 250x250) of the AC photo-current under constant voltage. Use focused laser beam and the constant voltage applied on the sample. Requires ohmic contacts on the sample.
Electroluminescence in 200-1600nm, 77-500K (using cryostat Oxford Instruments Optistat DN-V)	Apply ac voltage using power supply Kepco BHK 500-80MG and the frequency 1.5 Hz. Requires electrical contacts on the sample (typically PN junction in sandwich configuration).

Table 2 *Summary of the methods available with UV-VIS-NIR micro-spectrometer & laser scanning optical microscope (LSOM).*

The light sources are placed on left side (solid state lasers) or on right side (monochromatic light provided by the Xe lamp and the monochromator SP150). The light source is selected by rotating the flat mirror M1. Since the laser beam is focused on the spot size below 10 μm, an additional visible light for the microscope is provided by the white scattering paint on right side of the aperture A2 illuminated by the 50 W quartz tungsten halogen lamp. The aperture A2 together with the lens L5 and L6 act as a space filter and a beam expander (10x). There is a mechanical high frequency chopper Ch1 (300□1000 Hz) to periodically modulate the laser beam intensity.

The 75 W Xe lamp attached to the Acton Research SpectraPro SP150 monochromator equipped with UV and VIS/NIR gratings provides the incident light illumination in the spectral range 200–1000 nm. There are a mechanical low frequency chopper Ch2 (0-50 Hz) and a filter wheel F2 with band pass filters attached to the exit slit of the monochromator. The monochromatic light is collimated by the fused silica lens L7. For the purpose of the photoluminescence spectroscopy, an additional narrow band filter F3 placed into then parallel beam must be used. Available narrow band filters have band width about 10 nm and the maximum transparency at 250, 300, 350, 375, 400, … , 1075, 1100 nm. The spot size of the focused laser beam is below the Ø10 μm depending on the wavelength and divergence of the laser beam. The spot size of the monochromatic light from Xe lamp is several hundreds of micrometers depending on the objective used. When the spherical mirror M2 is used for the illumination then the illuminated spot on the sample equals about Ø2 mm. The intensity of the light illuminating the sample S is monitored by the calibrated Si photodiode Newport Si918-UV placed in the position D2 or D3 depending of the source of the light and method to be used. The beam-splitter B3 (fused silica window) reflects about 8% of the light intensity to the auxiliary detector D3, the broad band beam-splitter B1 (Al polka-dot fused silica) splits the light by 50 to 50%. The polka-dot beamsplitter is also used as B2. If the laser beam is used for the illumination, the beam-splitter optimized for the laser light wavelength must be used at B2 to avoid the multi-reflections and interferences. The light reflected from B2 is focused by the lens (objective) L1 on the sample S. The lens L1 also collects the light from the sample. The image of the sample is then displayed by the plano-convex lens L2 onto the aperture A1. The minimal aperture of the iris diaphragm (Ø 0.4 mm) corresponds to the selected sample area Ø 200 μm or Ø 100 μm depending on the objective used. Smaller apertures can be achieved using the precision pinholes Ø 200, 100, 50 and 20 μm. It should be noted that in any case the center of the aperture must be in the optical axis of the lens L1, L2, L3 and L4. The biconvex lens L3 images the aperture A1 onto the videocamera VC as well as on the entrance slit of the monochromator H10. Filters F1 have multiple purposes depending of the applied spectroscopy method. To work efficiently, they are placed into the parallel beam in front of the lens L2. The broad band beamsplitter B1 (polka-dot fused silica) splits the light onto the videocamera VC and the input slit of the monochromator H10. Thus, both image of the aperture A1 and the signal intensity can be monitored simultaneously. Monochromatic videocamera is capable to detect the image at wavelength range 350–1100 nm. The lens L3–L4 are fused silica lens without antireflection coating to be transparent in a broad spectral range 200–2000 nm. However, our μ-spectrometer suffers a large chromatic aberration in UV making the UV micro-spectroscopy not reliable.

When adjusting the μ-spectrometer, I advise to follow these steps:

1. Illuminate the aperture A1 from lefts side, adjust the distance between A1 and L3 to be about 100 mm and focus the distance between the lens L3 and the camera and input slit of H10 by moving the camera and H10.
2. Remove the objective L1 and use the parallel beam from right side to focus the L2 onto the A1 without moving A1
3. Put back the objective L1 and focus the sample in the reflectance mode

SIGNAL DETECTION AND PC CONTROL

The μ-spectrometer is PC controlled via USB and RS232 interfaces. The PC control comprises the control of both monochromators, the filter wheel F2, the XY sample stage and the detectors D1, D2 and D3 a well as video-camera VC. In the case of the electrical measurements (LBIC and DBP) the photocurrent induced in the sample is also recorded automatically by PC via the PC control of the lock-in amplifier. The photocurrent is usually measured in ac mode using current preamplifier and lock-in amplifier referenced to the internal oscillator or to the mechanical chopper frequency. The auxiliary detectors D2 and D3 are connected via coaxial cables to the Perkin Elmer/Signal Recovery #5105 lock-in amplifier where the photocurrent from Si photodiode is converted to voltage by 100 kΩ resistor. The photocurrent from the main detector D1 or from the sample (in the case of LBIC or DBP) is connected by coaxial cable to the Salford Research SR570 current preamplifier (typical gain used 10 nA/V to measure ac current down to 10 fA) and Salford Research #SR830 lock-in amplifier. The constant voltage up to 500 V

required for LBIC and DBP spectroscopy is supplied by Keithley 6487 Picoammeter/Voltage Source. The Keithley 6487 Picoammeter/Voltage Source can be also used for dark current measurements in dc mode and for measuring the volt-ampere curve. The ac voltage required for electroluminescence measurements is supplied by Kepco BHK 500-80MG (max 500 V, 80 mA) that allows to trigger the switch on/off by TTL pulses provided by the internal oscillator from SR830 (no chopper used in this method). The lock-in amplifiers #5105 and SR830 are connected to PC via RS-232 port that allows the reliable data rate transmission about 50 ms/reading. The data transition rate 1 ms/reading can be achieved by reading the SR830 analog voltage output by USB the Keythey 2000 digital multimeter (USB connected).

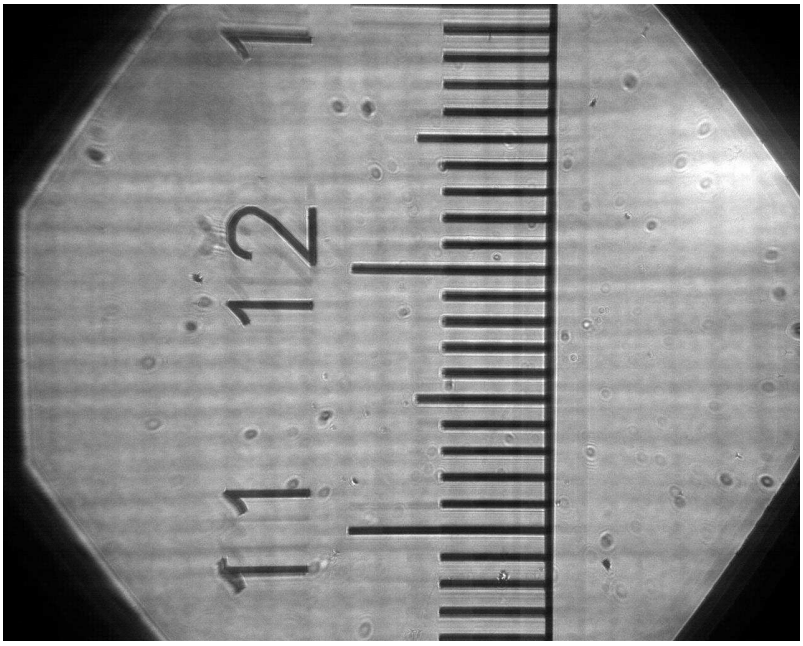

Figure 2 Image created in transmittance mode on videocamera with magnification 50x using objective N.A. 0.25, green light, almost fully open aperture and the scale on plastic as a sample. The minor tics are separated by 0.1 mm, the major ticks with numbers by 1 mm.

The sample is always placed vertically in the μ-spectrometer and must be therefore mechanically fixed on the stage. The sample can be placed either on manually driven XYZ stage equipped with the micrometer screws or on the PC controlled XY stage with manual focus. Focusing is done by moving the sample towards the objective L1. The PC control is essential to perform LBIC, reflectance and photoluminescence 2D mapping and it is also useful for profiling in laser scattering. The PC controlled XY stage consists of two motorized linear actuators with the maximum travel distance 13 mm, accuracy 12 μm, backlash 2 μm, repeatability 0.3 μm and resolution 0.1 μm. They are connected to PC via RS-232 port, therefore 2D scanning is done in continuous moving mode with equidistant time readings (typically 10 ms/reading, thus 250x250 map takes about 20 min). Previously, we did 2D in step scan mode and the 250x250 scan took several hours. All drivers and control software is written in Labview 8.

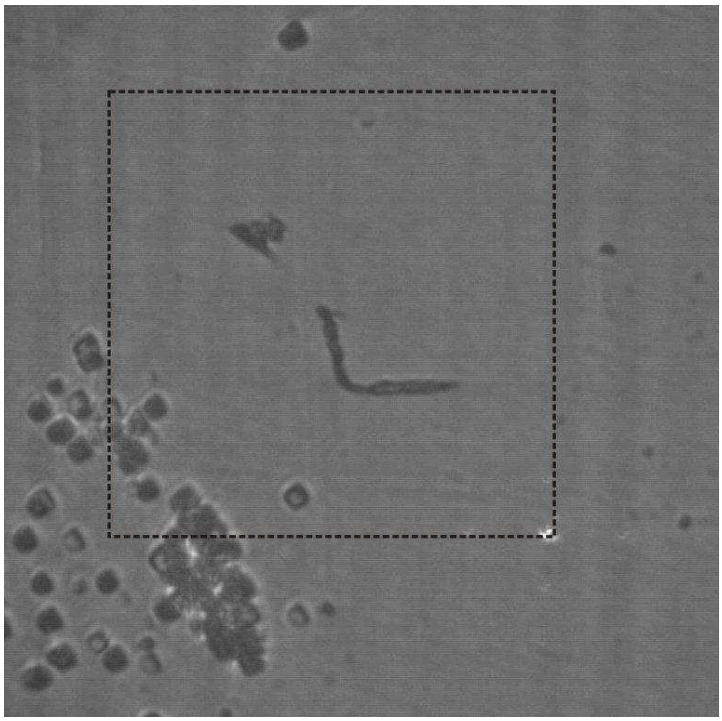

Figure 3 *The transmission optical image of the single crystal CVD diamond with about 10 µm thick homoepi B-doped layer. The area 600x600 µm scanned by laser beam is shown as square with the focused laser spot in the right bottom corner.*

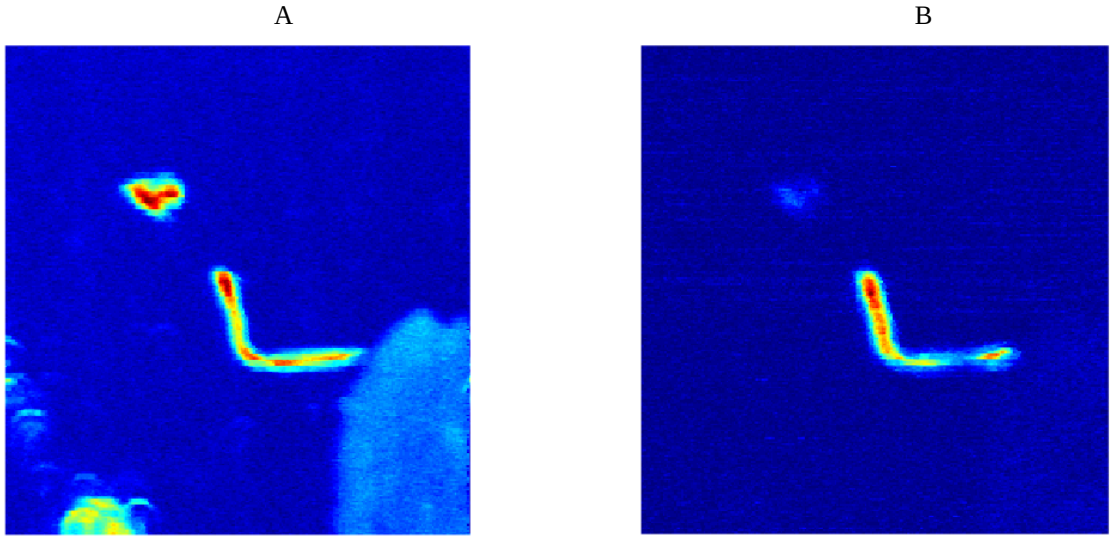

Figure 4 *A) LBIC and B) 600 nm PL scan 250 x 250 steps (area 600 x 600 µm) with green laser 532 nm.*

EXAMPLE OF THE LBIC AND PHOTOLUMINESCENCE MAPPING

The correlation between LBIC and green laser photoluminescence scans is demonstrated on 2D mapping of the defects in homo-epitaxial B-doped diamond layer grown on single crystal 100 oriented type IIa diamond substrate. Nowadays, many types of single crystal diamond substrates are available on the market showing various degree of the crystalline quality, in particular misorientation, dislocation and defect density as well as surface roughness. Recently, it has been shown that the ultra-smooth, defect-free single crystal diamond surfaces are necessary to achieve the highest quality of the B-doped homoepi layer [3]. However, for the purpose of this paper to demonstrate the LBIC and PL mapping, the size 3 x 3 x 0.5 mm^3 optical grade (low N content) single crystal CVD synthetic diamond substrate purchased from ElementSix (http://www.e6.com/en/) was sent to CNRS/Grenoble, where the about 10 µm thick B-

doped homoepi layer has been grown by MW plasma enhanced CVD without the substrate surface polishing. The surface of B-doped homoepi layer was oxidized in RF plasma After the grown and the two coplanar contacts separated by 2 mm where evaporated. Since boron is a rather deep acceptor in diamond with the activation energy 0.36 eV, the sample is photosensitive when illuminated by 10 mW green laser at wavelength 532 nm. The dark dc current was about 100 μA at room temperature under the voltage bias 13 V. The ac photocurrent at 333 Hz generated locally by the focused laser beam was in the order of hundreds of pA up to 10 nA. The difference between LBIC and PL mapping was just "one cable switch" – instead of detecting the LBIC directly from the sample, PL was measured with the current preamplifier connected to Si photodiode detector detecting the scattered light through the optical filters. The razor edge filter was used to cut off 6 orders of magnitude of green 532 nm to measure PL spectra. Thus, using green laser and Si photodiode the PL maps can be eventually done at different wavelengths above 536 nm. The red photoluminescence at 600 nm was chosen for mapping because it gave the maximum PL signal.

The optical image in Fig. 3 shows various defects such as surface pyramids of the size of few tens of μm. These pyramids are probably located at spots where substrate dislocations reach the surface catalyzing the secondary nucleation growth. 2D LBIC and PL maps are shown in Fig. 3a and Fig. 3b in false colors using freeware software GNU Octave (http://www.gnu.org/software/octave/) and command image(A), where A is a matrix of signals measured in each step with respect to the XY position. Blue color represents low signal, red color high signal. The enhancement of the photosensitivity as well as photoluminescence in the vicinity of cracks is probably related to the enhanced boron concentration. The enhanced boron concentration may also appear in pyramids, though here the photocurrent enhancement may be just related to the thicker thickness.

SUMMARY OF THE AVAILABLE METHODS.

Several different experimental methods available with the μ-spectrometer are summarized in **Table 2**. Since the optical components are mounted on the optical rails placed on the optical table, they can be easily interchanged to provide different measurement methods. The adjustment of the optical path was done using laser beam.

Acknowledgement The paper was supported by the Institutional Research Plan No AV0Z10200521, project MEB0810081 (MŠMT ČR) and the agreement of the international cooperation between AS CR and CNRS France: *Optical, optoelectronic and transport properties of the high quality CVD diamond* (2009-2010).

REFERENCES

[1] In *Characterization of Material*, 2 volume set, E. N. Kaufmann, ed., John Wiley & Sons, New Jersey, 2003

[2] Z. Remes, in *Study of defects and microstructure of amorphous and microcrystalline silicon films and polycrystalline diamond using optical methods*, PhD-Thesis, Faculty of Mathematics and Physics of the Charles University (1999), http://www.fzu.cz/~remes/thesis/remes.pdf

[3] T. N. Tran Thi, B. Fernandez, D. Eon, E. Gheeraert, J. Härtwig, T. Lafford, A. Perrat-Mabilon, C. Peaucelle, P. Olivero, E. Bustarret, *Ultra-smooth single crystal diamond surfaces resulting from implantation and lift-off processes*, physica status solidi (a) 208 (2011) pp. 2057–2061

DIAMOND CHEMICAL VAPOR DEPOSITION

Alexander Kromka

Institute of Physics AS CR, v. v. i. , Cukrovarnicka 10, CZ-16253 Praha 6, Czech Republic

kromka@fzu.cz

Abstract Present paper reviews growth of diamond thin films by various chemical vapor deposition processes. Basic characteristics and common features of processes are pointed out with a respect to quality of grown films and standard process parameters. Novel and non-standard diamond syntheses techniques are briefly discussed.

Keywords*:* diamond, thin film, chemical vapor deposition, hot filament, microwave plasma

INTRODUCTION

Growth of diamond thin films by chemical vapour deposition (CVD) processes provides new vistas for their industrial applications. The rapidly developed CVD process seems to be very interesting in the importance for the next decade. The diamond CVD growth is achievable at *low temperature* (400°C-1000°C) and at *low pressures* (below one atmosphere). The first CVD growth was achieved from a mixture of H_2 (converted to H^0) and CH_4 in the 1970's [1]. A listing of deposition techniques demonstrated up to know are mostly presented by various *plasma assisted chemical vapour depositions* (microwave, RF, or DC frequencies) or *hot filaments.* Less common CVD techniques includes *electron, UV* and *laser assisted CVD, ion beam,* and *halogen-carbon thermal CVD processes* have achieved films [2]. In coming chapter it will be shown that after a decade of established beyond a shadow of a doubt – the even very dense phase could be grown from a very low density gaseous phase, far from the equilibrium conditions.

COMMON FEATURES OF DIAMOND CVD PROCESSES

All CVD process above mentioned can be characterized by common features. One of the most common features of CVD growth processes is the presence of gas-phase nonequilibrium in immediate vicinity of the substrate, generated by some sort of gas-phase „activation". The gas phase must contain from a carbon carrier or a specific diamond-forming growth species and powerful selective etchants (*e.g*. atomic hydrogen, oxygen, fluorine *etc*.), in order to remove non-diamond carbon phases from the growing diamond film. The nonequilibrium situation is kept under vacuum conditions and required chemical reactions are stimulated by external sources of energy like surface of hot filaments, oxy-acetylene flame, or through plasma activation. The underlying principles which are operative in the mostly used CVD methods are described below.

HOT FILAMENT CVD

Basic principle: In the hot filament process, atomic hydrogen and other radicals critical to the chemical vapor deposition of diamond films are generated by thermal dissociation. Thermal energy is provided by a refractory metal filament (tungsten, wolfram or rhenium), heated to high temperatures 1900-2500°C. At temperatures as high as 2400°C, at least 10% of hydrogen molecules are dissociated into atomic hydrogen which are further used for chemical reaction, stabilization of diamond surface and selective etching of non-diamond carbon phases [3-5].

Reactor: In a hot filament CVD system flows a carbon gas (methane) over a heated filament to the substrate. Substrate is commonly held about 5-15 mm away from the filament, Fig. 1. Presently, more complex growth systems have been developed to allow, for example, dc biasing of the substrate stage with respect to the filament or to the hot filaments (like in dual plasma CVD process) to control the nucleation procedure and/or growth conditions[6,7].

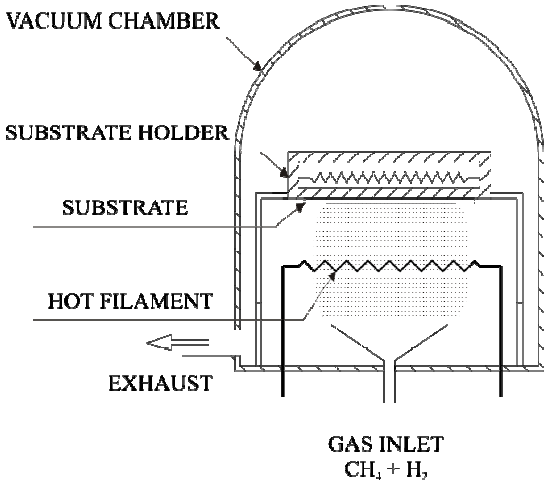

Figure 1: *A schematic drawing of HF CVD reactor*

Growth: The diamond growth by the hot filament CVD has been successfully presented by many research and industrial groups. Typical growth conditions include: <3% of methane in hydrogen, <1000 sccm total gas flow, total pressure <10 kPa, substrate temperature ~800°C, filament temperature of 2000-2200°C and a silicon or molybdenum substrate. Growth rates are generally on the order of 1-10 μm/hr.

Advantages and Disadvantages: The primary advantages of the hot filament CVD process are that highly faceted diamond films can be produced over large areas at moderate growth rate and relatively low capital cost. The HF CVD is commonly used to overcoat cutting drills. Uniform deposition over large areas is feasible rather than point sources (typical plasmas and most combustion processes). The HF CVD system is optimal to R&D activities like kinetic studies and modeling of the gas chemistry, fluid mechanics, etc. However, there are several drawbacks to hot filament systems, such as the filament changes both chemically (carbudization) and physically (length enlargement and diameter decreasing) with time, contamination of grown film from the filament, and limited amount of methane (due to carbudization of filament and its further over-growth by graphitic phases) or oxygen content (due to filament burning).

PLASMA ASSISTED CVD

Basic principle: In the plasma assisted CVD diamond growth, first plasma is ignited by constant or time-varying electric field of sufficient strength to ionize the gas under vacuum conditions. In the plasma assisted (or enhanced) diamond CVD growth, the activation of the reactant gases is accomplished through inelastic collision between high temperature (~5000°C) electrons and relatively cool (~800°C) neutral species. The most commonly used frequencies in diamond synthesis are commercially available 2.45GHz (microwave frequencies) or 915 MHz [8-11]. Less common used radiofrequency is radiofrequency at 13.56 MHz which resulted in a growth of low quality films [12]. Finally lower frequencies and DC has been used too [13].

Growth: The diamond growth by the plasma assisted CVD process is mostly provided at microwave frequencies (2.45 GHz), at total power up to 6 kW in a continuous mode. Typical growth conditions include up to 3% methane in hydrogen, <1000 sccm total gas flow, and total pressure 3-5 kPa, substrate temperature 650-850°C. Growth rates are generally on the order of 1-5 μm/hr for films of optical grade. A schematic diagram of diamond growth systems driven by radiofrequency and electron cyclotron resonance microwave plasma are shown in Fig. 2**.**

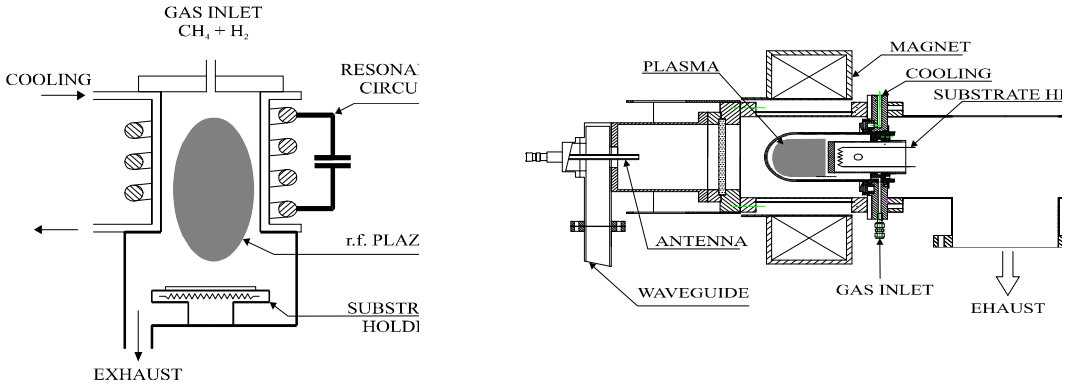

a) **b)**

Figure 2: *A schematic diagram of inductively coupled radiofrequency (a) and electron cyclotron resonance microwave (b) plasma assisted CVD system.*

Advantages and Disadvantages: The primary advantage of a plasma over purely thermal process is that radical species can be generated from high energy electrons while gas and substrate remain relatively coll. Typical gas temperatures are <1000°C, compared with ~2000°C in the HF CVD. Oxygen containing gas mixtures can be used which results in improvement of film quality and growth rate, respectively. DC plasmas up to 4 inches in diameter have been presented. However, they are less attractive due to impurities from the cathode. RF technology resulted in a growth of sp^2 containing diamond films due to low efficiency in hydrogen decomposition. Microwave plasmas are the most employed systems used for diamond CVD growth and such reactors are commercially available. Presently, large area systems are under intensive studies. A disadvantage to plasma-based diamond growth system is that in situ diagnostics are more difficult than the HF CVD system. In addition, the plasma becomes less stable in cavity-like systems (i.e. focused ball) when the argon reach gas mixture is used.

PLASMA TORCH ACTIVATED CVD

Basic principle: Plasma torch systems are presently less favorable. Only briefly, high power density plasmas provide the gas phase activation in the torch. Gas activation is so efficient that the highest diamond growth rates in the world have been reported. The high power density produces electron temperatures of about 10 000 K and gas temperature of about 2 100 K [3-14].

Advantages and Disadvantages: The two major advantages to plasma torch driven growth of diamond are that *i)* growth rates are the highest of any diamond growth technology (max .~1mm/hr) and that *ii)* the resulting films are predominantly sp^3 bonded and highly faceted. Major disadvantages of this system are the need for very gas flows (1-100 liters per minute range), the large power supplies required, and the small growth area (~1 cm in diameter).

COMBUSTION ACTIVATED CVD

Basic principle: In the combustion process, gas phase activation is provided through the highly exothermic chemical reaction between acetylene and oxygen. Reactor hardware is minimal, especially since growth is often performed without vacuum chamber[3,15,16]. For atmospheric pressure combustion reactors, the chemistry of the feather is generally considered to be at thermodynamic equilibrium at the adiabatic flame temperature (~3 700K). The substrate is kept in direct contact with the flame and must be actively cooled. Growth rate is less dependent on diffusion through the boundary layer and more dependent on the mass transport.

Advantages and Disadvantages: The primary advantages of combustion growth of diamond are high growth rate (up to 100 μm/hr), primarily sp^3 bonding, and low capital cost. As limitation is a considerable secondary nucleation because of the thin boundary layer which results in growth of highly rough films. In addition, temperature and chemistry varies with flame diameter resulting in a formation of highly defective crystal.

A summary of advantages/disadvantages for the diamond growth technologies and typical ranges for critical growth parameters are given in **Table I.**

Table I: *Technical data and characteristics of diamond CVD techniques [2-17]*

Method	Rate [μm/h]	Area [cm^2]	Quality [Raman]	Substrates	Advantages	Drawbacks
Flame	30-200	1-100	+++	Si, Mo, TiN, Al_2O_3	simple, rate	area, stability, uniformity
Heated filament	1-10 40*	100-1000	+++	Si, Mo, Al_2O_3, silica, etc.	simple, large area	contaminations, stability
DC discharge (low P*)	<0.1	70	+	Si, Mo, Al_2O_3, silica, etc.	simple, large area	Quality, low growth rate
DC discharge (medium P*)	20-250	<2	+++	Si, Mo, Al,. Al_2O_3	rate, quality	area, contamination
DC plasma jet	10-930	2-100	+++	Mo, Si, W, Ta, Cu, Ni, Ti, stainless steel	highest rate, quality	area, stability, homogeneity
RF (low P*)	<0.1	1-10	-/+	Si, Mo, Ni, silica, BN,	scale up	quality, rate, contaminations
RF (thermal, 1atm)	30-500	3-78	+++	Mo	rate	area, stability, homogeneity
Microwave (0.9-2.45 GHz)	1 (low pressure) 30 (high pressure)	40	+++	Si, Mo, silica, WC, etc.	quality, stability (reasonable rate and area)	rate, area**
Microwave (ECR 2.45 GHz)	0.1	<40	+/-	Si	area, low pressure	quality, rate, cost, contaminations

* - in plasma assisted HF CVD systems

** - newly, linear antenna systems become attractive due to scale-ability up to large area [18]

NON-STANDARD CVD METHODS

In spite of the variety CVD technologies used for diamond film growth, a development of new deposition methods is attractive regarding to find an effective process for low temperature CVD diamond growth over large areas and at higher quality, etc. **Ion ablation** has been not successful due high amount of non-diamond bonded carbon [19]. Similarly to the ion ablation process is the **ion implantation process.** The formation of diamond films by ion implantation of carbon ions into non-diamond substrates has been proposed Prins [20]. The basic requirement is using the substrate with a lattice parameter similar to that of diamond (such as Cu, Ni). However, up to know, no breakthrough has been presented in the diamond growth ar reasonable quality and quantity. **Laser-based irradiation techniques** employ a high energy phonon source for gas phase excitation. The laser frequency may be optimized for a given gas phase chemistry, the beam can be precisely controlled in terms of position and other parameters.

Generally, in all of these laser-enhanced CVD depositions produced individual crystallites rather than complete films [21-23]. An interesting CVD alternative represents **Atomic Layer Epitaxy (ALE)** which is based on diamond surface termination by hydrogen- or halogen-based chemistries as the self-stopping step growth [24,25]. The ALE process has been proposed as promising techniques for many applications, such as the deposition of ultrathin, extremely uniform, precisely controlled, and atomically abrupt diamond (mono-) layers. Finally, well known technique is the Hybrid HPHT/CVD process in which firstly, diamond films are grown by high-pressure high-temperature process (HPHT) and then by the microwave CVD process. This technique allows growth of high-purity and high-quality diamond single crystals.

CONCLUSIONS

Until early 70s of the 20 century, diamond was known and available exclusively as more or less bulky single crystals. However, the rapidly developed low-pressure chemical vapor deposition techniques opened novel possibilities of easily forming relatively extensive two-dimensional diamond thin films. These thin-film and coating technologies are now routinely employed to produce diamond. Some of them have technologically reached high improvements and were adopted by industry. In the short term, the microwave plasma CVD technique seems to be the most promising process which will continue to dominate over the diamond film community as the method for growing high purity and high quality diamond for electronic applications. In the long term, improvements of microwave resonators (i.e. chamber), simulations, design of new modifications or some yet to be invented higher frequency systems may be even more useful for commercial applications.

Acknowledgement Author thank for financial support of national projects KAN400100701 (ASCR), P108/11/0794 (GACR) and bilateral project MEB0810082 (MSMT-Kontakt).

REFERENCES

[1] B. V. Derjaguin, D. V. Fedoseev: Growth of Diamond from Gas Phase, Nauka (1977 Moscow), p. 114.

[2] H. Li, D. S. Dandy: DIAMOND CHEMICAL VAPOR DEPOSITION-Nucleation and Early Growth Stages, NOYES PUBLICATION (New Jersey 1995).

[3] L. S. Plano: *Growth of CVD Diamond for Electronic Applications*, in *DIAMOND: Electronic Properties and Application*, edited by L. S. Pan, D. R. Kania, KLUWER ACADEMIC PUBLISHER (1995 Boston), pp. 61-138.

[4] F. Jansen, M. A. Machonkin, D. E. Kuhman: *The deposition of diamond films by filament techniques*, J. Vac. Sci. Technol A8 (5) (1990), pp. 3785-3790.

[5] J. Yang, Z. Lin, L. Wang, S. Jin, Z. Zhang: *Structural study of diamond film formed on silicon wafer by hot-filament chamical vapour deposition method*, Appl. Phys. Lett. 65 (25) (1994), pp.3203-3205.

[6] V. Malcher, A. Kromka, V. Dubravcová, M. Kubovič: *Investigation of diamond films in double bias-enhanced deposition on molybdenum*, Metallic Materials 39 (6) (2001) 388-395 (ISSN: 0023-432X).

[7] Kromka, T. Daniš, F. Balon, J. Janík, M. Vaněček: *Influence of nucleation parameters on growth of diamond thin films by hybrid hot filament CVD*, Diamond and Related Materials 12 (3-7) (2003) 356-360.

[8] S. H. Kim, Y. S. Park, S. K. Jung: *Effect of the substrate state on the formation of diamond films in a low temperature microwave-plasma-enhanced chemical vapor deposition system*, J. Vac. Sci. Technol. A, Vol. 13 (No 3) (1995), pp. 1620-1623.

[9] H. C. Shih, C. P. Sung, W. L. Fan, W. T. Hsu: *Growth and morphological changes of chemically vapour deposited diamond in the presence of argon*, Thin Solid Films 232 (1993), pp. 41-46.

[10] Z. Feng, M. A. Brewer, K. Komvopoulos, D. B. Bogy: *Diamond nucleation on unscratched silicon substrates coated with various non-diamond carbon films by microwave plasma-enhanced chemical vapor deposition*, J. Mater. Rec Vol 10 (No 10) (1995), pp. 165-174.

[11] Z. Ring, T. D. Mantei*: Low-temperature diamond growth in a pulsed microwave plasma*, J. Vac. Sci. Technol. A, Vol. 13 (No 3) (1995), pp. 1617-1618.

[12] R. B. Jackman, J. Beckman, J. S. Foord: *Chemical vapour deposition of diamond from a novel capacitively coupled r.f. plasma source*, Materials Science and Engineering B10 (1995), pp. 216-219.

[13] K. Kumagai, K. Miyata, K. Nishimura, K. Kobashi: *Growth of (110)-oriented diamond films by electron assisted chemical vapor deposition*, J. Mater. Res. Vol 8(No 2) (1993), pp. 314-320.

[14] K. Kurihara, K. i. Sasaki, M. Kawarada: *Diamond synthesis using DC plasma jet CVD*, Fujitsu Sci. Tech. J. 25 (1) (1989), pp. 44-47.

[15] R. Philips, J. Wei, Y. Tzeng: *High quality flame-deposited diamond films for IR optical windows*, Thin Solid Films, 212 (1992), pp. 30-34.

[16] T. Abe, M. Suemitsu, N. Miyamoto: *Microcrystalline diamond deposition using inert-gas curtain combustion flame method*, Journal of Crystal Growth 143 (1994), pp. 206-212.

[17] C. P. Klages: *Chemical Vapor Deposition of Diamon*d, Applied Physics A - Solids and Surfaces 56 (1993), pp. 513-526

[18] Kromka, O. Babchenko, T. Izak, K. Hruska, B. Rezek: Linear antenna microwave plasma CVD deposition of diamond films over large areas, Vacuum, in press (doi: 10.1016/j.vacuum.2011.07.008).

[19] D. V. Fedoseev, B. V. Derjaguin, R. Roy: *Possible connection of laser-irradiation solid phase synthesis to CVD diamond processes*, in *New Diamond Science and Technology*, edited by R. Messier, J. T. Glass, J. E. Butler, R. Roy, Materials Research Society (1990 Pitsburgh), pp. 439-442.

[20] J. F. Prins: *Ion implantation and diamond: some recent results on growth and doping*, Thin Solid Films 212 (1991), pp. 11-16.

[21] N. Ohya, H. Maeda, K. Kusakabe, S. Morooka*: Enhancement of diamond growth under UV irradiation*, in *Applications of Diamond Films and Related Materials: Third International Conference*, edited by NIST (August 1995, Washington), pp. 369-372.

[22] P. A. Molian, A. Waschek: *CO2 laser deposition of diamond thin films on electronic materials*, J. Mat. Sci. 28 (1993), pp. 1733-1736.

[23] J. Singh, M. Vellaikal, J. Narayan: Laser enhanced synthesis and processing of diamond films from liquid hydrocarbons, J. Appl. Phys. 73 (9) (1993), pp. 4351.

[24] B. B. Pate: *The diamond surface: Atomic and Electronic Structure*, Surf. Sci. 165 (1986), pp.83-88.

[25] R. Gat, T. I. Hukka, M. P. D'Evelyn: *Progress toward atomic layer epitaxy of diamond using radical chemistry*, in *Proceeding of the third international symposium on Diamond materials*, edited by J. P. Dismukes, K. V. Ravi, The Electrochemical Society (1993), Pennington NJ 08534-2896, pp.516-512.

GROWTH OF DIFFERENT CARBON NANOTUBES FORMATIONS BY CVD

Mário Kotlár[1,2], Viliam Vretenár[2], Marian Veselý[1], Robert Redhamer[1]

[1]*Department of Microelectronics, Slovak University of Technology, Ilkovičova 3, 812 19 Bratislava, Slovakia*

[2] *Danubia NanoTech, s.r.o., Ilkovičova 3, 841 04 Bratislava, Slovakia*

mario.kotlar@stuba.sk

Abstract Carbon nanotubes with different morphologies were synthesized on SiO_2 substrates by using the chemical vapor deposition technique. The role of bimetal catalyst composition (Al/Fe, Al/Ni) on creation of nanoparticles with different diameter and density was examined. In dependence on pretreatment and growth conditions two different growths of carbon nanotubes formations has been observed, namely multi-walled carbon nanotubes forests and single-walled carbon nanotubes plane networks. The experiments were evaluated using Raman analysis and SEM. The influence of catalyst composition together with temperature and time of annealing is discussed.

Keywords*:* carnon nanotubes, chemical vapor deposition, Raman spectroscopy, SEM

INTRODUCTION

A carbon nanotube is a cylindrical shaped structure made of carbon atoms. Carbon atoms are arranged in a hexagonal crystal lattice. We can consider a carbon nanotube as one graphite layer that is rolled up into cylinder having diameter of nanometer and length of micrometer order. Due to their unique structure, carbon nanotubes (CNTs) have many interesting electronic, mechanical and chemical properties. CNTs are prepared by many techniques, but chemical vapor deposition is simplest and probably mostly used technology for their growth. In this process the thermal decomposition of hydrocarbon is achieved in the presence of metal catalysts on the surface of substrate. The pretreatment and synthesis conditions, as well as morphology and structure of catalytic nanoparticles play an important role in determining both diameter d_t and chirality (n, m) of CNTs synthesized by catalytic-chemical vapor deposition (CVD) [1]. There exist many theories of growth mechanism for carbon nanotubes. Widely accepted mechanism is based on so-called dissolution – diffusion - precipitation model. In this model a hydrocarbon is decomposed into carbon and hydrogen on the surface of the catalytic nanoparticle, released hydrogen flies away and the carbon diffuses into metal particle. When a supersaturated state in the catalyst is reached, carbon starts to precipitate in a crystalline tubular form [2]. By controlling both the catalyst particle size and synthesis temperature the selective growth of Multi Walled Carbon Nanotubes (MWCNTs) or Single Walled Carbon Nanotubes (SWCNTs) may be achieved. The particle size strongly depends on the catalyst composition and an annealing temperature (pretreatment conditions). As catalyst Ni, Fe, Co or Mo can be used because of two main reasons: high solubility of carbon and high carbon diffusion rate in these metals [2]. In recent years bimetallic catalysts such as Ni-Co, Fe-Co [3] and Fe-Mo [3, 4] and three-layered catalysts with Al [5, 6] have been reported. The Al layer promotes the formation of very small bimetallic particles that can catalyze the growth of CNTs. Recently it has been reported a three-layered Al-Cu-Fe ultrathin film [1] that can play key role in selective synthesis of armchair CNTs.

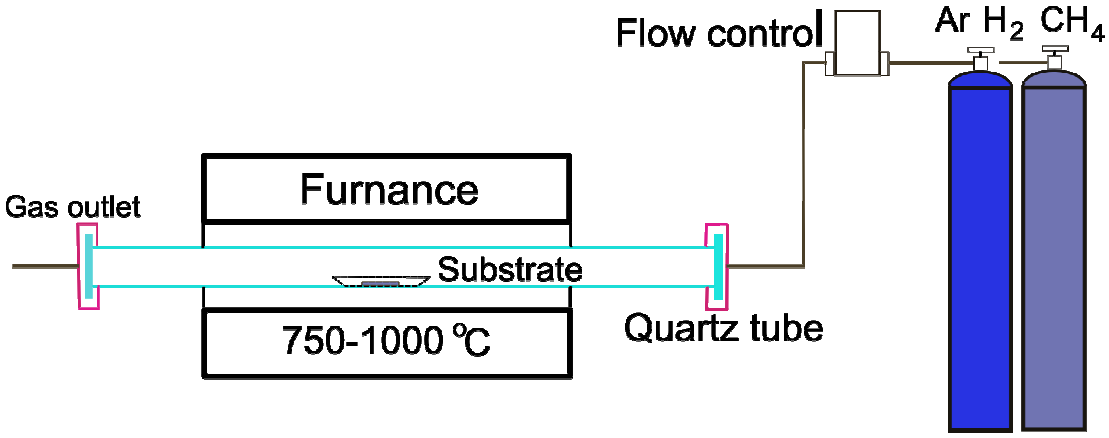

***Figure 1**. Schematic draw of CVD apparatus.*

In this work, the effect of catalyst composition and pretreatment conditions on growth of different types of carbon nanotubes was studied. Experiments were performed using the thermal CVD. Schematic drawing of CVD reactor is shown in the Fig. 1. Bimetallic thin films of Al/Fe and Al/Ni with different thicknesses have been used as catalytic layer, where Al/Fe catalysts promoted the growth of MWCNTs "forest" (vertically aligned and densely packed carbon nanotubes) and Al/Ni catalysts enforced the synthesis of SWCNTs "networks" (horizontally aligned CNTs).

EXPERIMENTS

Experiments were carried out in a tube furnace with quartz tube of 40 mm inner diameter. The furnace was placed on to a rail to be easily moved into different positions relative to the sample. Thanks to this solution the samples can be heated and cooled in few minutes and experiment can run at different temperatures continuously. CNTs were grown on small substrates (5x5 mm^2) cut off from Si (100) single crystal wafer (n-type) having thermally oxidized surface as a diffusion barrier for dopants. Methane (CH_4) was used as a source of hydrocarbons.

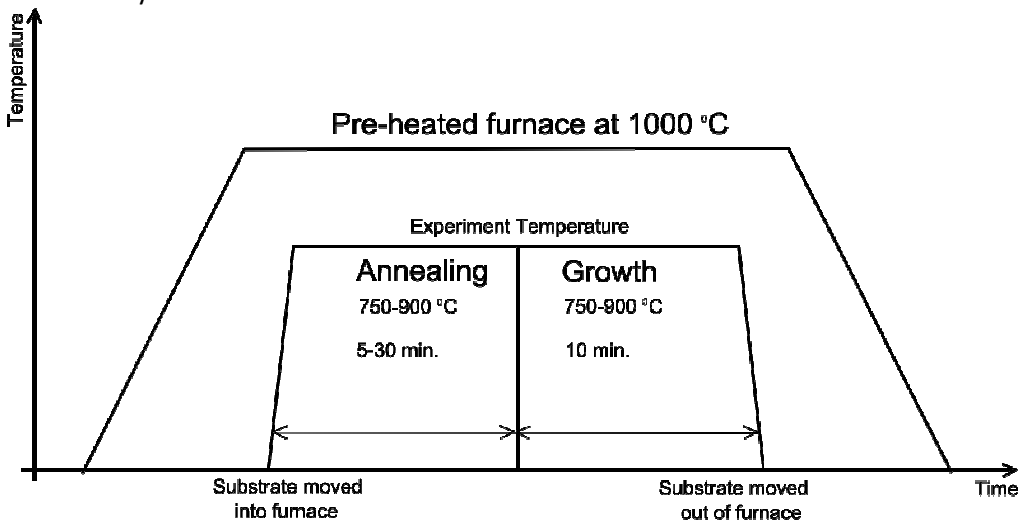

***Figure 2.** Process description.*

For the synthesis of MWCNTs, Al(6 nm)/Fe(2.5 nm) two-layered films were deposited on SiO_2 substrates by thermal evaporation. The temperature of the furnace was ramped up to 1000 °C (Fig. 2.) and stabilized. After that the samples were moved into the furnace at region with 750 °C of temperature and the process started as follows: first, the nano-particles were formed from metallic layer by sample annealing in Ar/H_2 mixture (atmospheric pressure and flow rate of 200/25 sccm) for 5 - 20 min and then by adding 100 sccm of methane CH_4 the synthesis of CNTs took place for 10 min.

For the growth of SWCNs "networks", Al(8 nm)/Ni(2 nm) two-layered films were used as catalyst. Substrates were annealed in the flow of Ar/H_2 mixture (200/30 sccm) for 10 - 30 min, whereas the growth was performed in the flow of $Ar/H_2/CH_4$ mixture (200/30/80 sccm) for 10 min. Both processes were run at same temperature ranging from 750 to 900 °C.

After experiments the samples were examined by Raman spectroscopy with 632.8 nm He-Ne laser. The structural morphologies of synthesized CNTs were characterized by SEM.

RESULTS AND DISCUSSION

The growth of carbon nanotubes was investigated using different catalyst layers. It's known that different catalysts create nanoparticles with different diameter and density on the substrate surface, which directly affects the way of the carbon nanotubes growth. In the Fig. 3, the SEM picture of MWCNTs grown on the surface with Al/Fe bimetal catalyst is presented. Carbon nanotubes are highly oriented and densely packed, forming "forest structure".

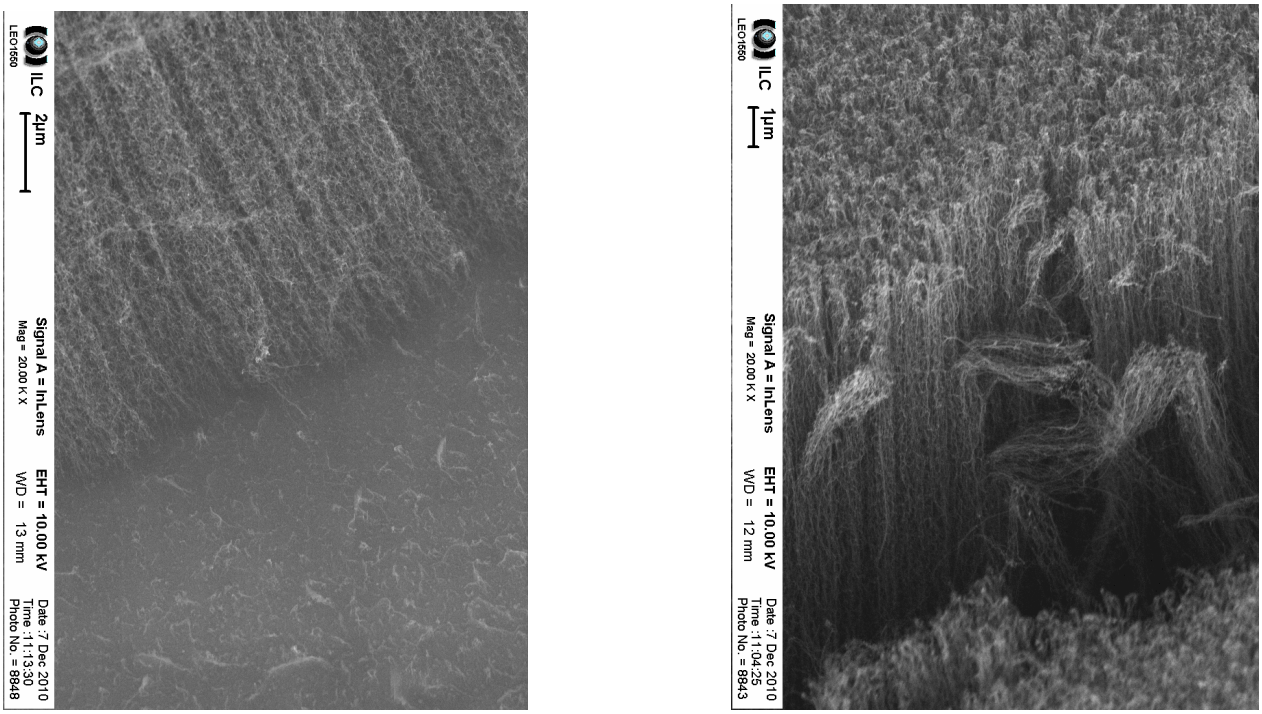

Figure 3. *SEM images of MWCNTs "forests".*

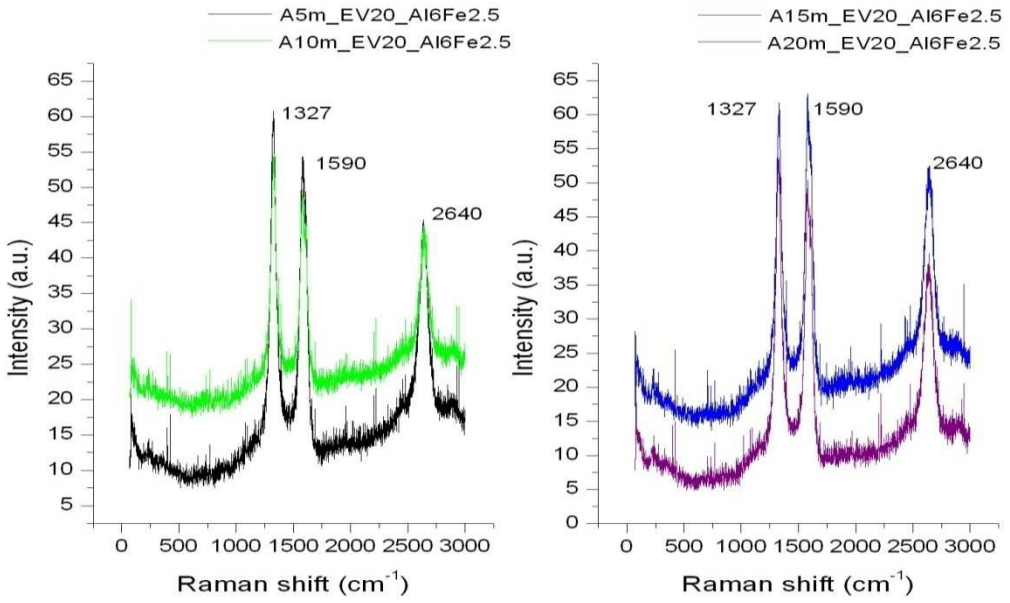

***Figure 4**. Raman spectra of the MWCNTs in the dependence on different annealing times.*

By performing series of experiments it was found out that the best temperature for annealing process and consequential growth of MWCNTs is 750 °C. In addition better results were achieved for bimetallic catalyst with Alumina as supporting layer than for Iron layer itself.

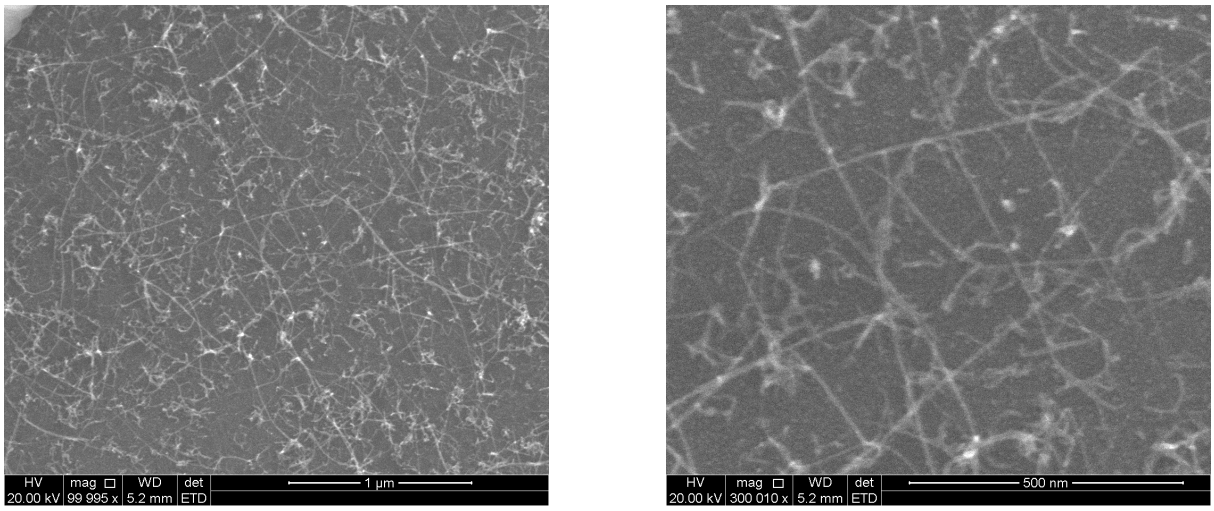

***Figure 5**. SEM images of SWCNTs "networks".*

For higher temperatures the growth was significantly weaker. The influence of annealing time of catalyst layer on growth of CNTs was examined in the following way. The samples were annealed for different times varying from 5 to 20 minutes and then, after the growth, examined by the Raman spectroscopy. Measured Raman spectra showed typical characteristics of MWCNTs growth by chemical vapor deposition (Fig. 4). Since the Raman signal is taken from the upper side of the samples, which are covered with vertically highly oriented carbon nanotubes, only just their ends carrying high amount of defects are measured in majority. That is probably the reason for high D mode found in Raman spectra. No significant differences in Raman spectrum of MWCNTs were found for different annealing times (see

Fig. 4). In the Fig 5., SEM pictures of the SWCNTs networks are shown. Carbon nanotubes were growth on the surface of SiO_2 substrate covered with Al/Ni catalyst layer. The growth of carbon nanotubes was inspected for different temperatures (750 - 900 °C) and annealing time (10 - 30 minutes). The measured Raman spectra of the SWCNTs samples are depicted as a function of the temperature (Fig. 6) and annealing time (Fig. 8).

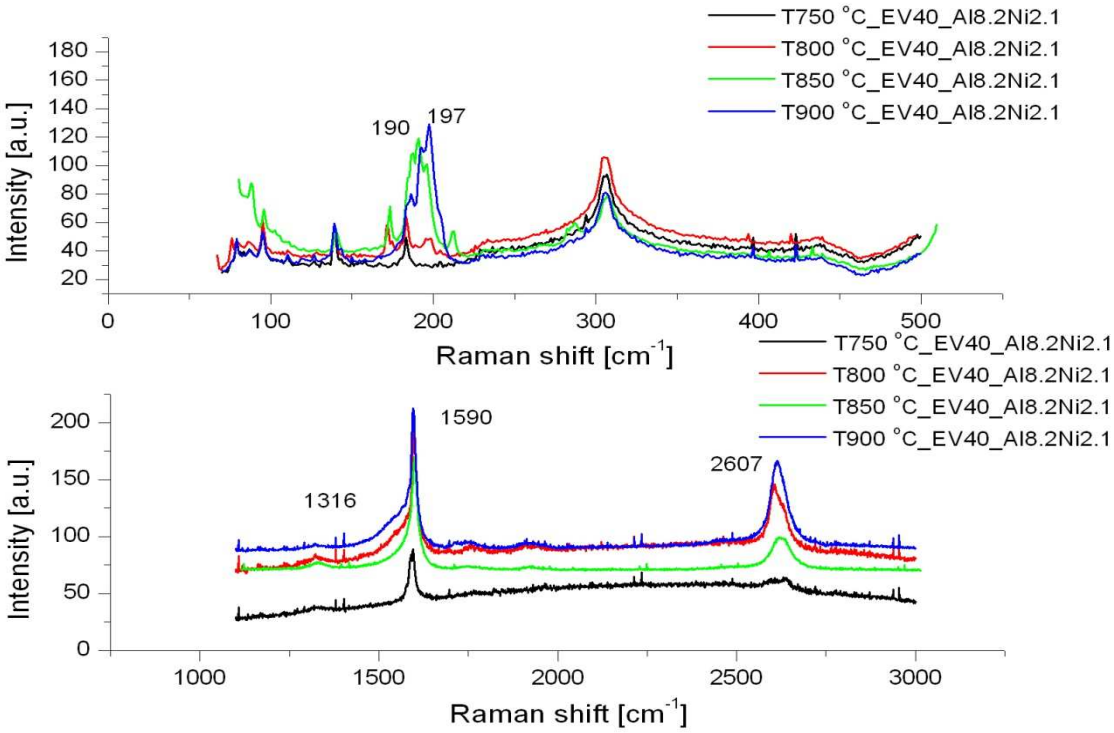

Figure 6 *Raman spectrum of the SWCNTs "networks" for different temperatures.*

With help of the Raman spectroscopy the quality and crystallinity of the carbon nanotubes might be characterized. In the upper part of Raman spectrum (Fig. 6, different growth temperatures two strong peaks, G and 2D at position of 1590 cm^{-1} and 2607 cm^{-1}, respectively and one weak peak, D at 1316 cm^{-1}, can be seen. The G band is related to the stretching of C - C bonds in two dimensional hexagonal crystal lattice of graphite, whereas the D band is related to the disorder carbon or diamond like carbon structures. The quality of carbon nanotubes is then estimated according to the ratio of individual peaks, I_D/I_G ratio. Dependence of I_D/I_G ratio on the temperature (see Fig. 7) is showing lower values for carbon nanotubes grown at higher temperatures (850 - 900 °C), which indicates their better quality in comparison with carbon nanotubes grown at lower temperatures (750 - 850 °C). Typical RBM modes related to the SWCNTs structures can be seen in the lower part of Raman spectrum (Fig. 6) with two distinct peaks positioned at 190 cm^{-1} and 197 cm^{-1}, respectively.

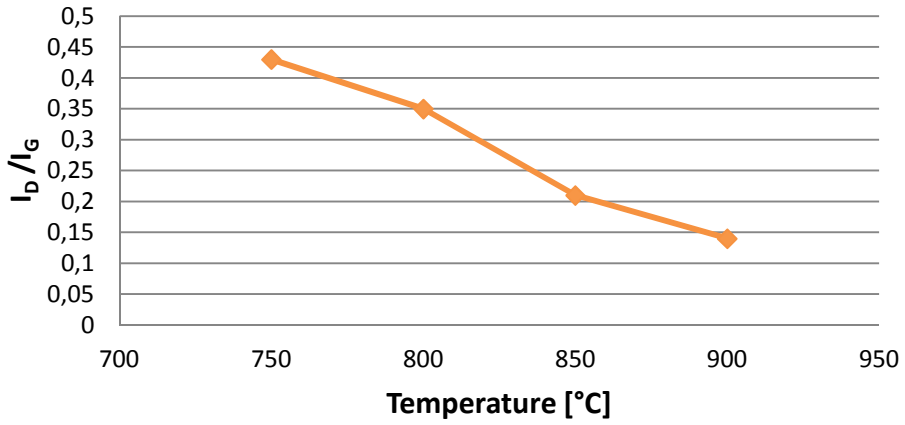

Figure 7. *I_D/I_G ratio calculated from SWCNTs Raman spectrum for different temperatures.*

In the case of Raman spectra as a function of different annealing time (Fig. 8), no significant difference in I_D/I_G ratio (Fig. 9) was observed between the samples. Potential changes in morphologies of SWCNTs are highly questionable and need to be investigated by SEM in details.

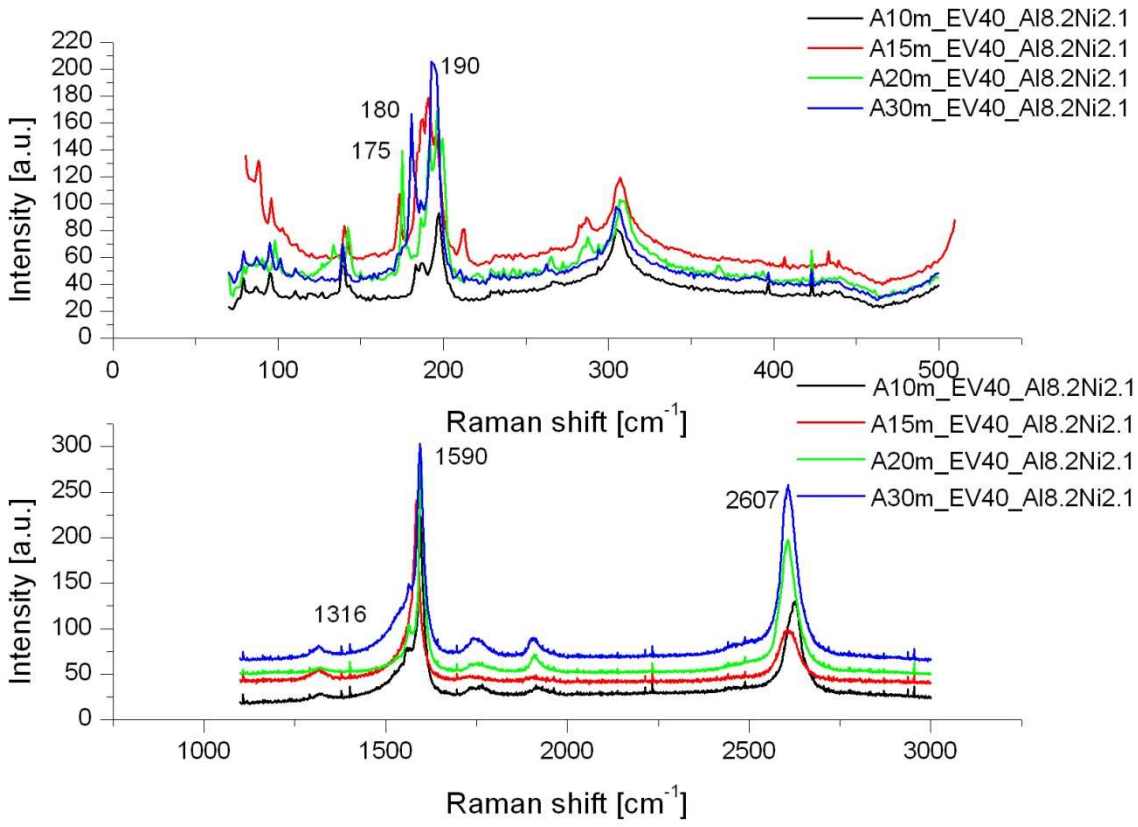

Figure 8. *Raman spectrum of the SWCNTs "networks" for different annealing time.*

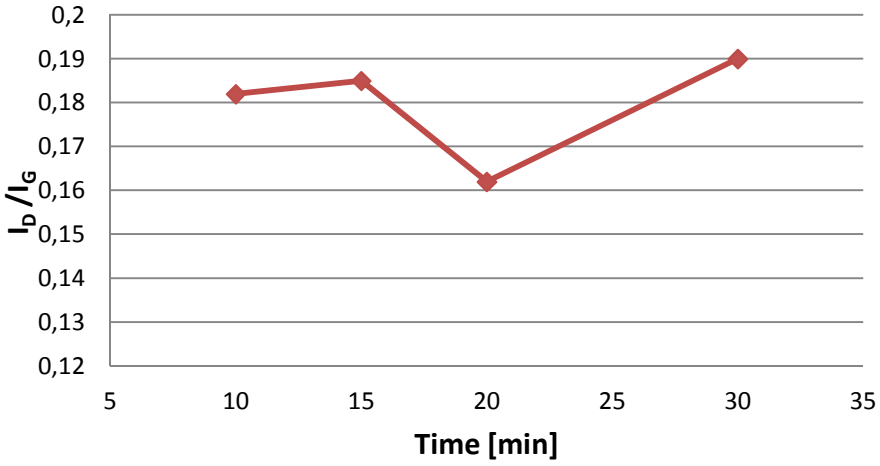

Figure 9. *I_D/I_G ratio calculated from SWCNTs Raman spectrum for different annealing time.*

CONCLUSION

In this work the growth of carbon nanotubes by chemical vapor deposition was studied. The role of different catalyst composition was examined and it can be concluded that different catalysts create nanoparticles with different diameter and density on the surface of substrate affecting in such way the growth of carbon nanotubes. For MWCNTs the use of Al/Fe catalyst and for SWCNTs the use of Al/Ni catalyst were found as the best growth promoters. According to Raman spectroscopy the annealing time did not affect the quality of grown carbon nanotubes. On the other hand, the temperature was a significant parameter which affects their quality. As a matter of fact, different catalyst morphology (Al/Fe, Ni ratio) along with different annealing and growth temperatures need to be investigated in more details.

Acknowledgement This work was done in Center of Excellence CENAMOST (Slovak Research and Development Agency Contract No. VVCE-0049-07) and was financially supported also by grants APVV-0628-06, APVV-0548-07, SK-CZ-0139-09, LPP-0094-09, LPP-0246-06, LPP-0149-09, and VEGA 1/0807/08, 1/0857/08, 1/0746/09, 1/0390/08.

REFERENCES

[1] K. Kajiwara, S. Suzuki, Y. Matsui, H. Sato, and K. Hata, *Characterization of quasicrystalline Al-Cu-Fe nanoclusters as catalysts for the synthesis of carbon nanotubes*, Journal of Physics: Conference Series 226 (2010), p. 012008.

[2] M. Kumar and Y. Ando, *Chemical Vapor Deposition of Carbon Nanotubes: A Review on Growth Mechanism and Mass Production*, Journal of Nanoscience and Nanotechnology 10 (2010) pp. 3739-3758.

[3] Ansaldo, M. Haluska, J. Cech, J. Meyer, D. Ricci, F. Gatti, E. Dizitti, S. Cincotti, and S. Roth, *A study of the effect of different catalysts for the efficient CVD growth of carbon nanotubes on silicon substrates*, Physica E: Low-dimensional Systems and Nanostructures 37 (2007) pp. 6-10.

[4] Singh, S. Cho, K. Bartwal, N. Hoa, and H. Ryu, "Synthesis of MWNTs using Fe–Mo bimetallic catalyst by CVD method for field emission application," Solid State Communications 144 (2007), pp. 498- 502.

[5] Chiu, C. Chen, N. Tai, and C. Tsai, "Growth of high-quality single-walled carbon nanotubes through the thermal chemical vapor deposition using co-sputtering Fe–Mo films as catalysts," Surface and Coatings Technology 200 (2006), pp. 3199-3202.

[6] B.H. Choi, H. Yoo, Y.B. Kim, and J.H. Lee, *Effects of Al buffer layer on growth of highly vertically aligned carbon nanotube forests for in situ yarning*, Microelectronic Engineering 87 (2010) pp. 1500-1505.

[7] Y. Chen, J. Huang, J. Hu, C. Yang, and W. Kang, *Synthesis of single-walled carbon nanotubes produced using a three layer Al/Fe/Mo metal catalyst and their field emission properties*, Carbon 45 (2007) pp. 3007-3014

DEPOSITION OF CARBON NANO-TUBES BY MW PE CVD METHOD

O. Babchenko[1,2], M. Davydova[1,3], K. Hruška[1], A. Kromka[1]

[1]*Institute of Physics AS CR, v. v. i., Cukrovarnická 10, 162 53 Praha 6, Czech Republic*

[2]*Faculty of Nuclear Sciences and Physical Engineering, Czech Technical University in Prague, Czech Rep.*

[3] *Faculty of Civil Engineering, Czech Technical University in Prague, Czech Republic*

babcenko@fzu.cz

Abstract We investigate the influence of plasma type onto growth of carbon nanotubes from CH_4/H_2 gas mixture. Experiments were performed in the pulsed linear antenna microwave plasma system employing two different catalyst materials (Ni or Co). The observation from scanning electron microscope shows that efficient growth was achieved applying combination of microwave and radiofrequency activated plasmas.

Keywords: *carbon nanotubes CNT, microwave plasma*

INTRODUCTION

Carbon nanotubes (CNTs), as one of carbon allotropes, were firstly discovered by S. Iijima in 1991 in the form of soot [1]. The nanotubes are tubular structures with one or several walls (graphene sheets) composed from sp^2 hybridized carbon atoms. Interest to those structures is attracted due to possible wide-range applications such as: hydrogen storage, scanning tunneling microscope tip, atomic force microscope probe, electronic transistor, electrical field emitter of flat panel display, composite materials with enhanced electrical conductivity, mechanical strength, etc [2, 3].

Since nanotubes were discovered, a large number of researches have intensively investigated ways of their synthesis by various processes. Carbon nanotubes are typically grown by catalyst-supported chemical vapor deposition (CVD) process. Iron, cobalt, nickel or their derivatives are the most often used as the catalyst [2, 3].

Recently we have reported synthesis of CNTs by focused microwave plasma reactor with ellipsoidal cavity [4] or by pulsed linear antenna microwave system [5, 6].

In the present study we report on the synthesis of CNTs employing the large area CVD plasma system with two linear antennas. We compare the influence of different types of plasma discharge, i.e. microwaves (MW), radiofrequency (RF) and their combination (RF/MW), on the CNTs synthesis. Finally, we compare the CNTs growth by using two types of catalyst material (Ni or Co).

EXPERIMENTAL PART

As substrates, 550 µm thick Si (100) wafers with 1.5 µm SiO_2 layer on the smooth side and in size 1x1 cm^2 were used. Prior to CNTs synthesis, substrates were coated with 3 nm thick catalyst layer (Ni or Co) by thermal evaporation. Next, samples were annealed in linear antenna CVD system by hydrogen plasma ignited at following conditions: microwave power 2500 W with on/off pulse cycle 6/3 ms, at pressure 0.2 mbar maintained by 300 sccm H_2 flow for the 10 min. The heater temperature during this process was 600°C. The annealing results in a fragmentation of continuous metal film into nanoislands, as shown in our previous studies [4, 5, 7].

After the annealing, the CNTs growth stage followed. The nanotubes were synthesized for 30 min from methane-in-hydrogen gas mixture (30% of CH_4 in H_2) maintained at pressure 0.2 mbar. The plasma discharge was initiated by a) RF generator at power 600 W and bias 500 V, or by b) MW generator at power 2000 W with on/off pulse cycle 6/3 ms, or by c) their combination (MW+RF). The heater temperature during the process was 600°C. In the second series of experiments, i.e. comparing Ni and Co catalyst, the MW process power was reduced to 1700 W.

After the deposition, all samples were investigated by the scanning electron microscope (SEM, e_LiNE writer, Raith, GmbH).

RESULTS AND DISCUSSION

As has been shown in our previous work, annealing of the catalyst layer by MW plasma resulted into a formation of nanoislands (nanoparticles) in sizes 20-30 nm (not shown here). These nano-sized features are required to grow the CNTs. SEM images of as-grown structures are shown in Figure 1. Samples processed in the microwave plasma reveal only isolated catalyst nano-islands, which are similar to annealed layer. No sign of CNTs growth is observed (Fig. 1a). The CVD process using the RF plasma results in poor carbon nanotubes formation (Fig. 1b). Finally, in the case of combined RF and MW plasma we observed densely packed and vertically oriented nanotubes with diameter in the range of 20-30 nm (Fig. 1c).

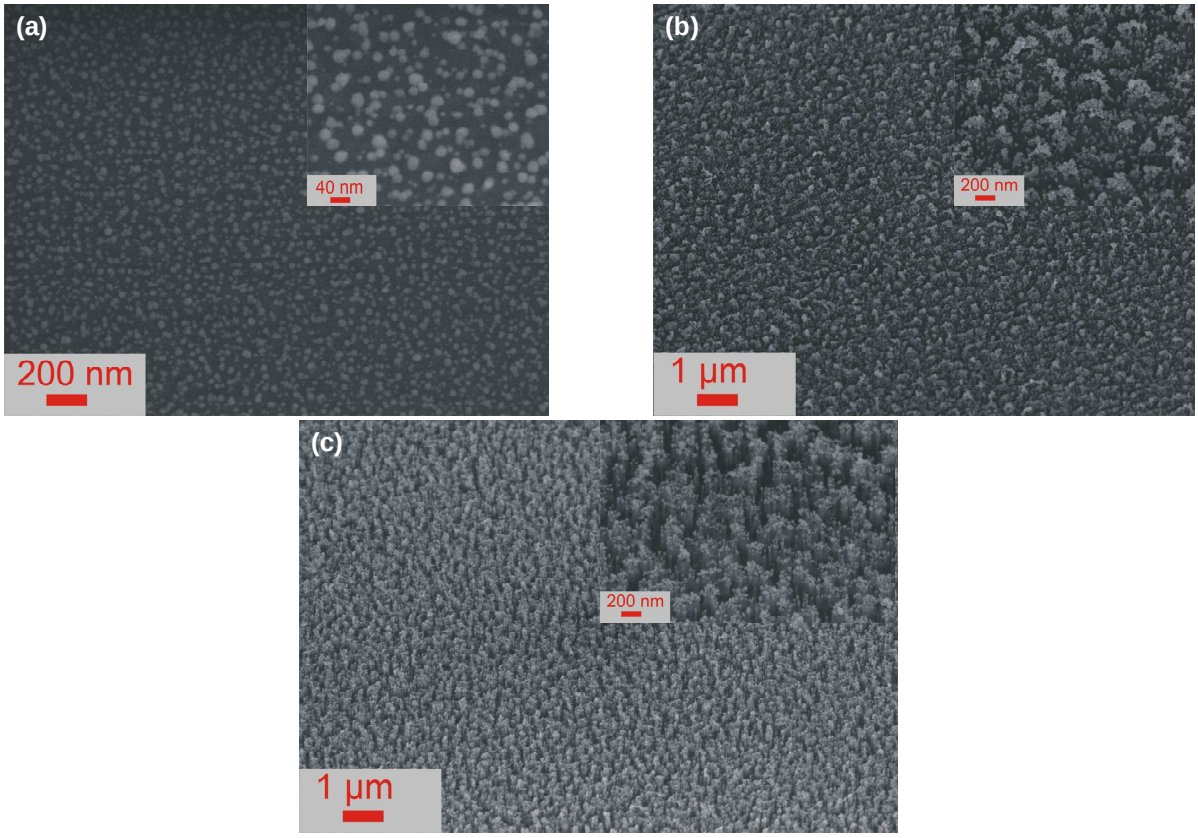

Figure 1. *SEM images of CNTs grown by CVD method where plasma discharge was ignited employing (a) microwaves (MW), (b) radiofrequency waves (RF), and (c) combined MW and RF plasma.*

We propose that in the case of using only MW plasma, despite known evidence of decomposition the CH_4, there is lack of formation growth species transported to the substrate. On the other hand, using the RF plasma intends an efficient flow of species to the growth surfaces, but in the same time the growth species are not found as optimal for proper growth of CNTs. Nevertheless, the efficient growth of nanotubes by RF plasma systems using the same gas mixture is achievable at higher substrate temperatures [2, 3]. As observed in Fig. 1c, the synthesis of CNTs in the linear antenna system requires employing of both plasmas. In this combined arrangement, microwave energy effectively decomposes working gases to growth species and RF helps to drive these species to the substrate surface where the synthesis reactions take place. Thus CNTs are formed vertically aligned in the direction of electric field.

Growth of CNTs using either Ni or Co catalyst is summarized in Fig. 2. CNTs synthesized from Ni catalyst seem to be denser and easily distinguished from each other. The diameter of carbon nanotubes follows the primary catalyst nanoparticles (20-30 nm). Carbon structures grown from the

Co catalyst are found in island-like forms with a conical shape. Here the diameter of nanostructures seems to be smaller (effect of material). The origin for this observation is not fully clear and is under study.

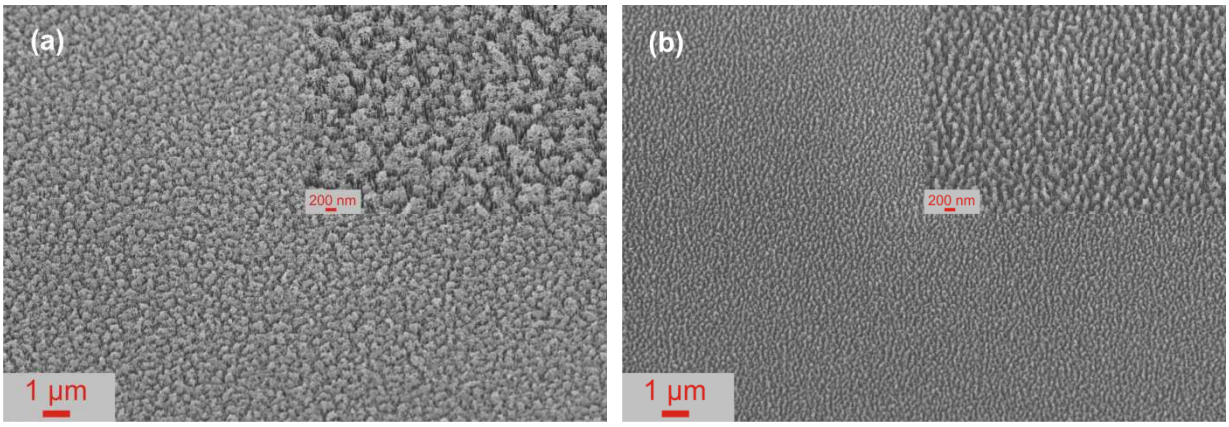

Figure 2. *SEM images of CNTs grown by combined MW and RF plasma CVD method using: (a) Ni or (b) Co as the catalyst.*

CONCLUSIONS

The carbon nanotubes were grown in the pulsed linear antenna microwave plasma system from CH_4/H_2 gas mixture. We observed that for the used deposition apparatus, the applying of only MW or RF plasma was not enough effective to form well ordered CNTs. Employing the combined MW and RF plasma, and using Ni as catalyst, resulted in growth of nanotubes 20-30 nm in diameters. Using of Co as the catalyst material, resulted in formation compressed-like structures which consisted of nanostructures with diameter below 20 nm. These results open new vistas for deposition of CNTs on areas as large as $1x1m^2$. The further work on characterization of formed carbon nanostructures is in progress.

Acknowledgement This work was supported by the grants KAN400100701, MEB0810082, SGS10/125/OHK1/2T/11 and Purkyne Fellowship.

REFERENCES

[1] S. Iijima: *Helical microtubules of graphitic carbon*, Nature 354 (1991) pp. 56-58.

[2] S.B. Sinnott, R. Andrews: *Carbon nanotubes: synthesis, properties, and applications*, Critical Reviews in Solid State and Material Sciences 26 (2001) pp.145-249.

[3] A.V. Melechko, V.I. Merkulov, T.E. McKnight, M.A. Guillorn, K.L. Klein, D.H. Lowndes, M.L. Simpson: *Vertically aligned carbon nanofibers and related structures: Controlled synthesis and directed assembly*, J. Appl. Phys. 97 (2005) 041301.

[4] O. Babchenko, A. Kromka, J. Potmesil, K. Hruska, M. Vanecek: *Growth of carbon nanotubes by microwave plasma in ellipsoidal-cavity reactor*, Proceedings of the 14-th International Conference on Applied Physics of Condensed Matter, June 25-27, 2008, KRU Bystrá, Liptovsky Ján, Slovak Republic, ISBN 978-80-227-2902-4, pp. 19-23.

[5] A. Kromka, O. Babchenko, T. Izak, M. Davydova, S. Potocký, and B. Rezek: *Growth of diamond films and carbon nanotubes over large areas by linear antenna microwave plasma CVD deposition*, Proceedings of the 20th Joint Seminar Development of Materials Science in Research and Education, Eds. K. Nitsch, Z. Kožíšek, September 1 - 3, 2010, Bořetice, pp. 33-34, ISBN 978-80-254-7237-8.

[6] A. Kromka, O. Babchenko, T. Ižák, Š. Potocký, M. Davydova, N. Neykova, H. Kozak, Z. Remeš, K. Hruška, B. Rezek: *Pulsed linear antenna microwave plasma – a step ahead in large area material depositions and surface functionalization*, NANOCON 2011, Conference Proceedings, 3rd International Conference, September 21-23, 2011, Hotel Voronez, Brno, Czech Republic, ISBN 978-80-87294-23-9

[7] O. Babchenko, A. Kromka, K. Hruska, M. Michalka, J. Potmesil, M. Vanecek: *Nanostructuring of diamond films using self-assembled nanoparticles*, Cent. Eur. J. Phys. 7 (2009) pp. 310-314.

INFLUENCE OF METHANE CONCENTRATION ON DIAMOND FILM MORPHOLOGY AND GROWTH RATE

T. Ižák[a,b], A. Kromka[a], J. Potměšil[a] and K. Hruška[a]

[a]*Institute of Physics AS CR, v. v. i., Cukrovarnická 10, 162 53 Praha 6, Czech Republic*

[b]*Department of Microelectronics, FEI STU, Ilkovičova 3, 812 19 Bratislava, Slovak Republic*

izak@fzu.cz

Abstract In this study we investigated the influence of methane concentration on the diamond film growth. The experiments were carried out in focused microwave chemical vapour deposition system. The methane concentration was varied from 0.5% to 10 % of CH_4 in H_2 atmosphere. The final film morphology, chemical composition and growth rate were investigated by scanning electron microscopy (SEM), Raman spectroscopy and optical reflectance measurement. We observed, that increasing of CH_4 concentration enhances the growth rate, but at the expense of the diamond film quality.

Keywords: microcrystalline, nanocrystalline diamond, methane concentration, SEM, Raman

INTRODUCTION

Growth of diamond films by chemical vapour deposition have been intensively investigated during the past two decades. The basic growth chemistry is based on the low methane concentration (1-2%) diluted in H_2 gas system and the growth is realized commonly at high process temperatures. The role of hydrogen is etching of non-diamond carbon species; further the creation of new surface sites and enhancing the insertion of adsorbed hydrocarbon species into the diamond lattice. In general, the morphology (crystal size, roughness) combined with such intrinsic properties as transparency, conductivity, etc. of diamond films is important parameter for a variety of applications. The film morphology and physical properties could be changed by varying of deposition conditions, e.g. by addition of different gases (argon, nitrogen, boron, halogens, oxygen containing gases, etc.), by applying the negative substrate bias, ion bombardment, or by changing the process pressure and growth temperature [1-2]. The simplest way to change the surface morphology is the variation of CH_4/H_2 ratio. It is well-know that increasing of methane content in the gas mixture leads to the enhanced growth rates, but at the expense of the diamond film quality [3]. Higher CH_4 content means more carbon species and hydrocarbon radicals, and therefore more sp^2 graphitic phases. From earlier studies it was confirmed that usually ≥20% of CH_4 in H_2 resulted in amorphous carbon film with a low content of sp^3 diamond bonds [4]. It was also observed that at very low methane concentrations (<1% or 0.25% of CH_4 in H_2) dominates etching instead of growth process [5]. It is caused by not sufficient amount of carbon source and by dominance of hydrogen atoms.

As useful method, methane variation was used by A. Kriele et al. for fabrication of nano-porous diamond materials as membranes used as filter applications [6]. By variation of methane they changed the film morphology from micro- to nanocrystalline and using suitable annealing they burned out the sp^2 amorphous carbon phases from grain boundaries.

In this study we have investigated the influence of methane concentration on diamond films morphology and growth rate by focused microwave plasma chemical vapour deposition (FMWP) system.

EXPERIMENTAL PART

The substrates (p-type Si with sizes 10x10 mm^2) were cleaned by isopropyl alcohol for 15 min in ultrasound bath, then washed in DI water, dried by nitrogen flow, and finally ultrasonically pre-treated in suspension of DI water and ultradispersed detonation diamond powder in diameter 5-10 nm. During diamond deposition the process time was kept constant (1 hour), only the concentration of CH_4 was changed from 0.5% to 10% in H_2 atmosphere. The other process conditions were the same: microwave power 2500 W, total gas pressure 50 mbar, temperature ~750°C, and hydrogen flow rate 300 sccm.

Next, based on our results from first set of experiments, we performed depositions at low (1%) and high (5%) methane concentration. The aim was obtain same film thicknesses in order to better comparison and characterization of the methane influence. Regarding to growth rate the process time was 5h for low and 2h 51 min for high CH_4 concentration, respectively. The other conditions were the same as in the previous set (pressure 50 mbar, microwave power 2500 W, temperature ~750°C, hydrogen flow rate 300 sccm).

The surface morphology of diamond films was analysed by Scanning Electron Microscopy (SEM, e_LiNE writer, Raith GmbH) and the chemical composition was investigated by Raman Spectroscopy (Renishaw In Via Reflex Raman spectrometer, excitation wavelength of 325 nm). The film thickness was evaluated from optical reflectance measurements [7].

RESULTS AND DISCUSSION

Influence of methane – the same deposition time

Fig. 1 shows SEM images of diamond films deposited at different methane concentration. In this case all samples had the same deposition time (1 hour). For the lowest methane concentration (0.5%) the surface morphology reveals small and homogeneous diamond crystals with size 90÷130 nm. With increasing of CH_4 concentration appears bigger crystals up to ~200 nm in diameter at 5% CH_4. We suppose that the increasing of diamond crystals size is due to increased growth rates from 164 nm/h at 0.5% of CH_4 to 360 nm/h at 5% of CH_4 respectively (Fig. 3). Moreover, at higher methane concentration the crystal size distribution is not as homogeneous as at 0.5% of CH_4 - besides larger crystals appear smaller crystals. With further increasing of CH_4 (up to 10%) the surface morphology is getting to nanocrystalline-type with enhanced content of sp^2 carbon bonds. This was confirmed also by Raman spectroscopy as discussed below.

Fig. 2a shows Raman spectra of samples normalized to diamond peak at 1332 cm^{-1}. Beside diamond peak Raman spectra consist of broad G-band (graphite-band) at 1580 cm^{-1} characteristic for sp^2 carbon bonds, and a peak at 1150 cm^{-1} which corresponds to trans-polyacetylene groups. At higher methane concentration (>3% of CH_4) appears also the D-band at 1350 cm^{-1}, which is induced by disordered carbon atoms. Increasing of methane concentration causes broadening and enhancing of D-band together with G-band. That observation is in a good agreement with SEM images, and is related to higher presence of sp^2 carbon bonds in diamond films.

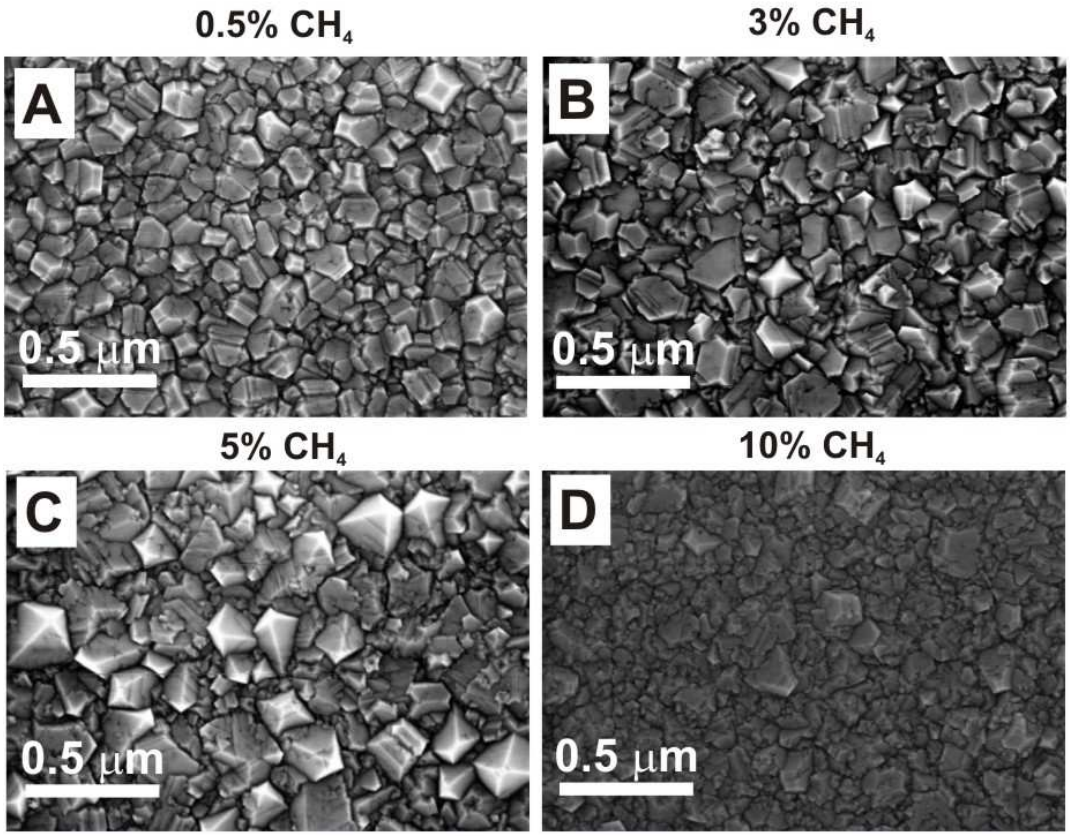

Figure 1 *SEM images of samples deposited at different methane concentration: a.) 0.5%, b.) 3%, c.) 5% and d.) 10% of CH_4 in H_2 gas system*

Further, the film quality was determined by calculation of diamond (sp^3) to non-diamond (sp^2) content. As first, Raman spectra of the samples were fitted in OriginLab software. Then the ratio of sp^3/sp^2 was calculated by dividing the diamond-peak area (A_{diam}) by sum of the other peaks areas (A_D+A_G). The calculated diamond/non-diamond ratio decreases with increasing methane concentration (Fig. 2b). Its value drops from an initial value 18 (0.5% CH_4) to 4 (10% CH_4).

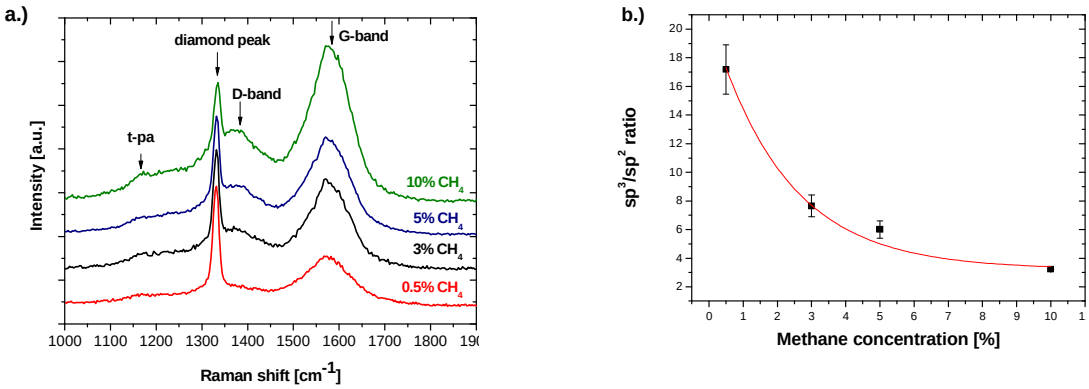

Figure 2 *Raman spectra of samples deposited at different methane concentration normalized to 1332 cm^{-1} diamond peak (a) and diamond to non-diamond ratio as a function of methane concentration (b)*

As we mentioned above, the increased methane content enhance the growth rate of diamond film. We observed that from 0.5% to 5% of CH_4 concentration the growth rate nearly linearly increased, while at 10% of CH_4 there is only a small enhancement. The growth rate increasing with increased methane concentration is due to higher amount of CH_3 radicals which act at the growth surface reactions. At the highest methane concentration appears a saturation of those CH_3 radicals, and that leads to decreasing of nanocrystalline diamond film growth rate.

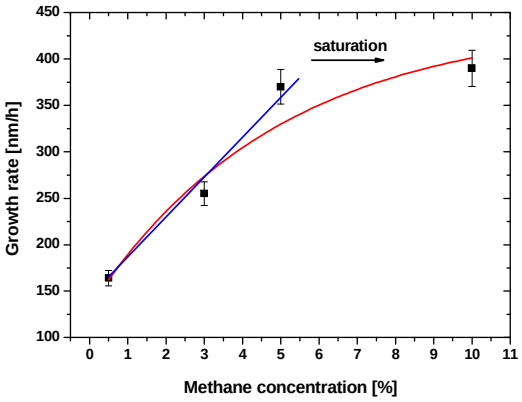

Fig. 3 *Growth rate as a function of methane concentration*

Influence of methane – the same film thickness

Based on previously results, long-time deposition were carried out at low (1%) and high (5%) methane concentration for better comparison of methane influence (i.e. for getting more obvious differences between the samples). The process time for each deposition were calculated from previously results in order to achieve the same film thicknesses. The measured film thickness was evaluated to 1180 nm and 1197 nm for 1% and 5% of CH_4, respectively. The surface morphology of samples is shown in Fig. 4. In the case of the low CH_4 concentration the diamond film consists of homogeneous diamond layer with crystals in diameter 100-400 nm, while for high CH_4 concentration the diamond film shows nanocrystalline character: beside larger non-uniformly situated diamond crystals dominates very fine granular structures. Raman spectroscopy with excitation wavelength 325 nm confirmed the micro- and nanocrystalline character of the diamond films (Fig. 4c). The origin for this film character could be assigned to high secondary nucleation during the CVD growth.

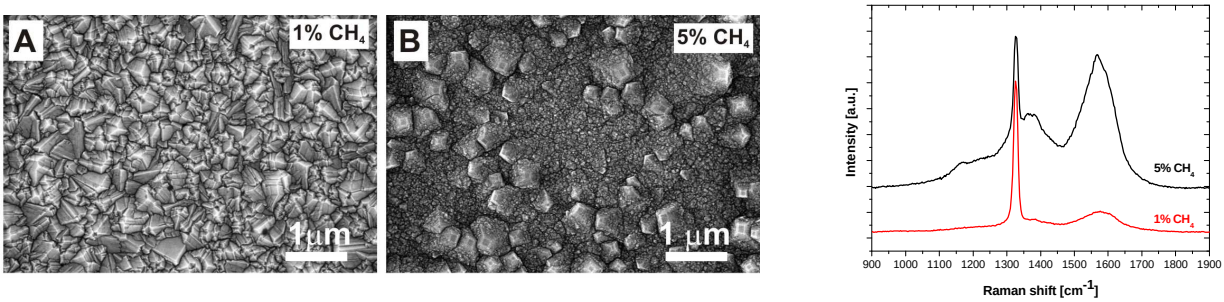

Fig. 4 *SEM images of diamond layers deposited at low (1%) and high (5%) methane concentration (left) and Raman spectra of samples normalized to 1332 cm^{-1} diamond peak (right)*

CONCLUSION

We have investigated the influence of methane concentration on diamond film morphology and growth process. The experiments were carried out in focused microwave plasma chemical vapour deposition system. The methane concentration varied from 0.5% to 10 % of CH_4 in H_2 atmosphere. As first, the film morphology, chemical composition and growth rate was investigated at the constant process time (1 hour). In the second case, long time deposition was performed at 1% and 5% of CH_4 in H_2 atmosphere in order to get better evaluation of the methane influence. In this case, the film thicknesses were the same (~ 1.2 μm), only the process time was varied.

We observed that increasing of CH_4 concentration in H_2 gas system leads to change the film morphology from high quality diamond layer to nanocrystalline character with smaller crystal sizes

and enhanced amount of sp^2 carbon bonds (amorphous carbon phases). In addition, increasing of methane concentration resulted in enhanced growth rates. The growth rate linearly increased from 160 nm/h to 360 nm/h for 0.5 to 5% of CH_4, respectively. Further increase of CH_4 had minimal influence of growth rate due to saturation of hydrocarbons.

Acknowledgements *This work was supported by the grants KAN400100701, IAAX00100902, MEB0810081, MEB0810082, and Purkyne Fellowship. We would like to gratefully appreciate O. Rezek for technical support and M. Varga for optical measurements of thicknesses.*

REFERENCES

[1] M. Marton, T. Izak, M. Vesely, M. Vojs, M. Michalka, J. Bruncko, *Effect of argon and substrate bias on diamond thin film surface morphology,* Vacuum 82 (2007) pp. 154-157

[2] T. Izak, O. Babchenko, A. Kromka, S. Potocky, *From micro- to nanocrystalline diamond films*, in *Proceedings of School of Vacuum Tech.- Vacuum and Advanced Materials*, Strbske Pleso, 8-11. Sept 2011, ISBN 978-80-969435-9-3

[3] X. Li, J. Perkins, R. Collazo, R. J. Nemanich, Z. Sitar, *Investigation of the effect of the total pressure and methane concentration on the growth rate and quality of diamond thin films grown by MPCVD*, Diamond & Related Materials 15 (2006) pp. 1784–1788

[4] Q. Yang, S. Yang, Y.S. Li, X.Lu, A. Hirose, *NEXAFS characterization of nanocrystalline diamond thin films synthesized with high methane concentrations*, Diamond & Related Materials 16 (2007) pp. 730–734

[5] H. Sternschulte, T. Bauer, M. Schreck, B. Stritzker, Comparison of MWPCVD diamond growth at low and high process gas pressures, Diamond & Related Materials 15 (2006) pp. 542–547

[6] Kriele, O. A. Williams, M. Wolfer, J. J. Hees, W. Smirnov, Ch. E. Nebel, *Formation of nano-pores in nano-crystalline diamond films*, Chemical Physics Letters 507 (2011) 253–259

[7] Z. Remes, H. Kozak, O. Babchenko, S. Potocky, E. Ukraintsev, B. Rezek, A. Kromka, *Grazing angle reflectance spectroscopy of organic monolayers on nanocrystalline diamond films*, Diam. Rel. Mat. 20 (2011) pp. 882-885

INFLUENCE OF CO_2 CONCENTRATION ON DIAMOND FILM MORPHOLOGY IN PULSED LINEAR ANTENNA MW CVD SYSTEM

M. Domonkos[a,b], T. Ižák[a,c], O. Babchenko[a], A. Kromka[a] and K. Hruška[a]

[a]*Institute of Physics AS CR, v. v. i., Cukrovarnická 10, 162 53 Praha 6, Czech Republic*

[b]*Faculty of Nuclear Sciences and Physical Engineering, Czech Technical University in Prague, Czech Rep.*

[C]*Department of Microelectronics, FEI STU, Ilkovičova 3, 812 19 Bratislava, Slovak Republic*

domonkos@fzu.cz

Abstract The diamond films were deposited in a pulsed linear antenna microwave plasma system. The influence of CO_2 addition into the standard CH_4/H_2 gas mixture on the diamond film morphology was investigated. The concentration of CO_2 varied from 0% up to 80% in $CO_2/CH_4/H_2$ gas mixture. The film morphology, the growth rate and the ratio of sp^3/sp^2 carbon bonds were investigated. It was found that increasing of CO_2 concentration resulted in enhanced growth rate (from 20 up to 36 nm/h). However, at very high CO_2 concentrations (>40%) dominates etching instead of growth process. Moreover, we found that increasing of CO_2 enhances the diamond film quality.

Keywords: nanocrystalline diamond, large area growth, growth rate, CO_2 addition, SEM, Raman Spectroscopy

INTRODUCTION

CVD diamond deposition is commonly carried out in CH_4/H_2 gas system with 1-2% of CH_4. In such gas system dominates CH_3 radicals, which acts at the diamond growth surface reactions. Activation energy is one of the important parameters that characterized the surface chemistry and growth process. The activation energy in common CH_4/H_2 systems is about 22-30 kcal/mol [1]. It was shown that by addition of other gases (halogens, oxygen containing gases, argon, nitrogen) the activation energy decreases, its mean less energy is needed to diamond formation [2-4]. Moreover, decreasing of activation energy predetermines diamond films growth at much lower temperatures, then in standard deposition processes (800-900°C)

Theoretical studies showed that the addition of oxygen to the reaction gases (e.g. CO, CO_2, O_2 or alcohol) enhances the growth rate and extends the region of diamond formation in Bachmann-Leers-Lvdtin model [5]. One explanation is that during the process OH groups are formed and removes the non-diamond carbon at a rate comparable to that of diamond growth [6]. The mentioned low temperature diamond growth (LTDG) is possible because oxygen at lower temperature has stronger preferential etching behaviours than hydrogen. Another possible explanation about the role of atomic oxygen is the effective abstraction of surface hydrogen [7].

In our experiments we added CO_2 addition into standard CH_4/H_2 gas mixture in order to enhance the growth rate. We chose CO_2 gas because it was shown that CO_2 addition decreases the activation energy from 22-30 kcal/mol to 7 kcal/mol [3]. In our parallel studies we also obtained activation energy about 3-6 kcal/mol in pulsed linear antenna microwave plasma (PLAMWP) chemical vapour deposition (CVD) system depending on microwave power (not published yet).The influence of CO_2 concentration on diamond film morphology, sp^3/sp^2 carbon bonds and growth rate are discussed.

EXPERIMENTAL PART

As substrates p-type Si (with sizes 10x10 mm^2) and AF glass (1x3 $inch^2$) were used. The substrates were treated by standard cleaning process: 15 min in isopropyl alcohol and ultrasound bath, washing in DI water, cleaning by pure nitrogen flow and finally ultrasonically nucleated in

suspension of DI water and ultradisperzed detonation diamond powder in diameter 5-10 nm. Diamond deposition was carried out in a pulsed linear antenna microwave plasma (PLAMWP) CVD system [8]. The common experimental conditions were as follows: pulsed microwave power 2x2500 W, total gas pressure 0.2 mbar, temperature ~720°C (measured by pyrometer), process time 15h, the distance of substrates from the antennas was 8 cm, and gas composition 2.5% of CH_4. The CO_2 concentration was varied from 0% to 80% in CH_4/H_2.

The surface morphology of diamond films was analysed by Scanning Electron Microscopy (SEM, e_LiNE writer, Raith GmbH) and the sp^3/sp^2 carbon ratio was investigated by Raman Spectroscopy (Renishaw In Via Reflex Raman spectrometer with excitation wavelength 325 nm). The film thickness was evaluated from optical reflectance measurements [9].

RESULTS AND DISCUSSION

Fig. 1 shows optical view of layers grown on 1”x3” AF glass substrates. On samples deposited with ≤20% of CO_2 we observed light interferences which is caused by thin diamond layer. Samples deposited with higher CO_2 concentrations (≥40%) show only white or transparent characteristic. This observation actually does not mean that the substrates are without diamond layer, because thin high quality diamond layers could be transparent in visible lights.

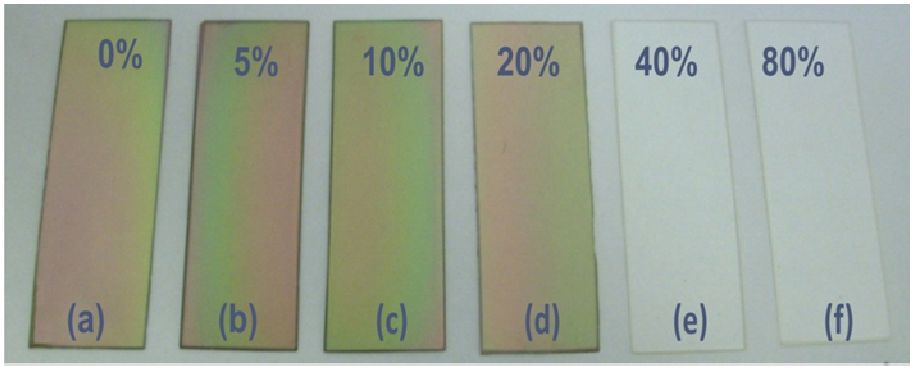

Figure 1 *Optical view of diamond layers deposited on AF glass substrates prepared at different CO_2 concentrations in CH_4/H_2 gas system*

Much more information of film quality is found from SEM images. Fig. 2 and 3 show surface morphology of diamond films deposited on Si substrates and on the AF glass, respectively. The morphology of grown films is nearly the same on the Si substrates and AF glasses. Small differences are observed only on samples deposited with higher CO_2 concentration (≥40%): Si substrates show clean surface, while on the AF glasses are detected small clusters (Fig. 3e), probably amorphous carbon species. That difference can be caused by different material properties of Si and AF glass: by thermal management, by low softening temperature of glass or by higher surface reactivity on the AF glass than on the Si substrates. Otherwise, it was proven, that at very high CO_2 concentration (≥40%) the CVD process is dominated by etching instead of growth process on both Si and AF glass substrates. Without CO_2 addition the diamond film features by ultra-nanocrystalline (UNCD) character with very fine granular structures. Raman spectroscopy confirmed UNCD character of the film (Fig. 4). Further increasing of CO_2 led to increasing the crystal sizes and the amount of sp^3 diamond bonds, hence this led to improving the quality of diamond films. That was reflected also in increasing diamond peak in Raman spectra.

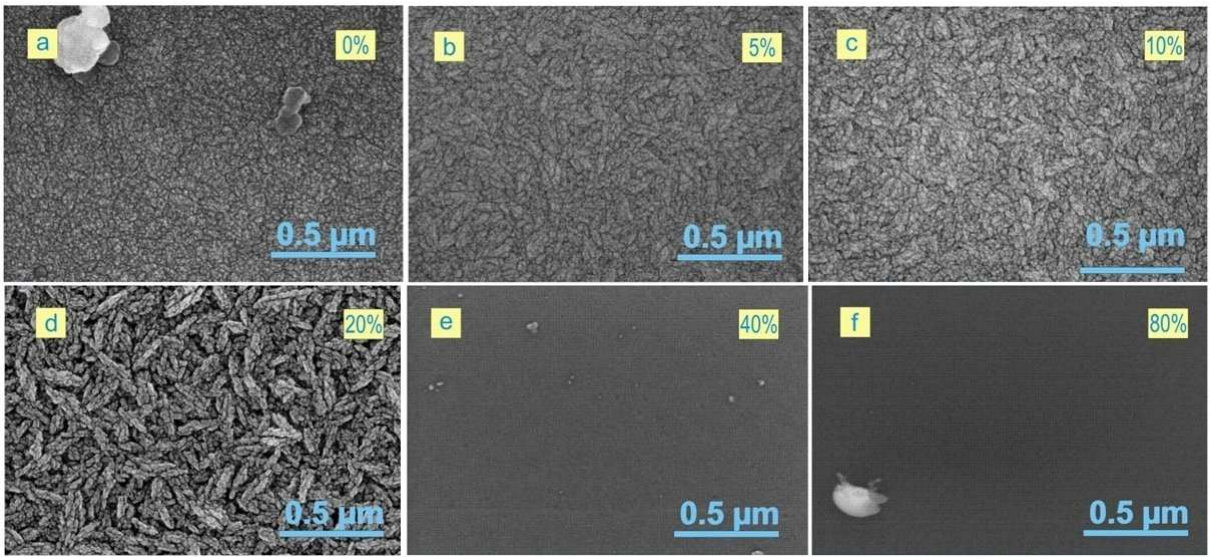

Figure 2 *SEM images of samples on Si substrates deposited at a) 0 %, b) 5 %, c) 10 %, d) 20 %, e) 40 % a f) 80 % of CO_2 in $CO_2/CH_4/H_2$ gas mixture (magnification is* 60 000x)

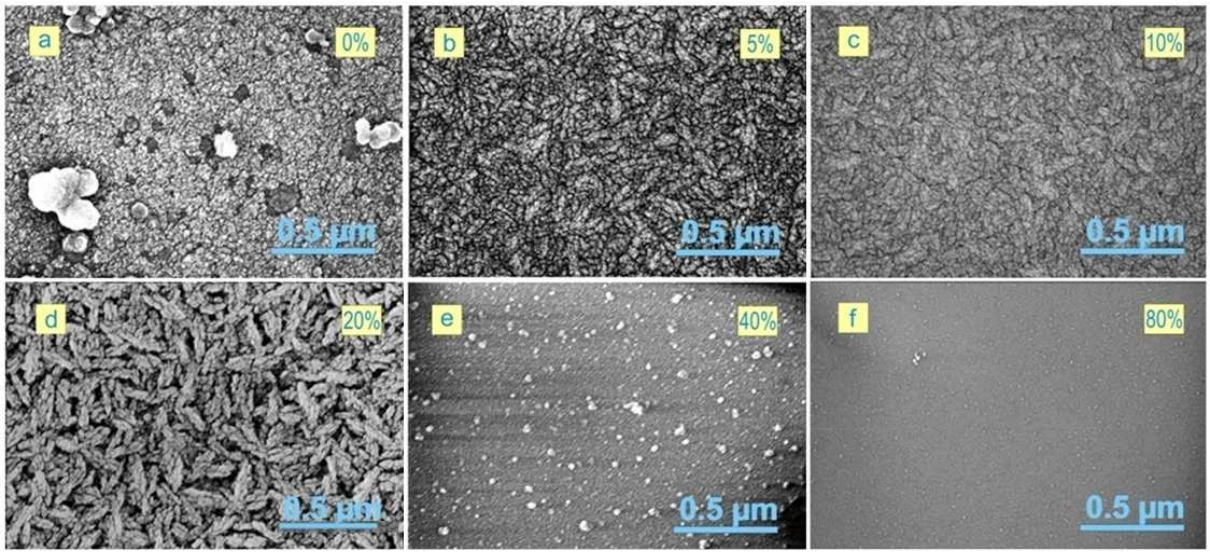

Figure 3 *SEM images of samples on AF glass substrates deposited at a) 0 %, b) 5 %, c) 10 %, d) 20 %, e) 40 % a f) 80 % of CO_2 in $CO_2/CH_4/H_2$ gas mixture (magnification is* 60 000x)

Beside the sharp diamond peak at 1332 cm^{-1}, which is related to sp^3 diamond bonds, Raman spectra are dominated by broad G-band (graphite-band at 1590cm^{-1}) and D-band (disordered- or defect-related graphite-band at 1350 cm^{-1}). G-band and D-band are known to be related to sp^2 amorphous carbon bonds and graphitic phases. Moreover, there is a peak at 1163 cm^{-1}, which is often attributed to trans-polyacetylene groups and characterizes indirectly the amount of hydrogen atoms in the film [10]. The Raman spectra of the samples deposited at higher CO_2 concentrations (≥40%) do not show any peaks except of sharp peak at 520 cm^{-1} related to Si substrate. Similar Raman spectra were measured on the samples with AF glass substrates (not shown here).

The film thicknesses were evaluated by optical reflectance measurements [9]. From thicknesses we calculated the growth rates for individual diamond layers (Fig. 4b). We observed that

by increasing of CO_2 concentration in gas system the growth rate increases from 20 nm/h to 36 nm/h (almost two times). It is caused by changed surface chemistry due to oxygen atoms as we mentioned earlier. The highest growth rate was measured for 5-10% of CO_2. By further increasing of CO_2 the growth rate decreases, and over 40% of CO_2 already dominates etching process.

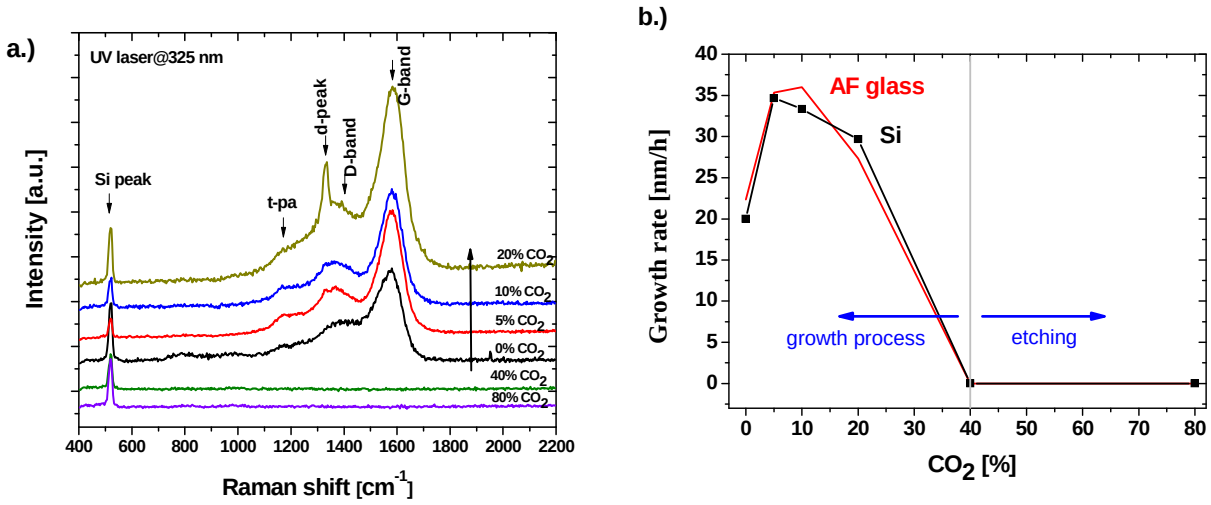

Figure 4 *Raman spectra of samples deposited on Si substrates (a) and the growth rate as a function of CO_2 concentration (b)*

Further experiments with CO_2 addition into the gas mixture showed that 10% of CO_2 added to the 2.5% CH_4 in H_2 resulted in high quality diamond layer with large diamond crystals (up to 430 nm) [8]. We suppose that the observed morphologies of NCD layers (published in this article) are caused by leakage, i.e. by air inlet into the reaction chamber. Further analysis of the diamond films composition is needed. On other hand, that observation not influences the fact, that with CO_2 addition increases the growth rate and at very high CO_2 concentrations (≥40%) dominates etching effect instead of growth process. The leakage was caused by not appropriate isolation of the quartz antennas from O-rings (high reflection of microwaves caused thermal degradation of teflon O-rings). The failure was removed and the deposition system was technically upgraded.

CONCLUSION

In this article the influence of CO_2 on diamond film morphology and growth process in pulsed linear antenna microwave plasma CVD system was studied. The concentration of CO_2 varied from 0% up to 80% in CH_4/H_2 gas mixture. It was found that increasing of CO_2 concentration resulted in enhanced growth rate from 20 nm/h to 36 nm/h up to 20% of CO_2. At further increasing of CO_2 (>40%) the CVD process is dominated by the etching instead of growth process. In addition, we found that increasing of CO_2 not only enhances the growth rates, but also improves the diamond films quality by etching of non-diamond carbon phases with oxygen. Repeated experiments showed that already 10% of CO_2 resulted in high quality diamond film with large crystal sizes (up to 430 nm). It means that the formation of NCD layers in our first early experiments was influenced by leakage/air inlet into reaction chamber. After removing the construction problem, on the CVD system technical upgrade was done.

Acknowledgements This work was supported by the grants KAN400100701, IAAX00100902, MEB0810081, MEB0810082, and Purkyne Fellowship. We would like to gratefully appreciate J. Potmesil and O. Rezek for technical support.

REFERENCES

[1] X. Xiao, J. Birrell, J. E. Gerbi, O. Auciello, J. A. Carlisle, *Low temperature growth of ultrananocrystalline diamond*, J. Appl. Phys. 96 (2004) pp. 2232–2239

[2] E. J. Corat, R. C. Mendes de Barros, V. J. Trava-Airoldi, N. G. Ferreira, N. F. Leite, K. Iha, *The activation energy for diamond growth from mixtures in a hot-filament reactor,* Diamond and Related Materials 6 (1997) pp. 1172- 1181

[3] J. R. Petherbridge, P. W. May, S. R. J. Pearce, K. N. Rosser, and M. N. R. Ashfold, *Low temperature diamond growth using CO2/CH4 plasmas: Molecular beam mass spectrometry and computer simulation investigations*, J. Appl. Phys. 89 (2001) pp. 1484-1492

[4] J. Lee, B. Hong, R. Messier, R. W. Collins, *Real time spectroellipsometry for optimization of diamond film growth by microwave plasma-enhanced chemical vapor deposition from CO/H-2 mixtures*, J. Appl. Phys. 80 (1996) pp. 6489–6495

[5] Y. Liou, A. Inspektor, R. Weimer, D. Knight, R. Messier, *Effect of oxygen in diamond deposition by microwave plasma enhanced chemical vapor deposition,* J. Mater. Res. 5 (1990) pp. 2305-2312

[6] S. T. Lee, Z. Lin, X. Jiang, *Quantitative analysis of polyvinyl alcohol on the surface of poly(D,L-lactide-co-glycolide) microparticles prepared by solvent evaporation method: Effect of particle size and PVA concentration*, Materials Science and Engineering, 25 (1999) pp. 123-154

[7] B. Sun, X. Zhang, Q. Zhang, Z. Lin, *Effect of atomic hydrogen and oxygen on diamond growth*, J. Appl. Phys. 73(9) (1993) pp. 4614-4617

[8] A Kromka, O.Babchenko, T. Izak, K. Hruska, B. Rezek, *Linear antenna microwave plasma CVD deposition of diamond films over large areas*, Vacuum xxx (2011) 1-4, article in press, doi:10.1016/j.vacuum.2011.07.008

[9] Z. Remes, H. Kozak, O. Babchenko, S. Potocky, E. Ukraintsev, B. Rezek, A. Kromka, *Grazing angle reflectance spectroscopy of organic monolayers on nanocrystalline diamond films*, Diam. Rel. Mat. 20 (2011) pp. 882–885

[10] H. Kuzmany, R. Pfeiffer, N. Salk, B.Gunther, *The mystery of the 1140 cm−1 Raman line in nanocrystalline diamond films*, Carbon 42 (2004) pp. 911–917

DIAMOND THIN FILM DEVELOPMENT AND ANALYSIS ON VARIOUS SUBSTRATES

Andrej Vincze[1,2], Pavol Michniak, Daniel Haško[1,2],Miroslav Michalka[1,2], Marián Varga[2,3], Edmund Dobročka[4]

[1] *International Laser Centre, Ilkovičova 3, 841 04 Bratislava, Slovakia,*

[2] *Institute of Photonics and Electronics, STU, Ilkovičova 3, 812 19 Bratislava, Slovakia*

[3] *Institute of Physics AS CR, v. v. i., Cukrovarnická 10, 162 53 Praha 6, Czech Republic*

[4] *Institute of Electrical Engineering SAS, Dúbavská cesta 9, 841 01 Bratislava, Slovak Republic*

vincze@ilc.sk

Abstract The contribution shows the possibilities of the diamond growth on various substrates. The thin film samples were prepared using hot filament CVD. The analysis of the diamond coatings were done by various methods. SEM, XRD, Raman spectrometry and SIMS were done in order to characterize the samples. The results of the diamond thin films are discussed.

Keywords: diamond thin films, hot filament CVD, SIMS, SEM, XRD, Raman spectroscopy

INTRODUCTION

Diamond is known as a material with superlative physical qualities, superlative properties of hardness, highest room temperature thermal conductivity, etc., most of which originate from the strong covalent bonding between its atoms. Except for the natural diamonds as gemstones also the artificial ones have similar properties. Those properties determine the major industrial application of diamond in cutting and polishing tools. Because of its extremely rigid lattice, fig. 1, it can be contaminated by very few types of impurities and thus the optical properties are remarkable. Combined with wide transparency, this results in the clear, colorless appearance of most natural diamonds. The diamond thin films are very useful for many applications, maybe the biological one [1] is the most attractive in these days. The superior properties like biocompatibility, homogeneity, chemical inertness, reproducibility, considerably low background current, predestinate the diamond thin films for in vivo electronic applications as well as a transducer material for biofunctionalization and biosensing [2].The recent development of material deposition methods leads also to thin diamond film production on various substrates. The technologies used for the diamond thin film formation are based on chemical vapour deposition.

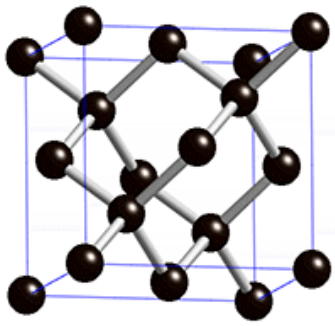

***Figure 1**: The diamond crystal structure [2]*

EXPERIMENTAL DETAILS

The diamond thin films were prepared by Hot Filament CVD. The conditions of seeding and also the growth process parameters can be varied [3, 4]. The morphology and the electrical

parameters are dependent on the growth process substrate biasing too and the process environment [5, 6]. The growth process evolution follows the various substrates of Si, SiO_2 and Fused Silica (JGS1).

Using the hot filament CVD method the reactor reaches almost 2000°C and the substrate temperature is usually in the range between 600°C and 800°C. The diamond thin film growth series contains one Si substrate, one Si substrate covered by thermally created Si/SiO_2, one SiO_2 substrate and one special fused silica (JGS1) [7] substrate. All other variables like the time of the deposition - 30 min, 15:300 for CH_4:H_2 ratio, 3 kPa pressure in the chamber and 600°C the temperature of the holder were used the same. The nucleation process was initiated using diamond powder in ultrasonic bath in acetone.

Optical microscopy, SEM investigations (LEO 1550), Raman spectroscopy measurements (Horiba Jobin Yvon, Labram with He-Ne laser in backscattering geometry) SIMS depth profile analysis (Ion TOF, Bi^+ primary ions for analysis and 2 keV Cs^+ for sputtering) and XRD measurements were performed in order to get an overview and quality information of produced diamond thin films. The diamond thin film samples were examined without surface chemical cleaning before the analysis.

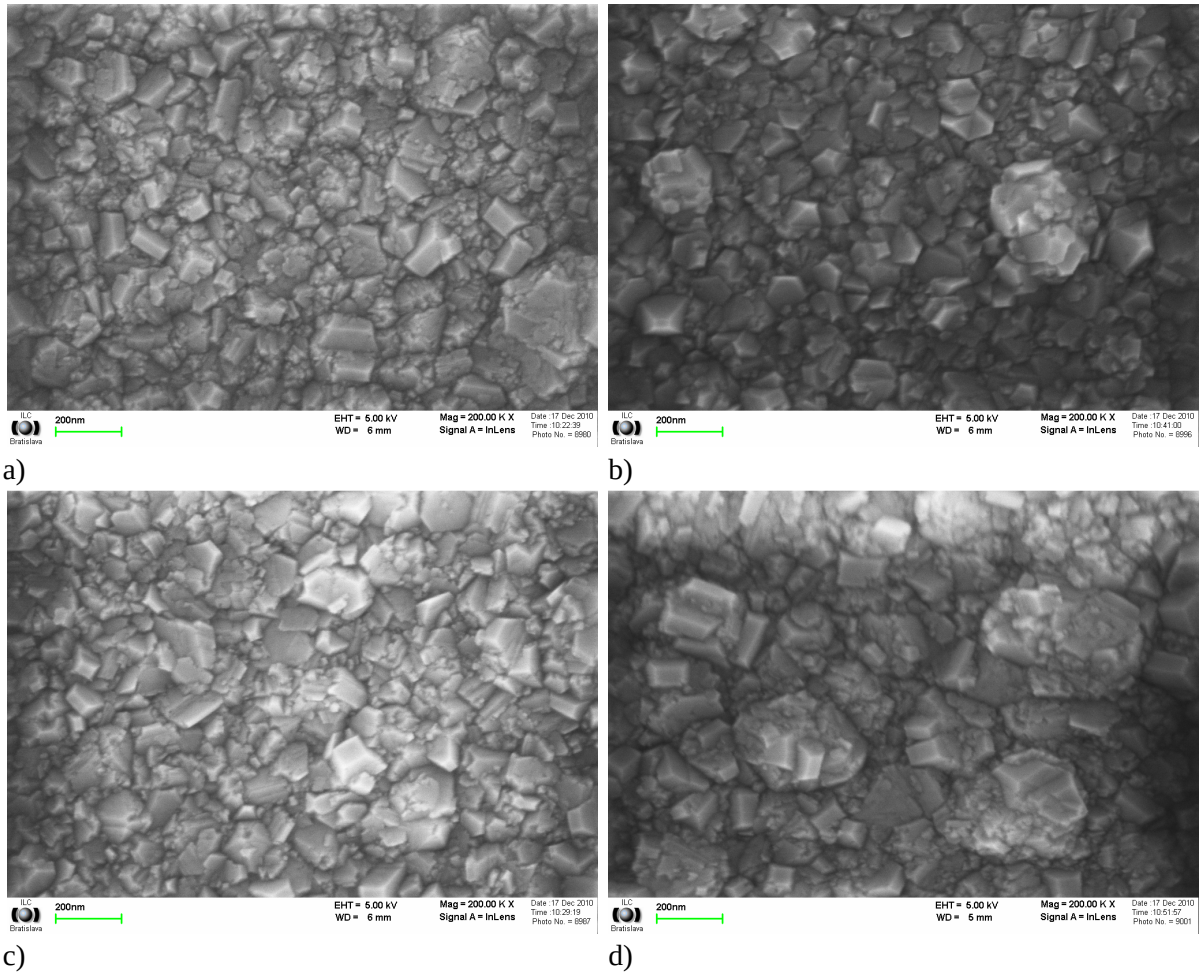

***Figure 2**: Diamond thin films from a SEM view a) on Si substrate b) on JGS1 substrate*

EXPERIMENTAL RESULTS

For experimental evaluation in first approach the optical evaluation and microscopy was used. The prepared diamond thin film surface in a view of SEM microscopy shows different size and cluster structures of diamond seeds, fig. 2. The surface coverage is homogeneous, larger and smaller crystal clusters were found in some specific parts of the surface. This effect of crystal clustering can be attributed to the nucleation results, where the nucleation was slightly different.

The Raman spectroscopy results confirmed the dimaond bonds at the peak 1333 cm^{-1}. The peak at 1580 cm^{-1} confirm the fact, that the diamond thin films also contains bonds to graphite, which are in these thin films dominating, fig. 3. At this point we started to investigate in paralel the diamond thin films using XRD to find the relations in the frowth parameters and also by the SIMS, where the composition can clarify the results.

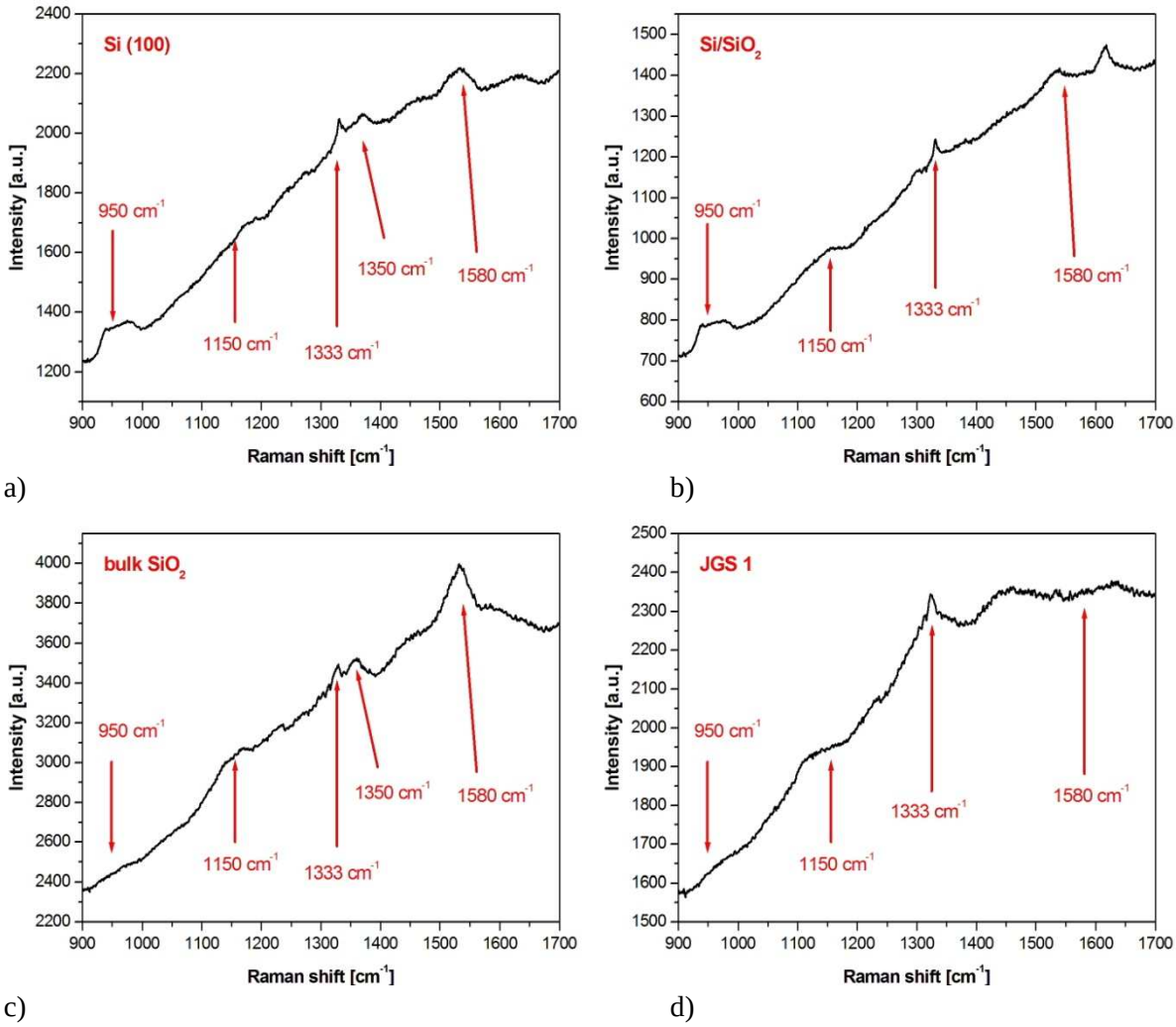

***Figure 3**: Diamond thin films from a Raman spectroscopy view on a) Si b) Si/SiO_2 c) SiO_2 and d) JGS1 substrates*

The XRD results shows very sharp peak at 44°, which is belong to the diffraction from the crystallographic plane (111). Also was detected the peaks at 75°, crystallographic plane (220) and in lower intensity at 92° assigned to plane (331), fig. 4.

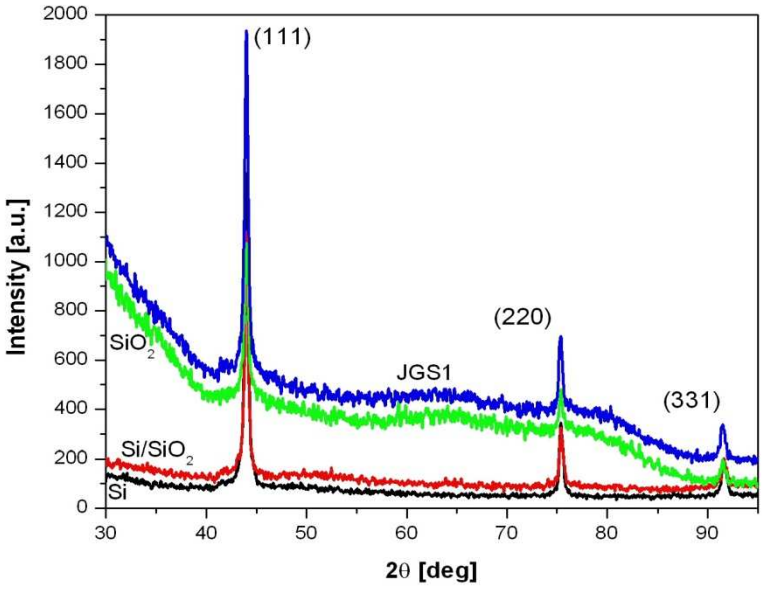

***Figure 4**: XRD patterns of the diamond thin films for all substrates*

The SIMS results revealed differences caused by growth conditions and seeding layers, which influence mainly the interface between substrates and diamond thin films. The main elements are the C, H, O for the diamond films, differences were found in the H and O concentration, which is increased in the surface region for the sample thermally Si/SiO_2 substrate, fig. 5.

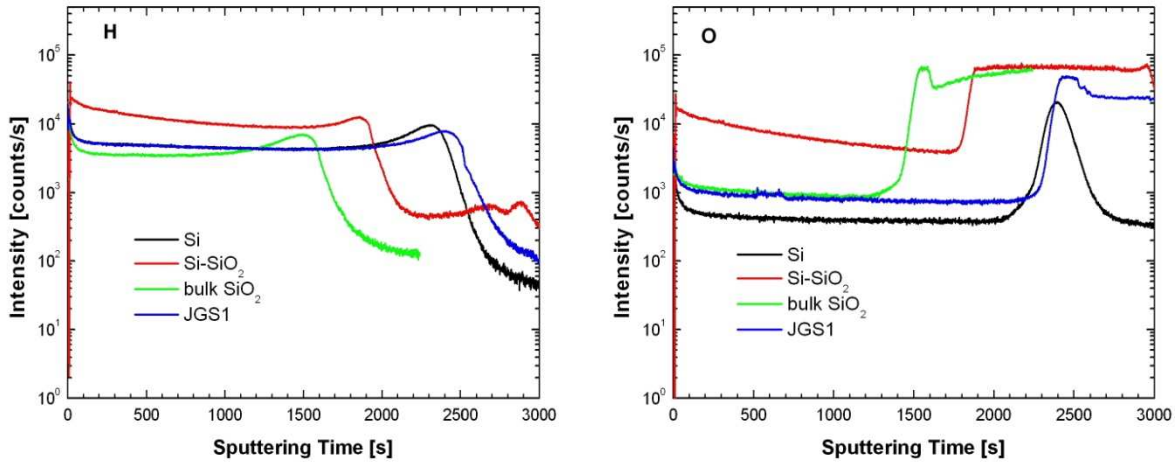

***Figure 5**: Comparison of H and O spectral lines in the depth profiles of diamond thin films on various substrates*

However the same deposition time was used for all samples, using the same sputtering ions and conditions the same diamond thin film thicknesses were expected. This is in fact not really true. The highest diamond thin film thickness was identified for Si substrate, a little bit lower for JGS1, substrate and then the thermal Si/SiO_2 followed by the SiO_2 substrate, fig. 6.

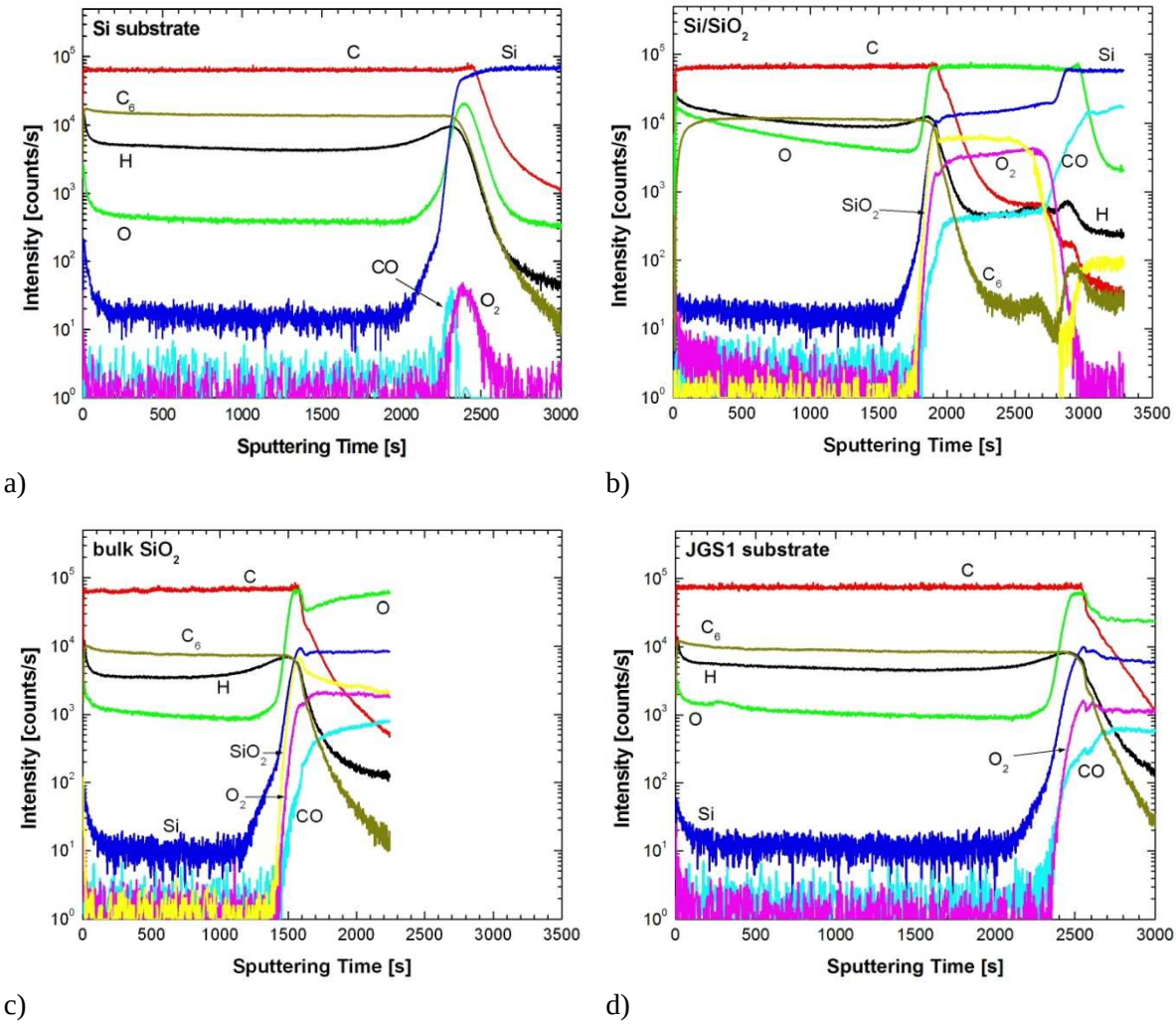

***Figure 6**: SIMS depth profiles for diamond thin films on Si, Si/SiO_2, bulk SiO_2 and JGS1 substrate*

The SIMS craters were visualised by using white light interferometry (Bruker Contour GT-K1) Utilizing white light interferometry three-dimensional surface measurements from nanometer-scale roughness through millimeter-scale steps with sub-nanometer resolution can be performed. The 2D representation reveals the diamond thin film thicknesses, fig 7 c and d.

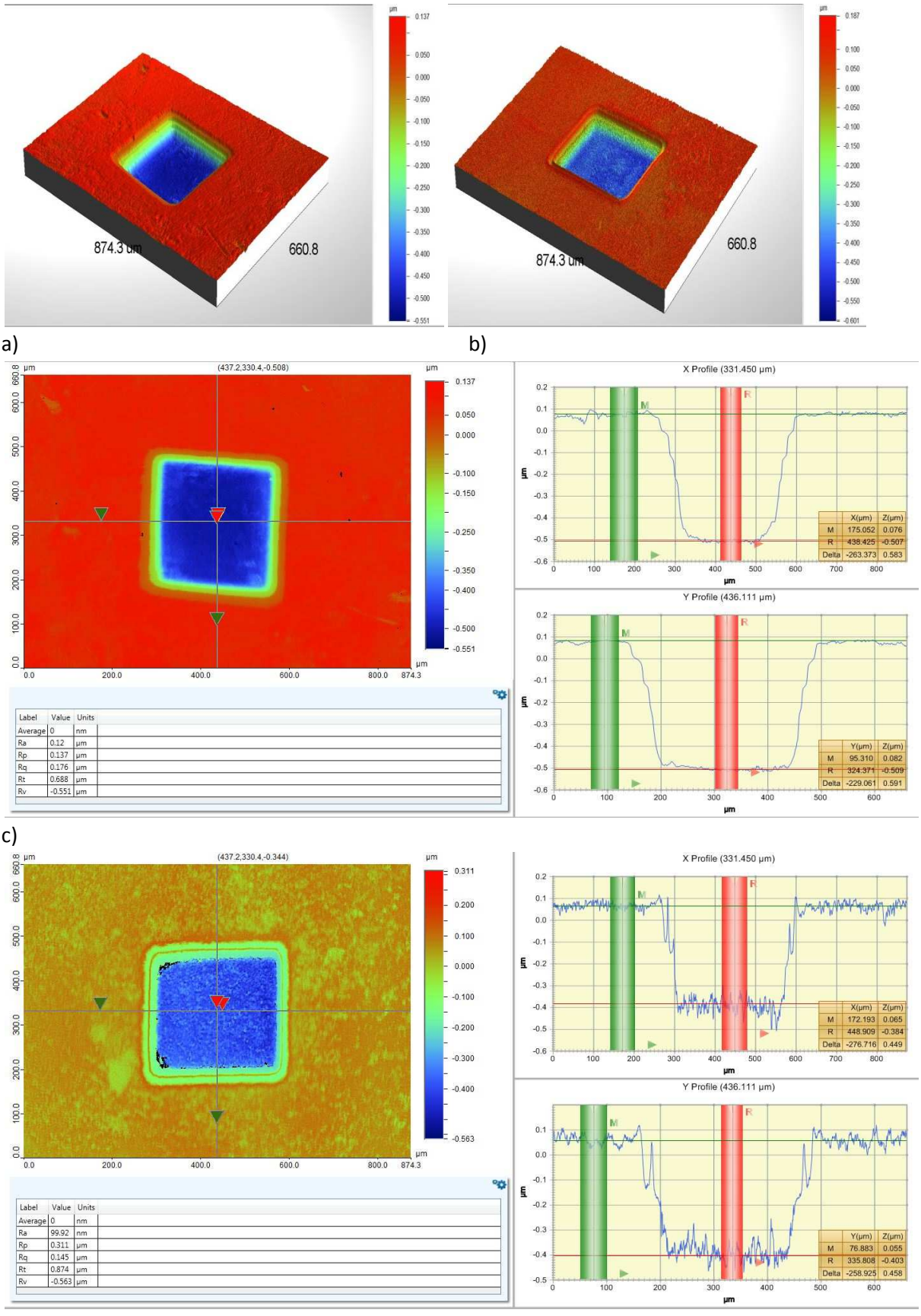

***Figure 7**: SIMS depth profile craters visualised using white light interferometry on a) Si b) JGS1 substrate in 3D representation and c) Si d) JGS1 substrate in 2D representation*

CONCLUSIONS

In this contribution we compared a series of diamond thin film samples produced by HF CVD method using the same conditions in different substrates. Characterization by methods of SEM, SIMS, XRD and Raman spectroscopy were done. XRD confirmed the crystalline planes, while RS clarified the evolution and that the diamond thin films contains bonds to graphite, which are in these thin films dominating. The SIMS depth profiles shows only small changes in the H, C at the surface region.

Acknowledgements This work was supported by the Slovak Grant Agency contract VEGA 1/0787/09 by grants of Slovak Research and Development Agency APVV-0548-07, SK-CZ 0148-09, SK-CZ 0139-09 and by the projects MŠMT ČR KONTAKT projects MEB0810081 and MEB0810082.

REFERENCES

[1] S.-Tong Lee , Zhangda Lin, Xin Jiang: *CVD diamond films: nucleation and growth*, Materials Science and Engineering 25 (1999) pp.123-154

[2] S. Koizumi, C. Nebel, and M. Nesladek, in *Physics and applications of CVD diamond*, Wiley-VCH (2008), ISBN: 978-3-527-40801-6

[3] T. Ižák, M. Marton, M. Varga, M. Vojs, M. Veselý, R. Redhammer, M. Michalka, *Bias enhanced nucleation of diamond thin films in a modified HFCVD reactor,* Vacuum 84 (2009) pp.49-52

[4] A. Kromka, O. Babchenko, B. Rezek, M. Ledinsky, K. Hruska, J. Potmesil, M. Vanecek, *Simplified procedure for patterned growth of nanocrystalline diamond micro-structures,* Thin Solid Films 518 (2009) pp.343-347

[5] M. Marton, T. Ižák, M. Veselý, M. Vojs, M. Michalka, J. Bruncko, *Effect of argon and substrate bias on diamond thin film surface morphology*, Vacuum 82 (2008) pp.154-157

[6] T. Ižák, M. Vojs, M. Veselý, J. Škriniarová, I. Novotný, M. Michalka, R. Redhammer, *Electrical property dependence on thickness and morphology of nanocrystalline diamond thin films*, Microelectronics Journal, 40 (2009) pp.615-617

[7] JGS1 specification http://www.newrise-llc.com/fused-silica.html

ZNO LAYERS PREPARED BY PULSED LASER DEPOSITION (PLD)

Jaroslav Bruncko, Andrej Vincze, Miroslav Michalka, Daniel Haško

International Laser Centre, Ilkovicova 3, 841 04 Bratislava, Slovak Republic

bruncko@ilc.sk

Abstract The article deals with ZnO as a perspective semiconductor material for optoelectronic applications in UV and near UV region. Thin layers with controlled properties are the key components for preparing of p-n junctions which can serve a base of the detectors or emitters. PLD is an important deposition technology for deposition and basic research of such layers. The article briefly summarizes advantages/disadvantages of PLD, its deposition parameters and some results which were achieved in International Laser Centre in Bratislava.

Keywords: ZnO, pulsed laser deposition

INTRODUCTION

Zinc oxide (ZnO) attracts intensified scientific interest as a perspective semiconductor material nowadays. Along with GaN it is considered as the most promising materials for optoelectronic applications in blue-VIS and near UV region. Moreover, relative abundance and non toxicity make ZnO an ideal material for massive production of solar cells, large area displays, etc. There were many references published which refer about successful demonstration of p-type doping; however there are still not fully resolved technological issues to produce ZnO films with desired properties. The crucial problem is to prepare doped ZnO as long time stable p-type semiconductor [1, 2].

Fig. 1 documents the rise of scientific interest in ZnO. The source of presented data was SCOPUS^{TM} – abstract and citation database of research literature. Two ways was applied for acquiring the data. First, the phrase “ZnO-keywords” represents the number of articles per year covered by SCOPUS for “Physical Sciences” which contained “ZnO” phrase in keywords. Second, “ZnO AND PLD” represents number of articles per year covered by SCOPUS for “Physical Sciences” which contained “ZnO” AND “PLD” phrase in abstract.

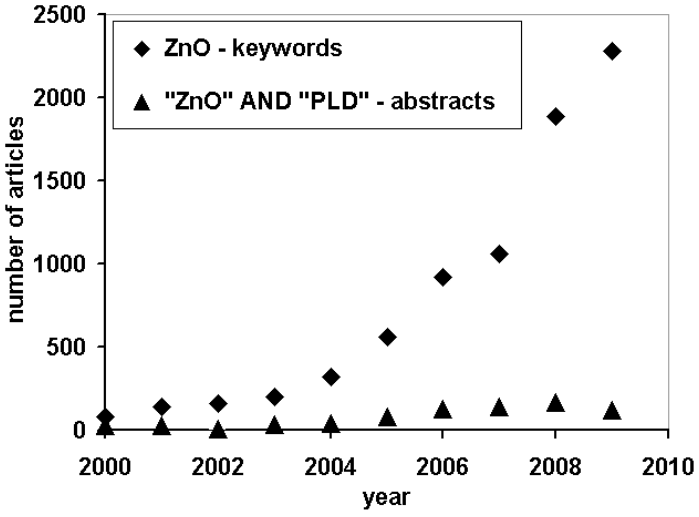

***Figure 1**. The rise of scientific interest in ZnO represented by data acquired from SCOPUS^{TM} database.*

ZnO is a direct band gap semiconductor (group II-VI) with E_g = 3.4 eV. The band gap level can be tuned via doping of different elements and the most interesting goal is to achieve p-type

conductivity. The most promising dopants are considered N, P, As with codoping containing Al, Mg, Ga, etc. Moreover, the structural defects in ZnO crystallographic structure contribute to the energy band gap shifting and whole complex of these circumstances cause difficulty to obtain reproducible results in final properties and time reliability of ZnO based devices. Tab. 1 sumarises the basic properties of undoped ZnO

The aim of this paper is to introduce the main features of pulsed laser deposition (PLD) at the example of ZnO. It deals with main technological conditions which influence the pulsed laser deposition of ZnO layers and demonstrates some results achieved in International Laser Centre Bratislava.

Table 1 *Properties of wurzite ZnO [3]*

Property	Value
Lattice parameter at 300K a_0 c_0	 0.32495 nm 0.52069 nm
Density	5.606 g/cm^3
Stable phase at 300 K	wurzite
Melting point	1975 °C
Refractive index	2.008, 2.029
Energy gap	3.4 eV (direct)
Intristic carrier concentration	< 106 cm^{-3}
Exciton binding energy	60 meV
Electron effective mass	0.24
Electron Hall mobility at 300K for low n-type conductivity	200 cm^2/Vs
Hole effective mass	0.59
Hole Hall mobility at 300K for low p-type conductivity	5 -50 cm^2/Vs

PULSED LASER DEPOSITION OF ZNO

According to [4] thin layers of ZnO can be deposited y a variety of technologies:

- Reactive / nonreactive magnetron sputtering
- Metalorganic chemical vapour deposition (MOCVD)
- Pulsed laser deposition (PLD)
- Evaporation
- Spray pyrolysis
- Sol-gel preparation
- Electrochemical deposition

Each of above mentioned method has own special features, advantages and disadvantages as well. PLD is largely used in laboratory research for its versatility, rather simple principles and possibility to vary technological conditions in wide range [5]. However, these universal properties of PLD sometimes lead to some different results at different deposition devices despite of otherwise similar parameters [6-8], which is caused probably by some additional and with difficulty defined processing circumstances.

Pulsed laser deposition (PLD) is a deposition technology which includes three basic components typical and inevitable for group of physical vapour deposition processes:

1) Source material (target),
2) Substrate where the layer is grown,

3) Energy supply to transport material from the source to the substrate during film deposition (in PLD it is an intense and properly focused pulse of laser energy) [9].

Among all physical vapour processes, the PLD hardware is the simplest and flexible. Fig. 1 shows the main parts of typical system for PLD. Advanced systems for PLD can include some additional components for diagnostics of deposition process, in situ investigation of the properties of grown film, modification of plasma plume etc. [10].

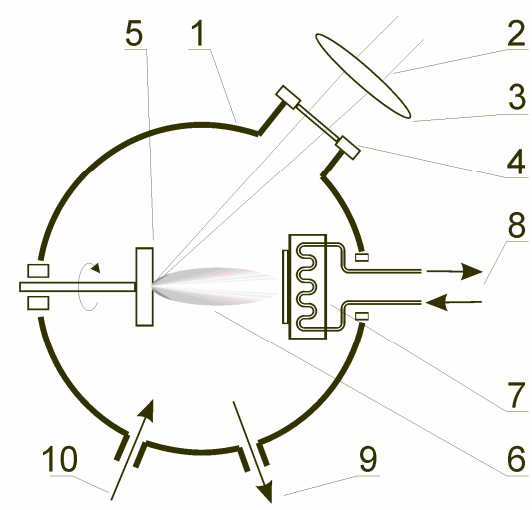

Figure 2 *The main parts of PLD equipment: 1 – vacuum chamber, 2 – pulsed laser beam, 3 – focusing lens, 4 – input window, 5 – rotating target, 6 – plasma plume, 7 – (cryogenically cooled) substrate holder, 8 – heating system, 9 – vacuum output,10 – buffer gas (O_2) input*

Combination of deposition parameters plays crucial role for final properties of prepared layers (crystallographic orientation, thickness, electrical / optical properties …). Among the most influential parameters we can include background gas pressure (optionally its composition), substrate temperature, laser beam wavelength, laser energy density, target to substrate distance, rate of laser pulses. Moreover, there are additional group of non-processing conditions such as type of substrate and properties of ablated target (chemical composition, inner structure and state of surface).

PLD can be applied in growth of simple layers of ZnO as well as for doped films in complex multilayered structures with homo/hetero junctions. On the other hand, there is rising interest in fabrication of ZnO nanostructures with PLD nowadays. A variety of nanostructures including an array of nano-rods/wires/needles etc. have been possible by PLD by carefully varying the deposition conditions and modifications in the processing chambers [11].

The main advantage of PLD is a wide material selection suitable for successful growth of thin films including pure elements or compounds and multilayer structures. Among them, oxides play important role in thin film structure. Oxides cover a wide range of physical and chemical properties. They are typically used as the electrical and diffusion insulating barriers, optical waveguides, mechanical anti-scratch coverings, and in countless special applications.

EXPERIMENTAL

The experimental equipment for PLD in International Laser Centre consists of subsequent main parts:

Pulsed laser - Nd:YAG laser Quanta Ray, output wavelength 1064, 532 and 355 nm, maximum pulse energy 400 mJ, pulse length 10 ns, pulse repetition rate 10 Hz.

Vacuum chamber - ambient pressure can be adjusted in the range 5.10^{-4} Pa – 35 Pa, substrate temperature 20 – 700° C. The chamber includes the target holder for 2 targets and for

better thickness homogeneity there are possible both rotation of target and eccentrically rotated focusing lens. Incident angle between laser beam and target surface is 45° and target to substrate distance can be adjusted in 35-60 mm range.

3.1 Thickness of the films prepared by PLD

The thickness of resulted layers can be controlled by proper combination of deposition parameters. Of course, more dense plasma plume and longer deposition time cause increase of the thickness. However, there are complicated relations among other circumstances so detailed modelling and prediction is rather complicated and still is empirical than based on theoretical modelling.

The density of the plasma plume is depends on laser beam parameters (wavelength, energy density, the angle of incidence with substrate surface, pulse width…), target properties (chemical composition, surface roughness, temperature…), arrangement in deposition chamber (substrate to target distance, position angle between them), and ambient atmosphere (pressure level and chemical composition of active gas – if applied).

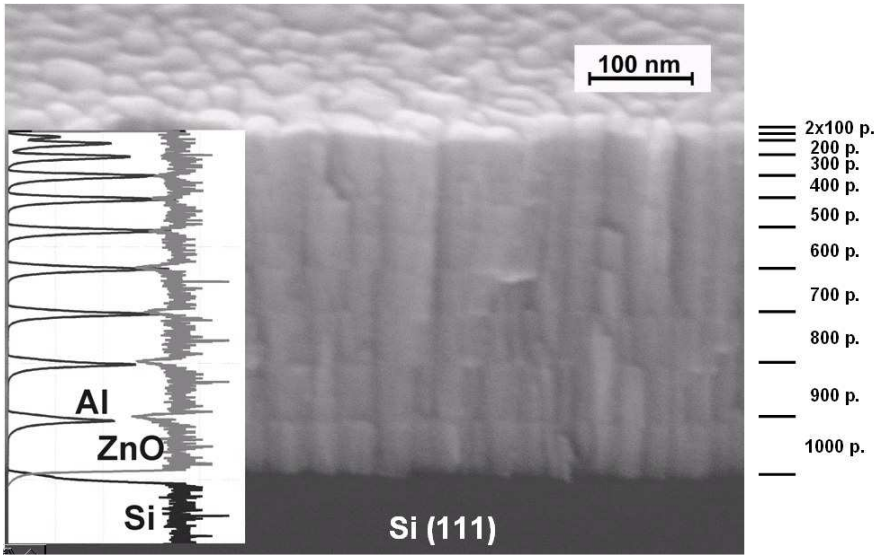

***Figure 3**. The multilayered experimental sample (ZnO / Al) deposited on Si (111). Deposition parameters: Buffer gas: 5 Pa O_2, Substrate deposition temperature: Si (111), 400°C, Laser pulse: wavelength 355 nm, pulse width 15 ns, Incident angle: 45°, Laser spot area 0.033 cm^2, Laser fluence 2,8 $J.cm^{-2}$, Target / substrate distance 50 mm.*

- Fig. 3 shows a layered sample of ZnO with metallic aluminium. The sample was prepared under application of subsequent parameters:
- Target: A: a sintered pellet of fine grained ZnO, target B: pure metallic Al,
- Buffer gas: 5 Pa O_2,
- Substrate deposition temperature: Si (111), 400°C,
- Laser pulse: wavelength 355 nm, pulse width 15 ns,
- Incident angle: 45°,
- Laser spot area 0.033 cm^2,
- Laser fluence 2,8 $J.cm^{-2}$,
- Target / substrate distance 50 mm

The different rate of ablation pulses (the exact number for each step is depicted in right side of figure) visibly correlates with different thickness of corresponding steps. The chemical analysis across the depth performed by SIMS confirms layers of ZnO and Al visible in SEM image. The relation between applied parameters and resulted thickness is subsequent: 1000 pulses give approximately 60 nm layer of ZnO, respectively for 1 nm of ZnO we need approximately 17 pulses.

3.2 Comparison of deposition ZnO from different targets

ZnO is the compound material which consists of two elements: Zinc and Oxygen, and therefore two deposition strategies can be applied:

- Direct deposition by ablation of compound ZnO target (in vacuum or O_2 atmosphere).
- Indirect deposition when a pure Zn target is ablated in O_2 ambient at certain pressure level. Removed atoms of Zn after ablation react with oxygen and create ZnO compound film at the target surface.

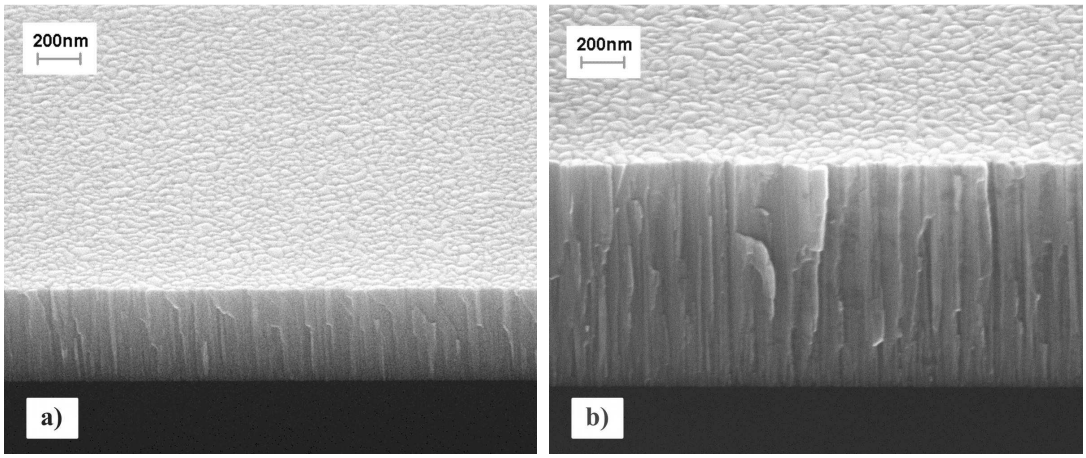

Figure 4. *ZnO thin films deposited on Si (111). Parameters: pressure 5 Pa of ambient O_2, deposition temperature 400°C, laser energy fluency 2.8 J.cm^{-2}. Fig. 4a – the sample deposited from Zn target. Fig. 4b – the sample deposited from ZnO target.*

We investigate the final properties of ZnO films in dependence of used target (a sintered ceramic pellet of ZnO in comparison with a pure metallic Zn target). Experimental depositions were performed at O_2 pressure levels: 1, 5, 10, 15, 25, and 35 Pa. Other technological parameters were fixed at the same level for all samples: deposition temperature (400° C), number of laser pulses (15,000), laser energy fluence (2.8 J.cm^{-2}). The samples were cooled after deposition without annealing. Chips of polished Si (111) were used as the substrate material and there was not applied any special cleaning process before deposition (rinsing in acetone and blowing by stream of pressurized nitrogen).

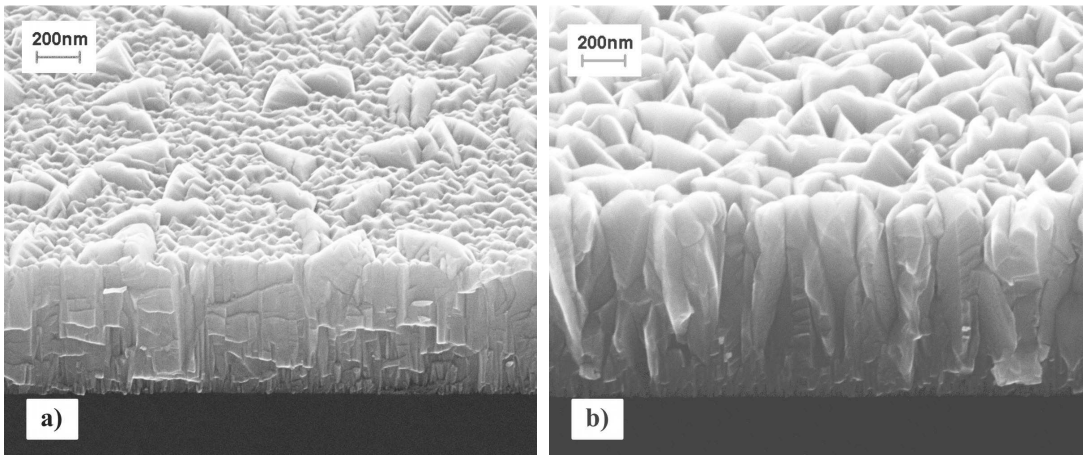

Figure 5*. ZnO thin films deposited on Si (111). Parameters: pressure 35 Pa of ambient O_2, deposition temperature 400°C, laser energy fluency 2.8 J.cm^{-2}. Fig. 5a – the sample deposited from Zn target. Fig. 5b – the sample deposited from ZnO target.*

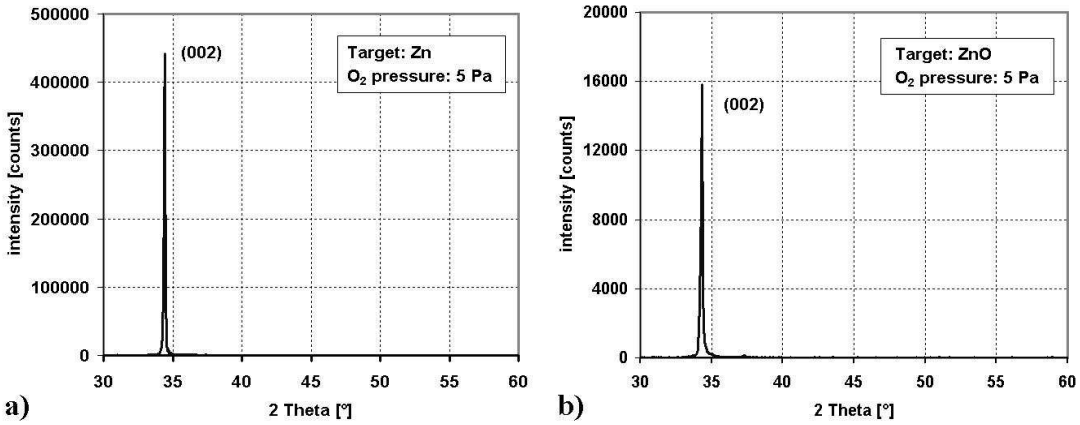

***Figure 6**. Examples of typical XRD patterns of prepared ZnO films. Parameters: pressure 5 Pa of ambient O_2, deposition temperature 400° C, laser energy fluency 2.8 J.cm^{-2}. Fig. 6a – the sample deposited from Zn target. Fig. 6b – the sample deposited from ZnO target.*

Fig. 4 and 5 represent typical examples of deposited films. Both contain a pair of pictures as a comparison of results achieved from different targets. Samples in Fig. 4 were deposited at 5 Pa of O_2, where Fig. 4a was grown from Zn target and Fig. 4b from ZnO target respectively. Samples in Fig. 5 were prepared at 35 Pa of O_2.

In XRD analyse all investigated samples exhibited nearly the same pattern: sharp, isolated peak of (002) line which slightly varied around 2 x angle of 34.5°. Some small differences occurred in case of samples which were prepared at 1 Pa of ambient oxygen (for both targets). These samples achieved much broader (002) line (it was around 0.7° at FWHM) than rest of prepared specimens (typical value was in the range of 0.1° – 0.3°). Measured results suggest that films are highly oriented and consist of columnar crystallites which are oriented perpendicularly on substrate surface.

Fig. 6 (a, b) consists of pair of XRD patterns which were recorded on samples grown at 5 Pa of oxygen pressure. Table 2 summarises measured data for investigated samples in dependence on type of target and applied pressure.

DISCUSSIONS

The analyses based on various analytical methods (SEM, SIMS, XRD) proved that deposition with applying of metallic Zn target is comparable with deposition from ZnO target at the pressures above 5 Pa of ambient oxygen. The thickness of layers was the main difference. The layers prepared from Zn target were typically thinner than their counterparts which were grown from ZnO target. Any other characteristics were very close. All XRD patterns consisted from intense, narrow (FWHM of 0.1 – 0.3°) isolated only peak of (002) at 34.5° of 2 theta angle which confirm highly oriented crystallographic structure.

SIMS analyses confirmed homogenous composition along the depth from the surface of film to the sharp interface between film and substrate with abrupt change of chemical composition. Presence of thin interface of SiO_2 suggests obvious oxidation process of substrate material which rises with O_2 pressure.

Pressure of ambient O_2 during the deposition process is very influential parameter. It is important for successful deposition from Zn target. Samples prepared at 1 Pa of O_2 substantially differed from their counterparts grown from ZnO target. Pressure of 1 Pa O_2 seems to be low for successful growth from Zn target. Samples exhibited wide (FWHM of 0.7°) XRD line for (002) and SIMS profile revealed large (approximately 70 nm) interface with mixed composition of ZnO, Zn, Si, and SiO_2.

CONCLUSIONS

Theoretical predictions and experimental results prove that PLD is the powerful experimental technique for ZnO deposition. There are increasing amount of papers which refer to successful fabrication of ZnO-based structures. Despite of relatively simple principles it offers a broad variety of scientific issues and there is still plenty of room for further experimental research.

Acknowledgment This work was supported by the Slovak Research and Development Agency under the projects no. SK-CZ-0148-09 and SK-CZ-0122-09 and by the MŠMT ČR KONTAKT projects MEB0810081 and MEB0810082.

REFERENCES

[1] Adachi, S., in *Properties of Group-IV, II-V and II-VI Semiconductors*, Wiley, New York (2005).

[2] Jagadisch, P. and Pearton, S.J., in *Zinc Oxide Bulk, Thin Films and Nanostructures: Processing, Properties and Applications*, Elsevier, New York (2006).

[3] Norton, D. P., Heo, Y. W., Ivill, M. P., Ip, K., Pearton, S. J., Chisholm, M. F. and Steiner, F., "ZnO: growth, doping &processing," Materials Today 7(6) (2004) pp. 34-40

[4] Ellmer, K., Klein, A. and Rech, B., in *Transparent conductive Zinc Oxide,* Springer-Verlag, Berlin & Heidelberg, (2008) pp. 56-57

[5] Vincze, A., Kovac, J., Novotny, I., Bruncko, J., Hasko, D., Satka, A. and Shtereva, K., *Preparation and properties of ZnO layers grown by various methods*, Applied Surface Science 255(4) (2008) pp. 1419-1422

[6] Chen, C. C., Yu. B. H., Liu, H. F., Dai, Q. R. and Zhu, Y. F., *Investigations of ZnO films on Si <111> substrate grown by low energy O+ assisted pulsed laser deposited technology*, Materials letters, 61(14-15) (2007) pp. 2961-2964

[7] Zhao, L. Hu, Z., Wang, J., Sun, J. and Wang, Z., *ZnO thin films on Si (111) grown by pulsed laser deposition from metallic ZnO target*, Applied Surface Science, 253(2) (2006) pp. 841-845

[8] Zhu, B. L., Zhao, X. Z., Su, F. H., Li, G. H., Wu, X. G., Wu, J., Wu, R. and Liu, R., *Structural and optical properties of ZnO thin films on glass substrate grown by laser ablating Zn target in oxygen atmosphere*, Physica B, 396(1-2) (2007) pp. 95-101

[9] Hoffman, D. M., Singh, B. and Thomas, III, J.H., in *Handbook of vacuum science and technology*, Academic Press, San Diego (1998) pp. 694-695

[10] Miller, J. C., and Haglund, R. F., in *Laser ablation and desorption*, Academic Pres San Diego (1997)

[11] Lorenz, M., Kaidashev, E. M., Rahm, A., Nobis, Th., Lenzner, J., Wagner, G., Spermann, D., Hochmuth, H. and Grundman, M., *MgxZn1–xO(0 ≤ x<0.2) nanowire arrays on sapphire grown by high-pressure pulsed-laser deposition,* Appl. Phys. Lett., 86(14) (2005) 143113.

RAMAN MICRO-SPECTROSCOPY AND TEMPERATURE DEPENDENCE OF CRYSTALLINE SILICON RAMAN SPECTRA

Robin Schilhart

Institute of Physics of the AS CR, v.v.i., Cukrovarnická 10, Prague 6, 160 00, Czech Republic

schil@fzu.cz

Abstract: This paper summarizes the essence of the Raman effect, Raman spectroscopy basic principles, advantages and its common applications. Furthermore Raman micro-spectroscope with broadband applications available in the lab of Institute of Physics of the ASCR is introduced together with detailed analyses of temperature dependent Raman spectra of crystalline silicon.

Keywords: carbon nanotubes CNT, microwave plasma

INTRODUCTION

Raman micro-spectroscopy is a widespread technique used mostly for chemical analyses of the matter. It is based on a process called the Raman effect, named after Sir Chandrasekhara Venkata Raman (1888-1970), who was an Indian physicist and Nobel Prize for Physics winner in 1930. He was the founder of a phenomenon called Raman scattering, inelastic scattering of a photon by matter. However, theoretical basics of this effect had been described by Adolf Smékal couple years ago, in 1923 [1, 5].

THE RAMAN EFFECT

When light enters the matter, it can interact in many possible ways. Photons interacting with the molecules are either reflected, absorbed or scattered.

Rayleigh scattering is the *elastic scattering* of the light by smaller particles than the wavelength of the light, (for instance atoms). Term elastic scattering refers to the fact that the incident photon has the same energy as the scattered photon.

When intensive light enters the matter, Raman have observed, that in spectrum of scattered light is not only the spectral line of the excitation frequency caused by Rayleigh scattering, but also symmetric and million times less intensive lines caused by so called Raman scattering. Distance (measured in wave numbers, usually in [cm^{-1}]) of these lines from the excitation wavelength is independent on its excitation frequency and is characteristic for the substance. This phenomenon is called the Raman effect. Its low probability (10^{-6}) is the reason, why progress in this scientific area started with the discovery of lasers strong monochromatic sources of light). What is the mechanism of this effect? Raman scattering is an inelastic scattering of a photon by a molecule. Photon interacts with the electron cloud of the functional groups bonds, exciting an electron from the ground state into a virtual state. This electron then relaxes into a different excited vibrational or rotational state.

The energetic difference between electron's initial and final state is compensated through emitting a photon. If the final state of the electron is higher than the initial state, emitted photon will have lower frequency compared to the incident photon (following the energy conservation law). Observing this frequency shift is the essence of Raman spectroscopy. Phenomenon described above is called Stokes Raman scattering. Anti-Stokes Raman scattering occurs when the final state of the electron is lower than the initial state and therefore the emitted photon will have lower frequency compared to the incident photon [2], see Fig. 1.

In Raman spectroscopy the Raman Stokes scattering is usually observed because of its higher intensity compared to the Anti-Stokes scattering, see Fig.2.

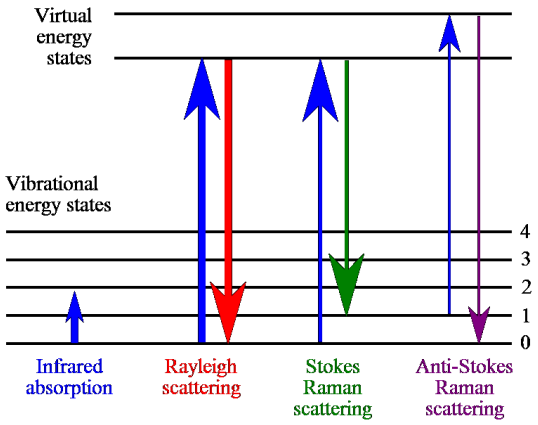

Figure 1. *Energy level diagram showing the states involved in Raman signal. Lines thicknesses are roughly proportional to the signal strength from different transitions. [http://en.wikipedia.org/wiki/File:Raman_energy_levels.jpg]*

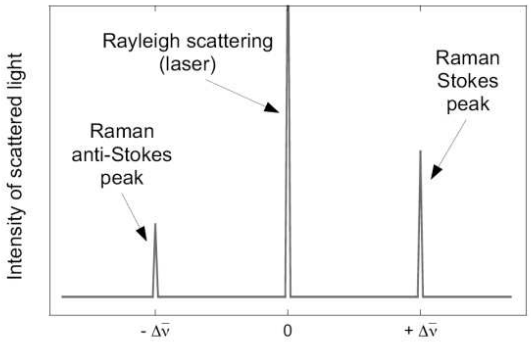

Figure 2. *Intensity of scattered light depending on the type of scattering; Stokes frequency shift used to be labelled as positive although it is a shift to lower frequencies [3].*

The reason is a higher probability for occupation the lower energetic states at thermodynamic equilibrium following the Boltzmann distribution law, where N0 and N1 stands for the absolute number of atoms in the ground and first vibrational state respectively, g0 and g1 express vibrational states degeneration, kB is the Boltzmann constant, T stands for the absolute temperature and EΔ is an energetic difference between ground state and the first vibrational state [3].

Let us consider Raman shift 1000cm-1 at room temperature. The probability of occupation the lower state to the higher state is 1000:1. The same ratio is visible between Stokes and Anti-Stokes lines in scattered light [2].

Of course absolute shift in frequency is only given by an energetic difference between the first excited vibrational state and the ground state and therefore the shift is the same for both – Stokes and Anti-Stokes scattering. It is possible to determine the temperature [7] of the sample from the intensity ratio between these two lines, Fig. 3, as it corresponds to the Boltzmann distribution law (1).

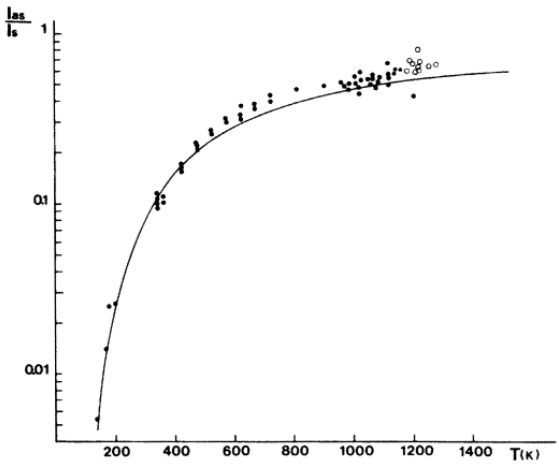

Figure 3. *Anti-Stokes to Stokes intensity ratio vs. temperature [7]. The solid line represents the theoretical curve* $exp(-\hbar\omega_0/k_BT)$.

ADVANTAGES OF RAMAN SPECTROSCOPY

Raman spectroscopy became a very useful and powerful tool for chemical and structural material analysis in last 10 years thanks to the coupling to an optical microscope, charge-coupled device (CCD) detection, confocal set-up or even to an atomic force microscope (AFM) [4].

It has many advantages. Firstly it is a non-contact and non-destructive method. Moreover there is not required special sample preparation. In addition, experiments in water solutions are allowed thanks to the weak water signal in Raman spectroscopy. Therefore Raman spectroscopy can be used for the analysis in solutions, liquids, gases and solids [5]. It is very important to mention that Raman spectroscopy is not only sensitive to the chemical compounds of the sample, but also to the distances, angles, polarizability and charges of their chemical bonds. The limiting spatial resolution is better than 1 µm. Aforementioned advantages open a wide field of applications in biology, medicine, material research and chemistry [5].

The Raman spectroscopy is a vibrational spectroscopy and therefore gives us similar information as infrared spectroscopy (IR), based on absorption. These methods can be complementary to each other depending on the selection rules. For example central symmetric molecules are active either in Raman spectra (if its vibrations are symmetric to the center of symmetry) or in IR (if its vibrations are anti-symmetric to the center of molecule symmetry) [3]. To disadvantages of IR spectroscopy belong worse spatial resolution around 20 µm and no ability for analysis in aqueous solutions while water presents very strong and broad absorptions in infrared. For IR is also impossible to reach the frequency range lower than 400 cm^{-1}, where some solid materials have their characteristic signals [4].

Raman spectroscopy is capable of differentiating undesirable and very strong luminescent signals from Raman signals by two different approaches. (Photoluminescence occurs after absorption of a photon. An electron-hole pairs returns back to the ground stage while emitting light of lower energy than was the excitation energy). It is possible to eliminate photoluminescence either by the choice of a different excitation wavelength or using time-domain Raman spectroscopy. Time-domain spectroscopy employs femtosecond pulses [6] and is capable of differentiation the fastest Raman scattering signal from the slower luminescent signal [2].

***Figure 4**. Renishaw InVia Reflex Raman micro-spectroscope [http://www.units.muohio.edu/mml/invia%20reflex.jpg]*

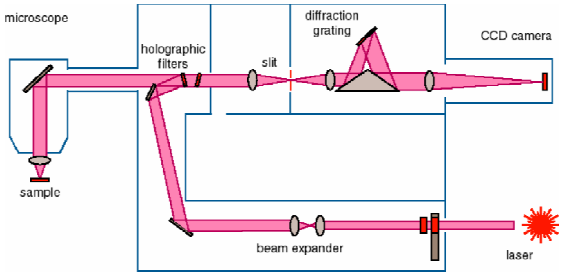

***Figure 5.** Scheme of InVia Reflex Raman micro-spectroscope [http://www.renishaw.com/en/raman-spectroscopy--6150]*

RAMAN MICRO-SPECTROSCOPE AT DEPARTMENT OF THIN FILMS AND NANOSTRUCTURES

Our laboratory is equipped with InVia Reflex Raman micro-spectroscope from Renishaw, see Fig. 4 and Fig. 5. Micro-spectroscope is equipped by Kimmon Company's HeCd dual laser with 325 and 442 nm excitation wavelengths and maximum laser power 3 or 40mW respectively. Additionally 785nm laser with output 200mW is available. For temperature dependence study it is possible to take an advantage of the temperature stabilized stage Examina 600 from Linkam, see Fig. 6. This setup enables to observe Raman spectra between -196°C and 600°C. We also benefit from a

combination of Raman micro-spectroscope and an Atomic Force Microscope made by NT-MDT. This combination allows studying chemical compounds of the sample together with surface topography giving us complementary information about multiple properties of the sample.

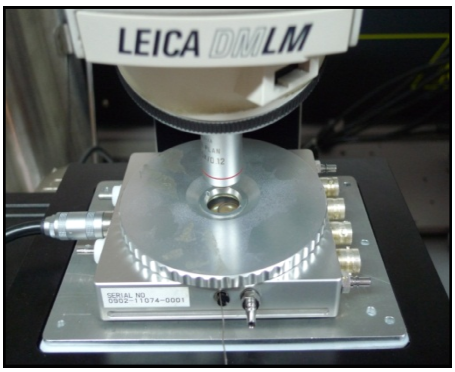

Figure 6. *Temperature stabilized stage Linkam Examina*

RAMAN TEMPERATURE DEPENDENT STUDIES ON CRYSTALLINE SILICON

Crystalline Silicon (CSI) is used as the etalon in Raman micro-spectroscopy for its sharp peak at 520,5 cm-1 at room temperature, which can be fitted precisely with Lorenz function, see Fig.7.

We observe shift to the higher frequencies and the peak's widening during warming up the sample of CSI in the Linkam stage, as is illustrated on Fig. 8. This phenomenon was described and theoretically calculated by M. Balkanski at al. in 1983 [7], Fig. 9.

My observation of CSI Raman shift on Fig. 10 is in good agreement with theoretical results on Fig. 11 [7]. My experimental results vary depending on the use of additional thermocouple or Linkam Examina inner thermocouple respectively. For future experiments more detailed analyses will be necessary.

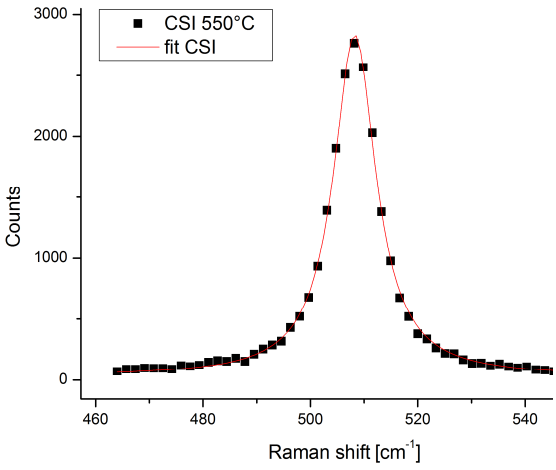

Figure 7. *CSI peak at 550°C fitted precisely with Lorenz function*

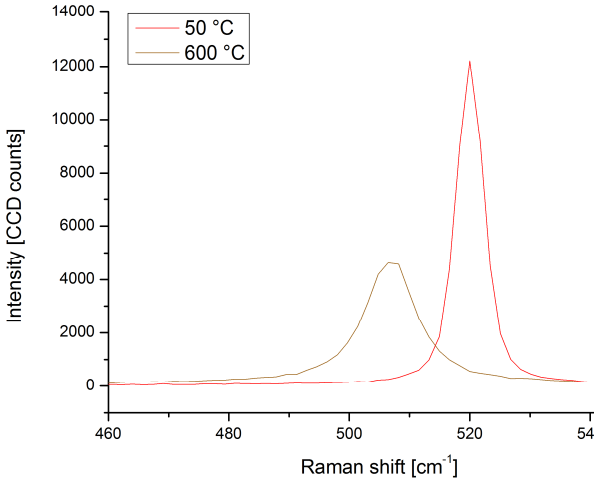

Figure 8. *First-order CSI Raman at 323 K and 873 K*

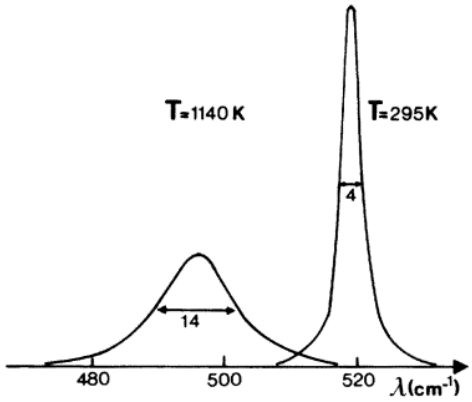

Figure 9. *First-order Raman spectra for silicon at 295 and 1140 K [7]*

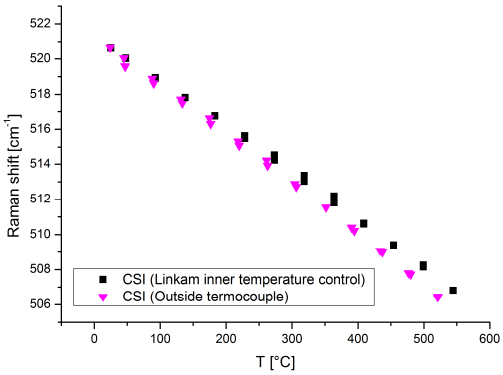

Figure 10. *Temperature dependent Raman shift of CSI*

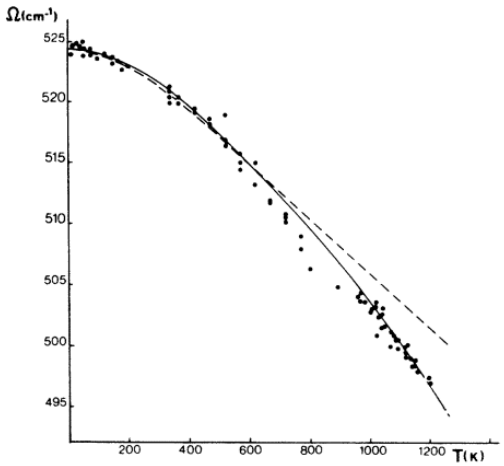

Figure 11. *Temperature dependence of the line position for Raman-active LO mode in silicon. The solid curve gives the theoretical fit using both three-and four phonon processes.*
The dashed curve gives the theoretical fit using only three phonon processes. [7]

REFERENCES

[1] R. Singh, *C. V. Raman and the Discovery of the Raman Effect*. Physics in Perspective 4, 1422–6944/02/040399–22 (2002), pp. 399-420.

[2] V. Prosser et. al. in *Experimental Methods in Biophysics* (in Czech). Prague, Academia (1989), ISBN 80-200-0059-3.

[3] M. Ledinsky in *Optoelectronical and Structural Properties of Thin Silicon Layers* (in Czech). Prague, PhD. Thesis. Charles University in Prague, Faculty of Mathematics and Physics (2009).

[4] P. V. Huong, *New Possibilities of Raman Micro-spectroscopy. Vibrational Spectroscopy* : Elsevier 11 (1996), pp. 17-28.

[5] G. Turrell, J. Corset et al., in *Raman Microscopy*. Elsevier (1996), ISBN 0-12-189690-0.

[6] S. Nath et al. *High-Resolution Raman Spectra with Femtosecond Pulses: An Example of Combined Time- and Frequency-Domain Spectroscopy*. Physical Review Letters 97, 267401 (2006).

[7] M. Balkanski, R. F. Walliss, E. Haro, *Anharmonic Effects in Light Scattering due to Optical Phonons in Silico*n. Physical Review B. 28 (1983), pp. 1928-1934

INFLUENCE OF NUCLEATION AND METHANE CONCENTRATION ON BUCKYPAPERS EXPOSED TO HOT FILAMENT CHEMICAL VAPOR DEPOSITION PROCESS

M. Varga[1, 4], M. Kotlár[1, 2], V. Vretenár[2], T. Ižák[1, 4], J. Šoltýs[3], A. Kromka[4], M. Veselý[1]

[1]Institute of Electronics and Photonics, FEI STU, Ilkovičova 3, SK-812 19 Bratislava

[2]Danubia NanoTech, s.r.o., Ilkovičova 3, 841 04 Bratislava, Slovak Republic

[3]ElÚ SAV, Dúbravská cesta 9, 841 04 Bratislava, Slovak Republic

[4]Institute of Physics of the ASCR,v.v.i., Cukrovarnicka 10, Praha 6, 16253, Czech Republic

marian.varga@stuba.sk

Abstract In this article we investigate the nanocomposite material formation, particularly the deposition of nanocrystalline diamond film on buckypaper (BP) substrate. The buckypapers were prepared from single-wall carbon nanotubes (SWCNT) mixture produced by laser ablation method. We have investigated the influence of the nucleation and methane concentration on buckypapers exposed to the hot filament chemical vapor deposition process. We found out that at low CH4 concentration (<5 % of CH4) the buckypaper was destroyed due to aggressive hydrogen-rich plasma. Finally we successfully deposited nanocrystalline diamond film on buckypaper substrate made of SWCNTs bundles and the best results were obtained at 5 % of CH4 in H2 atmosphere. Scanning Electron Microscopy and Raman spectroscopy were used for the surface morphology analysis and characterization of carbon phases.

Keywords: CNT, buckypaper, diamond film, HFCVD, SEM

INTRODUCTION TO CARBON ALLOTROPES AND CNTS

Recently, carbon allotropes are in the center of interests because of their properties and wide range of applications. There are several carbon allotropes, the well-known are graphite, diamond, amorphous carbon, nanotubes, fullerenes, graphene and carbon nanofoam (Fig. 1). Carbon nanotubes which were discovered by Iijima in 1991 [1] are the basic materials for buckypapers. The carbon nanotube is a tube-shaped material, made of carbon, having a diameter in nanometer scale [2]. CNTs are classified into two big groups: single-wall carbon nanotubes (SWCNTs) and multi-wall carbon nanotubes (MWCNTs) [3]. The graphite layer appears somewhat like a rolled-up chicken wire with a continuous unbroken hexagonal mesh and carbon atoms at the apexes of the hexagons [2]. There are many types of CNTs, differing in the length, thickness, and in the type of the helicity and the number of the layers. Due to their unique structure (high surface to volume ratio, diameter in nanometer scale and length in micrometer scale), CNTs have many interesting electronic, mechanical and chemical properties. However, their big disadvantage is related to their production, because in the most cases CNTs are

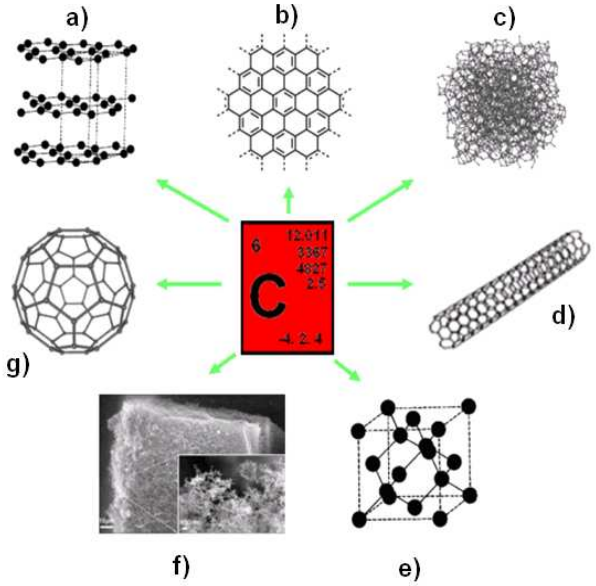

Fig. 1 *Schematic classification of carbon allotropes – a) graphite, b) graphene, c) amorphous carbon, d) carbon nanotube, e) diamond, f) carbon nanofoam, g) fullerene*

produced as a mixture with amorphous carbon, and in addition their different chiralities and diameters are observed. Up to now, there is no reliable method for individual precise manipulation and positioning of them.

Although CNTs are formed from graphite sheet, their electrical properties depend on their structure having metal or semiconductor behavior. Combination of carbon nanotubes with other materials leads to the formation of nanocomposites, which could be stronger, lighter, and capable of better thermal management than any known material [4]. Moreover, they could have a myriad of applications. However, integration of carbon nanotubes into composite materials is a complicated task because nanotubes have tendency to stick together and are not easily dispersed.

In the 1990's an inadvertent discovery resolved many of these problems, when researchers from Richard Smalley's laboratory managed to disperse nanotubes into a liquid suspension and then filter it through a fine mesh. By this method the nanotubes sticked to one another and were collected on a filter, forming a thin film disk of pure nanotubes, later dubbed as buckypaper. In our experiments the buckypapers made of SWCNTs were used as substrates for nanocrystalline diamond (NCD) grown by Hot Filament Chemical Vapor Deposition (HF CVD) technique.

PRODUCTION OF CNTS AND BUCKYPAPERS

Carbon nanotubes can be produced by several methods: arc discharge, chemical vapor deposition and laser ablation. Chemical vapor deposition (CVD) is the simplest and probably the most widely used technology, however, arc discharge and laser ablation method produce CNTs with superior quality. In the laser ablation technique a laser is used to vaporize the graphite target even in continual or pulsed regime. The graphite target consists of graphite and a catalytic metal (mostly bimetal - Ni/Co [5]). Further, the apparatus consists of a furnace, quarts tube and water cooled Cu collector. Graphite target is ablated by focused laser beam in the flow of Ar. Sputtered (or evaporated) carbon molecules and atoms condense with metal catalysts and form small nanoparticles from which carbon nanotubes are growing and collected on the cold copper collector. The final product has net-like structure and typically consists of SWCNTs grouped together by van der Waals forces and impurities in form of metal catalyst, amorphous carbon, etc.

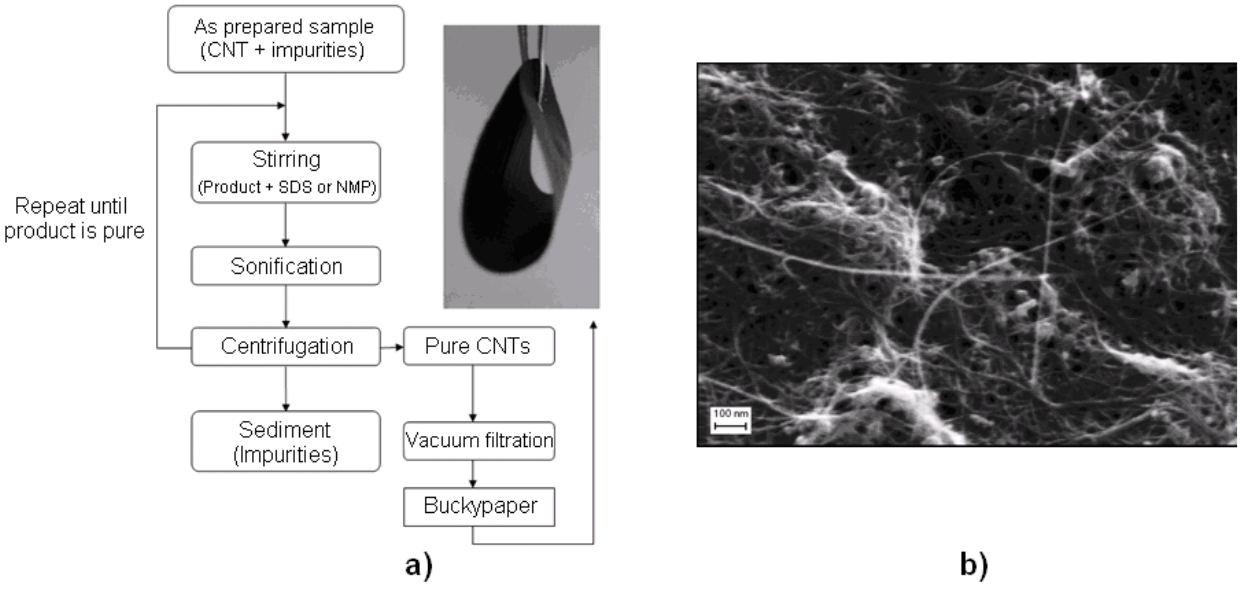

Fig. 2 a) *Preparation process of buckypapers with CNTs purification [7],*

b) *SEM image of the final buckypaper film surface morphology*

The CNTs mixture is commonly characterized by electron microscopies (SEM, TEM), thermo gravimetric analysis (TGA), Raman spectroscopy and ultraviolet-visible-near infrared (UV–vis-NIR) spectroscopy.

Before application it is very important to clean the product from impurities. Purification methods of CNTs can be basically classified into three categories: chemical, physical and the combination of both [6]. As chemical method – i.e. oxidation purification, is based on the idea of selective oxidation etching, wherein carbonaceous impurities are oxidized at a faster rate than CNTs. In general, chemical oxidation includes gas phase oxidation (using air, O_2, Cl_2, H_2O, etc.), liquid phase oxidation (acid treatment and refluxing, etc.), and electrochemical oxidation. The disadvantages of this method are that it often opens the end of CNTs, cuts CNTs, damages surface structure and introduces oxygenated functional groups (–OH, –C=O and –COOH) on CNTs. As a result, the purified CNTs in turn can serve as chemical reactors or a starting point for subsequent nanotube surface chemistry [13, 14]. Physical methods are based on sonification, centrifugation and filtration. Centrifugation is related to the effect of the gravity on particles in suspension (i.e. two particles of different masses settle in a tube at different rates in response to gravity). Commonly, the buckypapers are produced from pure SWCNTs by vacuum filtration. The processes included in buckypaper production are shown in Fig. 2a.

CVD DIAMOND FILMS

Diamond, as one of the well-known carbon allotropes, has sp^3 hybridization. There are two different types of diamond lattice: (i) a more common cubic and (ii) an unusual hexagonal lattice which was discovered in meteorites. For diamond lattice is characteristic that each carbon atom is covalently bonded to four other carbons in a tetrahedral structure. The distance between the atoms is 1.54 Å and their binding energy is 7.41 eV. This unique structure gives diamond special properties (wide optical transparency, high hardness, high thermal conductivity, chemical inertness and biocompatibility) hence it is very requisite for various applications (machinery, electronics, sensorics, optics, medicine) [8 - 10].

Diamond consisting of carbon atoms has some properties similar to CNTs. Therefore the combination of these two materials could lead to improve their particular properties. It was shown in earlier studies that diamond thin films on self-standing buckypapers improve the abrasion resistance and thermal conductivity of the final nanocomposite, and moreover diamond film makes buckypaper more stable [12].

Unique property of carbon is that chemical bond carbon-carbon can be in so called sp^1, sp^2 or sp^3 hybridization. In buckypaper, sp^2 bonds are present. For diamond, only sp^3 hybridization is dominant. Both hybridization types, sp^2 or sp^3, lead in differences of some intrinsic properties (hardness vs. softness, brittlenes vs. flexibility, optical transparency vs. opaque properties, etc.). It is proposed that combining/mixing both these carbon allotropes will lead in a new nanocomposit material with promising properties.

Figure 3 shows the typical Raman spectra of the single-crystalline diamond (SCD) (a), nano-crystalline diamond (b) and buckypaper (c). While in the spectra of SCD is observed only the diamond peak located at 1 332 cm^{-1} and which is related to sp^3 carbon bonds, in the NCD spectrum there are 3 additional bands: at 1 150 cm^{-1} (trans-polyacetylene-like fragments [11]), 1 350 cm^{-1} (D-band, disordered carbon) and 1 580 cm^{-1} (G-band, sp^2 carbon bonds) The typical Raman spectrum of SWCNT buckypaper shows an RBM (Radial Breathing Mode) mode at 240 cm^{-1}, the D (Defect)-mode at 1 332 cm^{-1}, the splitted G-mode at 1 580 cm^{-1} and 2D-mode at 2 650 cm^{-1}. In the case of combination of CNTs with CVD diamond film, the individual Raman spectra of such nanocomposite material is hardly deconvolute because of overlapping of peaks.

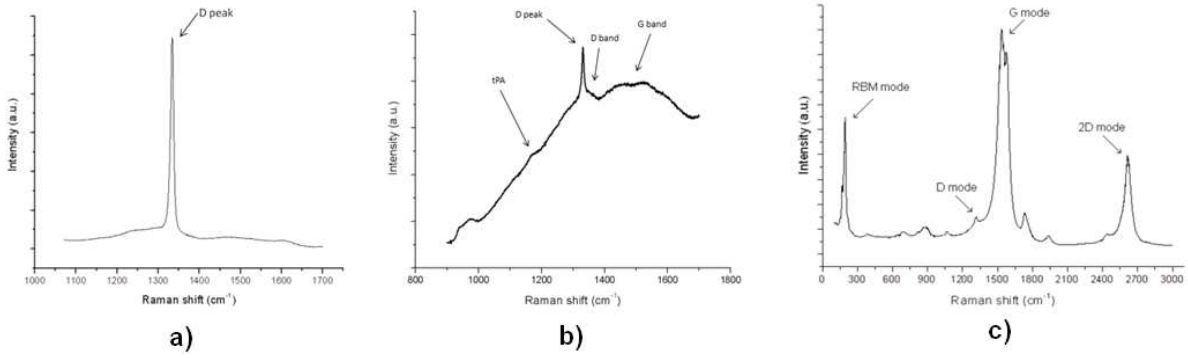

Fig. 3 *Raman spectra of* ***a)*** *single-crystalline diamond* ***b)*** *nano-crystalline diamond and* ***c)*** *buckypaper*

EXPERIMENTAL

SWCNTs were prepared by the laser ablation method and homogeneously dispersed in n-methyl pyrrolidone (NMP) solution by ultrasonic horn. Dispersed solution was filtered on nylon membrane (diameter 45 mm, pores size 0.45 um) by vacuum filtration apparatus. Membrane with CNTs deposit was dried in oven at 80 °C and afterwards removed buckypaper from the membrane was dried at 220 °C (to remove surfactant residua). For each deposition in HFCVD reactor were used 2 buckypaper samples. Before the deposition the first one was dipped in deionized water with nanodiamond powder (10 nm in diameter) for 2 hours and the second one was not nucleated. Then the buckypapers were placed into the HFCVD vacuum chamber and masked by pieces of silicon substrates on both sides. This led to dividing the buckypaper substrate for 2 different areas (covered and uncovered). The depositions were performed for 1 hour at the total gas pressure of 3 kPa. The working atmosphere consisted of the mixture of CH_4 and H_2 was activated by 5 tungsten filaments 0.6 mm thick, 120 mm long, heated to ~2 200 °C. Depositions were carried out at 1, 5 and 10 % of CH_4 in H_2 atmosphere (Tab. 1). After this step the samples were analyzed by Scanning Electron Microscope type Leo 1 550 and Raman spectroscopy using Renishaw In Via Reflex Raman spectrometer with the excitation wavelength of 442 nm.

Tab. 1 *Signification of the samples and deposition parameters*

Samples	Nucleation	CH_4:H_2 flow (sccm)	CH_4/H_2 ratio (%)	Substrate temperature (°C)
I-A-c / I-A-u	Dipped in solution	3:300	1	710
I-B-c / I-B-u	Not nucleated			
II-A-c / II-A-u	Dipped in solution	15:300	5	650
II-B-c / II-B-u	Not nucleated			
III-A-c / III-A-u	Dipped in solution	15:150	10	620
III-B-c / III-B-u	Not nucleated			

(Explanation: I, II, III = deposition, A = nucleated, B = not nucleated, c = covered, u = uncovered)

PRELIMINARY RESULTS

Fig. 4 shows SEM images of the analyzed parts of BP samples after the HFCVD process. It is visible that the influence of methane concentration as like as the nucleation takes effect on the

buckypaper resistance towards the hydrogen rich atmosphere during the deposition. At the deposition with 1 % of CH_4 in H_2 atmosphere the uncovered parts for both samples (nucleated and not nucleated) were completely destroyed. In the case of using gas mixture consisting of 5 % CH_4 was destroyed only the not nucleated-uncovered part (II-B-u). It indicates that diamond nanoparticles implemented on or into BP during the nucleation process formed the continuous diamond layer which protected the remaining buckypaper. We also found out that the nucleated-covered parts (set A-c) are overgrown by amorphous carbon in all cases and the not nucleated-covered parts of BP (set B-c) remained the same as before deposition.

Fig. 5 shows Raman spectra of the corresponding parts to SEM images in Fig. 4. In comparison with Raman spectra of initial buckypaper substrate (Fig. 3c) it is obvious that spectra of nucleated-uncovered parts changed markedly, spectra of not nucleated-uncovered parts are just a little bit misshaped and all covered parts are unchanged. The spectrum of the sample II-A-u represents the spectrum of NCD film. This diamond film is continuous and equally thick to completely press the signal from the BP substrate. Different result is observed for the sample III-A-u where the NCD film is not continuous so the Raman spectrum is a combination of the BP and NCD spectra. The most significant signs are the increased D mode, not splitted G mode and demonstrative photoluminescence broadband. In the case of the not nucleated-uncovered parts give out to a pressing of the G mode splitting what could be caused by a formation of different C form on the top or by the ratio changes between conductive and semi-conductive CNTs.

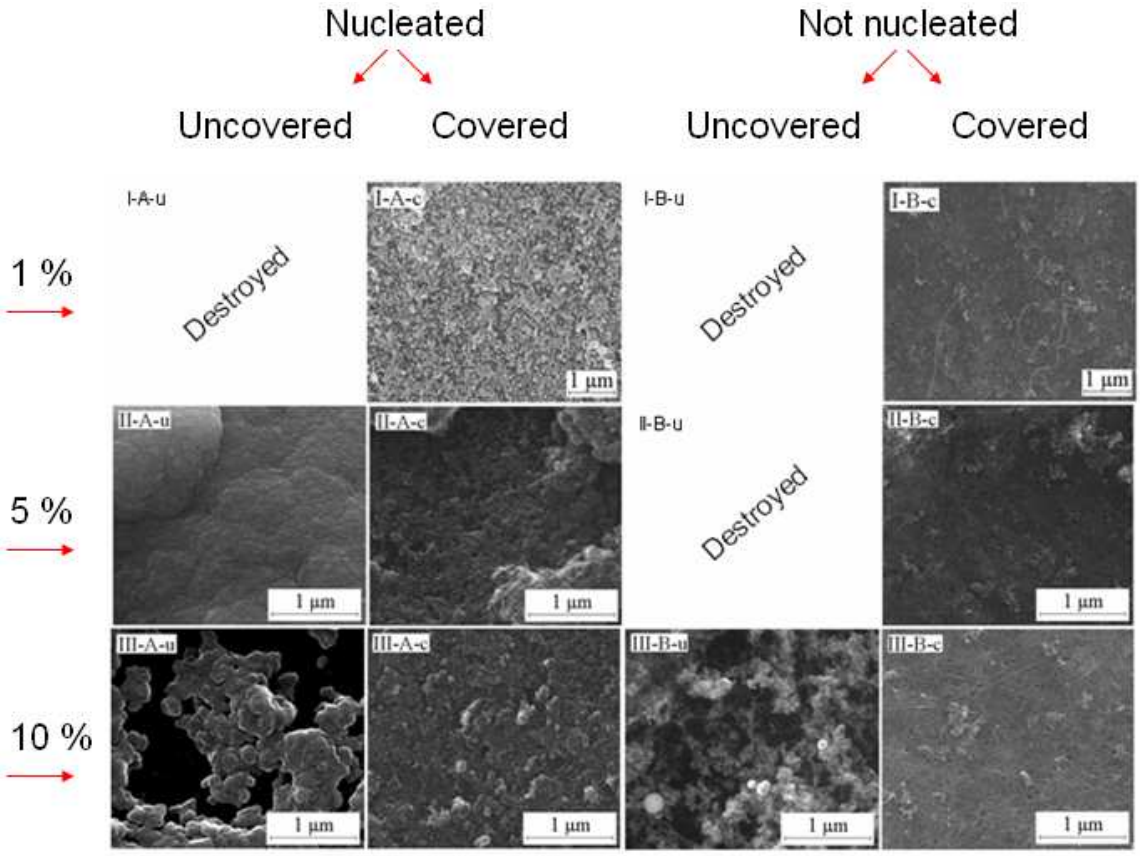

Fig. 4 *SEM images of surface morphology on buckypaper samples*

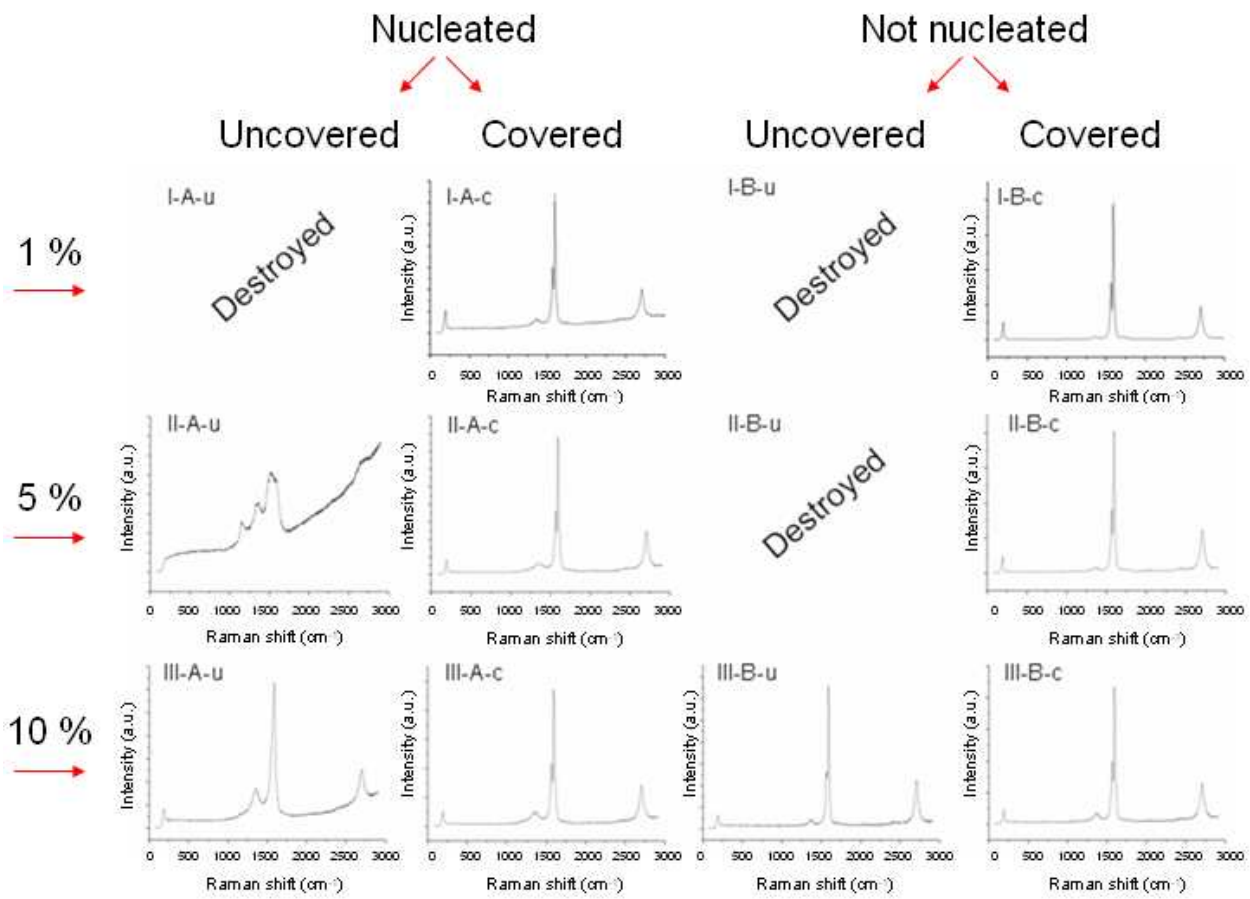

Fig. 5 *Raman spectra of buckypaper samples corresponding to SEM images (Fig. 4)*

CONCLUSIONS

In our work we have investigated the influence of the nucleation and methane concentration on buckypapers exposed to the HFCVD process. The obtained differences in results for each deposition are caused by various treatments of individual parts (nucleated vs. not nucleated, covered vs. uncovered). Due to increasing of methane concentration at the deposition we can notice the decreasing of the substrate temperature which could influenced the overgrowing effect. We found out that at low CH_4 concentration (<5 % of CH_4) the BPs were destroyed probably due to high temperature and aggressive hydrogen-rich plasma. Finally we successfully deposited nanocrystalline diamond film on BP substrate made of SWCNTs bundles. The best results were obtained at 5 % of CH_4 in H_2 atmosphere. We hope that further studies could optimize the carbon nanocomposite production and prove the enhanced properties of these materials.

Acknowledgement This work was done in Center of Excellence CENAMOST (Slovak Research and Development Agency Contract No. VVCE-0049-07) and was financially supported by the grants SK-CZ-0139-09 (MEB0810081), SK-CZ-0148-09 (MEB0810082) and VEGA 1/0746/09.

REFERENCES

[1] S. Iijima, *Helical microtubules of graphitic carbon*, Nature, vol. 354, no. 6348, pp. 56-58, 1991
[2] http://www.nanocyl.com/CNT-Expertise-Centre/Carbon-Nanotubes
[3] Y. Ando, *Carbon Nanotube: The Inside Story*, Journal of Nanoscience and Nanotechnology, vol. 10, no. 6, pp. 3726-3738, Jun. 2010.
[4] http://thefutureofthings.com/articles.php?itemId=24/61/

[5] T. Guo, P. Nikolaev, a Thess, D. Colbert, and R. Smalley, *Catalytic growth of single-walled manotubes by laser vaporization*, Chemical Physics Letters, vol. 243, no. 1-2, pp. 49-54, Sep. 1995.

[6] P. Hou, C. Liu, and H. Cheng, *Purification of carbon nanotubes*, Carbon, vol. 46, no. 15, pp. 2003-2025, Dec. 2008.

[7] http://www.materials.unsw.edu.au/research/batteries

[8] O. A. Williams, M. Nesladek, M. Daenen, S. Michaelson, A. Hoffman, E. Osawa, K. Haenen, R.B. Jackman, Diamond Relat. Mater. 17 (2008) 1080-1088

[9] P. Kulha, A. Kromka, O. Babchenko, M. Vanecek, M. Husak, O. A. Williams, K. Haenen, Vacuum 84 (2009) 53-56

[10] L. Michalikova, B. Rezek, A. Kromka, M. Kalbacova, Vacuum 84 (2009), 61-64

[11] F. Klauser, D. Steinmüller-Nethl, R. Kaindl, E. Bertel, and N. Memmel, *Raman Studies of Nano- and Ultra-nanocrystalline Diamond Films Grown by Hot-Filament CVD*, Chemical Vapor Deposition, vol. 16, Jun. 2010, pp. 127-135.

[12] N. Shankar, *Growth of nanodiamond/carbon-nanotube composites with hot filament chemical vapor deposition*, Diamond and Related Materials, vol. 17, no. 1, pp. 79-83, Jan. 2008.

[13] Banerjee S, Hemraj-Benny T, Wong SS. *Covalent surface chemistry of single-walled carbon nanotube*. Adv Mater 2005, 17(1):17–29

[14] Niyogi S, Hamon MA, Hu H, Zhao B, Bhowmik P, Sen R, et al. *Chemistry of single-walled carbon nanotubes*. Acc Chem Res 2002, 35(12):1105–13.